Seismic Retrofit of Cruciform-Shaped Columns in the Aurora Avenue Bridge Using FRP Wrapping

WA-RD 753.1

David I. McLean
Brian J. Walkenhauer

September 2010

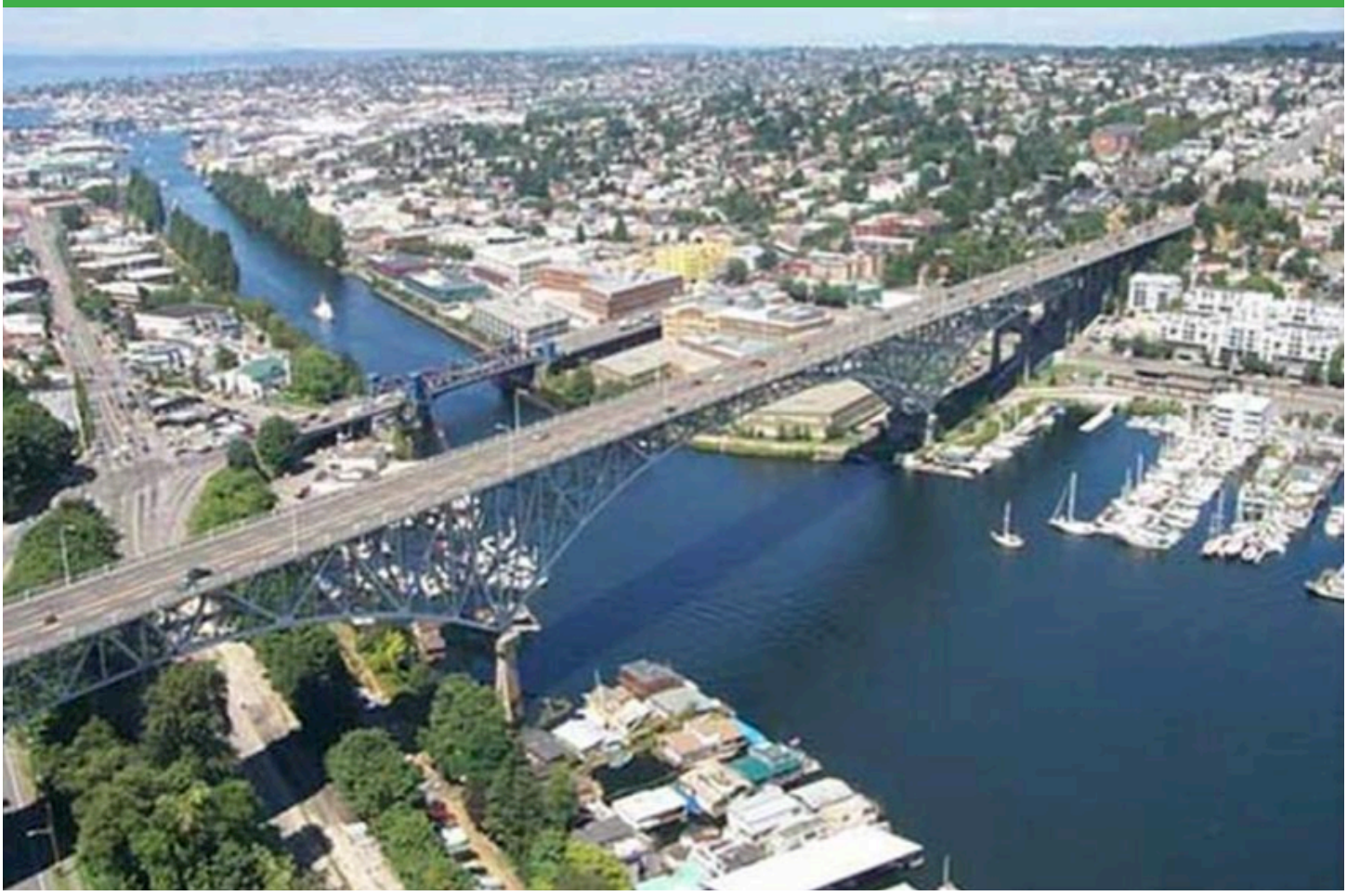

Washington State Department of Transportation
Office of Research & Library Services

WSDOT Research Report

Research Report

Research Project T4120-15
Aurora Avenue Bridge Retrofit Evaluation

SEISMIC RETROFIT OF CRUCIFORM-SHAPED COLUMNS IN THE AURORA AVENUE BRIDGE USING FRP WRAPPING

by

David I. McLean
Professor

Brian J. Walkenhauer
Former Graduate Student

Washington State Transportation Center (TRAC)
Washington State University
Department of Civil & Environmental Engineering
Pullman, WA 99164-2910

Washington State Department of Transportation
Technical Monitors
Craig Boone, Brian Aldrich and Chyuan-Shen Lee
Bridge Engineers

Prepared for

Washington State Department of Transportation
Paula J. Hammond, Secretary
Olympia, WA 98504-7372

September 2010

TECHNICAL REPORT STANDARD TITLE PAGE

1. REPORT NO.	2. GOVERNMENT ACCESSION NO.	3. RECIPIENT'S CATALOG NO.
WA-RD 753.1		

4. TITLE AND SUBTITLE	5. REPORT DATE
SEISMIC RETROFIT OF CRUCIFORM-SHAPED COLUMNS IN THE AURORA AVENUE BRIDGE USING FRP WRAPPING	September 2010
	6. PERFORMING ORGANIZATION CODE

7. AUTHOR(S)	8. PERFORMING ORGANIZATION REPORT NO.
David I. McLean and Brian J. Walkenhauer	

9. PERFORMING ORGANIZATION NAME AND ADDRESS	10. WORK UNIT NO.
Washington State Transportation Center (TRAC) Washington State University Department of Civil and Environmental Engineering Pullman, WA 99164-2910	11. CONTRACT OR GRANT NO. T4120-15

12. SPONSORING AGENCY NAME AND ADDRESS	13. TYPE OF REPORT AND PERIOD COVERED
Washington State Department of Transportation Transportation Building, MS: 7372 Olympia, WA 98504-7372	Research Report
	14. SPONSORING AGENCY CODE

15. SUPPLEMENTARY NOTES

This study was conducted in cooperation with the U.S. Department of Transportation, Federal Highway Administration.

16. ABSTRACT

Experimental tests were conducted on seven 1/3-scale column specimens to evaluate the vulnerabilities of existing cruciform-shaped columns and to develop appropriate retrofit measures that address the identified vulnerabilities. The specimens represented both solid and split columns in the Aurora Avenue Bridge in Seattle, Washington. The as-built specimens failed at low ductility levels due to shear distress. Fiber reinforced polymer (FRP) jackets with FRP inserts to anchor the jackets in the column reentrant corners along with steel confinement collars to provide confinement in the hinging regions were used to retrofit the column specimens. The retrofitted specimens developed plastic hinging in the column, with enhanced strength, energy and ductility capacities. Guidelines were presented for designing the various components of the retrofit measures.

17. KEY WORDS	18. DISTRIBUTION STATEMENT
Bridges, Columns, Retrofitting, Seismic response, Shear, FRP Jacketing, FRP Anchors	No restrictions. This document is available to the public through the National Technical Information Service, Springfield, VA 22616.

19. SECURITY CLASSIF. (of this report)	20. SECURITY CLASSIF. (of this page)	21. NO. OF PAGES	22. PRICE
Unclassified	Unclassified	96	

DISCLAIMER

The contents of this report reflect the views of the authors, who are responsible for the facts and accuracy of the data presented herein. The contents do not necessarily reflect the official views or policies of the Washington State Department of Transportation or the Federal Highway Administration. This report does not constitute a standard, specification, or regulation.

TABLE OF CONTENTS

Page

LIST OF FIGURES

LIST OF TABLES

Page

EXECUTIVE SUMMARY

This study investigated retrofit measures for improving the seismic performance of the cruciform-shaped columns in the Aurora Avenue Bridge located in Seattle, Washington. The primary objective of the study was to evaluate the effectiveness of fiber reinforced polymer (FRP) composite wrapping for enhancing the seismic shear strength of the columns. Seven 1/3-scale cruciform-shaped column specimens were subjected to increasing levels of cyclic displacements representative of seismic loading.

The experimental results of this study indicate that the cruciform-shaped columns in the Aurora Avenue Bridge have inadequate shear strength to develop ductile flexural hinging. Tests on column specimens representing as-built conditions resulted in shear failures at modest displacement levels, accompanied by severe strength, stiffness and physical degradation in the columns.

Tests on column specimens representing solid columns in the Aurora Avenue Bridge and which were retrofitted with FRP jacketing resulted in improved performance compared to that obtained for the column specimens representing as-built conditions. The solid column specimen retrofitted with an FRP jacket and no reentrant corner anchorage experienced pullout of the FRP from the corners, resulting in a shear failure. Solid column specimens retrofitted with an FRP jacket and reentrant corner anchorages developed flexural hinging and failed in a ductile manner with no evidence of shear distress. Failure in the specimen retrofitted with bent steel plate anchored in the reentrant corners with epoxied steel anchors was caused by bulging of the FRP jacket in the plastic hinge regions resulting in concrete degradation and failure of the epoxy anchors. The final solid column specimen was retrofitted with a grout-filled steel collar at the top and bottom of the column in addition to FRP anchors for reentrant corner anchorage. This

specimen achieved significant improvement in energy dissipation capacity and developed the full flexural capacity of the specimen without any bulging in the plastic hinge region. Failure in the specimen was due to extensive flexural hinging leading to low-cycle fatigue fracture of several of the longitudinal reinforcing bars.

Tests on column specimens representing split columns in the Aurora Avenue Bridge and which were retrofitted by providing cores over the full height of the split along with FRP jacketing anchored with FRP inserts and steel collars in the hinge regions resulted in a ductile response and good energy dissipation. The FRP jackets remained fully connected and no movement occurred between the two split sections throughout testing. Failures were due to extensive flexural hinging leading to low-cycle fatigue fracture of the longitudinal reinforcing bars.

The results of this study show that FRP jacketing is effective at providing the required shear strength enhancement to prevent a brittle shear failure. The FRP jacket needs to be anchored into the reentrant corners of the column in order to be effective. In addition, due to the cruciform shape of the columns, the FRP jacket does not provide adequate confinement in the hinge regions to develop ductile flexural hinging in the column. A steel collar filled with high-strength grout was effective at providing the required confinement. The final retrofit design incorporating both reentrant corner anchorage and steel collar confinement developed the full flexural capacity of the column and resulted in fracture of the column longitudinal reinforcing bars. Both the steel bent plates with epoxy anchors and the FRP anchors were effective at anchoring the FRP jacket into the reentrant corners of the column; however, the FRP anchors did not significantly alter the appearance of the bridge columns and were significantly easier to install.

INTRODUCTION

INTRODUCTION AND BACKGROUND

The 1971 San Fernando earthquake and other more recent earthquakes have demonstrated that bridges built using older design codes may be vulnerable to damage under seismic loading. Many of the interstate bridges in the United States were constructed in the 1950s and 1960s and incorporate deficiencies that must be addressed in order to avoid major damage or even collapse under strong ground motion.

Common deficiencies found in bridges built prior to 1971 are insufficient transverse reinforcement and inadequate lap splice length. In addition, poor detailing including lack of proper anchorage of the transverse reinforcement, rare use of crossties, and lap splices located in potential plastic hinge regions make older columns susceptible to failure. Possible failure modes of deficient columns are shear failure, premature flexural failure and lap splice failure.

It is not financially feasible to replace all deficient bridges, and hence retrofitting of existing deficient bridges is a necessary option. Several retrofitting techniques such as reinforced concrete jacketing and steel jacketing have been developed to rehabilitate structurally-deficient bridge columns. In the last decade, fiber reinforced polymer (FRP) composite wrapping has attracted the attention of researchers and bridge owners as an alternative method for retrofitting reinforced concrete bridge elements.

This report presents the findings of an experimental study conducted on cruciform-shaped columns retrofitted using FRP composite materials. Seven 1/3-scale column specimens representative of columns in the Aurora Avenue Bridge in Seattle, Washington were tested. Two unretrofitted specimens were tested to examine the performance of the as-built columns with deficient transverse reinforcement, and five specimens were tested after retrofitting with carbon

fiber FRP composite wrapping. Four of the retrofitted specimens also incorporated reentrant corner anchorage for the FRP, while the remaining retrofitted specimen did not have reentrant corner anchorage. All specimens were subjected to pseudo-static, reverse-cyclic loading. The performance of the tested specimens was evaluated based on failure mode, peak displacement levels attained before failure, and hysteretic behavior.

PROJECT OBJECTIVE

The objective of this study was to evaluate FRP wrapping as a retrofit method for improving the seismic performance of cruciform-shaped bridge columns with known structural deficiencies. To achieve this objective, four main tasks were performed:

1) Identify the vulnerabilities of the cruciform-shaped columns in the Aurora Avenue Bridge under seismic loading;
2) Evaluate FRP composite wrapping as a retrofit measure for improving the seismic performance of cruciform-shaped columns representative of those in the Aurora Avenue Bridge;
3) Evaluate various methods for anchoring the FRP wrapping in the reentrant corners of the column in order to develop the required capacity of the FRP wrapping; and
4) Draw conclusions on the feasibility and effectiveness of FRP composite wrapping for retrofitting deficient cruciform-shaped bridge columns.

THE AURORA AVENUE BRIDGE

HISTORY

The George Washington Memorial Bridge (commonly called the Aurora Avenue Bridge) is a cantilever truss bridge that carries Aurora Avenue North (State Route 99) over the west end of Seattle's Lake Union between Queen Anne and Fremont, as shown in Figure 1. The bridge is 2,945 ft (898 m) long, 70 ft (21 m) wide, and 167 ft (51 m) above the water. It is owned and operated by the Washington State Department of Transportation (WSDOT).

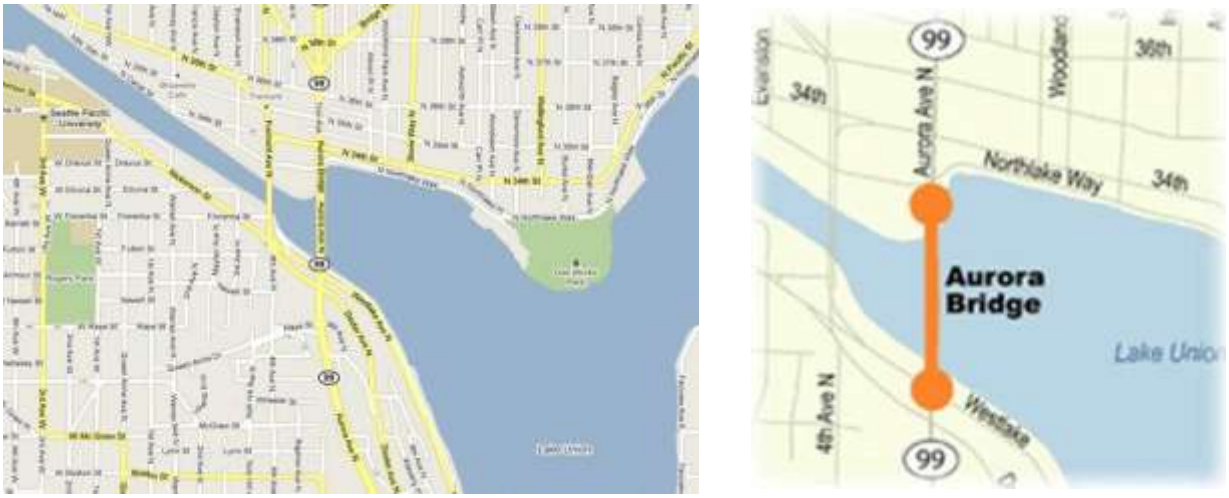

Figure 1 – Location of the Bridge

At the time of its construction, the Aurora Avenue Bridge was a highly controversial project. The state Highway Department wanted a new bridge to carry through traffic on U.S. Highway 99, the state's primary north-south route at the time, more efficiently through Seattle. Several routes for a high bridge over Lake Union were proposed, with possible crossings at Stone Way, Albion Place, Whitman Avenue, and Linden Avenue considered in addition to Aurora Avenue. On June 30, 1930, following the advice of city and state highway engineers, the Seattle City Council approved an ordinance extending Aurora Avenue through Woodland Park.

The council's decision to bisect Woodland Park's 200-acre (81-hectare) urban wilderness triggered outrage among park supporters and other bridge opponents. With the steadfast backing of the *Seattle Times*, speedway opponents gathered enough signatures to force a referendum on the council decision. However, despite these efforts, voters approved the speedway ordinance that November by a substantial margin, with more than 37,000 in favor and around 29,000 opposed. Despite the referendum's passage, the bridge remained a heated topic and the city and state agreed to split responsibility for the project. The state oversaw design and construction of the bridge itself, while the city took charge of constructing the bridge approaches, placing the controversy over the park route squarely in the city's hands. Construction of the bridge was finished in February of 1932, completing the final link of U.S. Highway 99 from Canada to Mexico. Currently the bridge has an estimated Average Daily Traffic (ADT) of over 100,000 vehicles, and it was added to the national register of historic places in 1982.

LAYOUT OF THE BRIDGE

The layout of the Aurora Avenue Bridge can be broken down into three distinct sections: the south approach, the main span, and the north approach. Figure 2 shows the overall layout of the bridge.

The south approach features three spans of reinforced concrete construction as well as three spans of steel deck truss. This section of the bridge is mostly hidden by the abundance of vegetation surrounding it and thus is not well known for its architectural features.

The main span of the bridge, however, is much more visible. It features three spans of steel deck truss cantilevered off of two large piers on opposite sides of the channel. At 1,450 ft (442 m) in length, the main span accounts for almost half of the total length of the bridge.

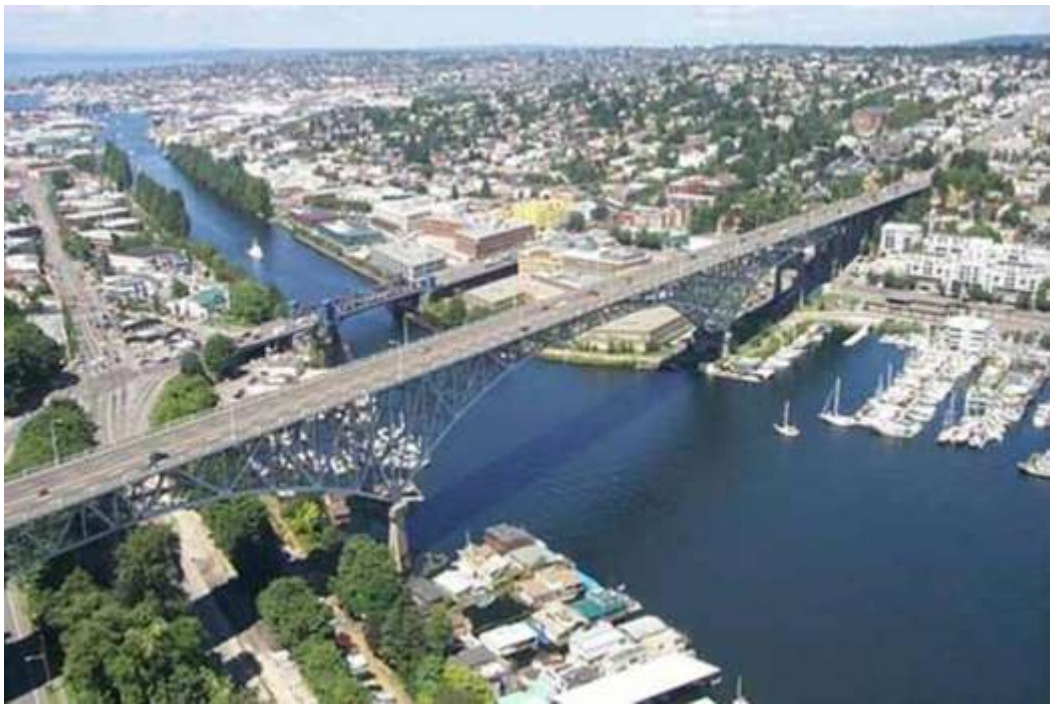

Figure 2 – Overall Layout of the Aurora Avenue Bridge

The north approach features twelve spans of reinforced concrete construction. These twelve spans are separated into five independent frames by split columns which allow for expansion and contraction of the bridge due to temperature and shrinkage effects. Figure 3 shows the layout of the north approach. The piers themselves are unusual in that they are in the shape of a cruciform (plus sign) and are tapered from top to bottom. Figure 4(a) shows a typical solid column and Figure 4(b) shows a typical split column in the north approach. The columns range in height from 13 ft (4 m) at the far north end of the bridge to 87 ft (27 m) where the north approach connects with the main span. The north approach is very accessible to the public as it passes directly over Troll Avenue. At the end of Troll Avenue sits a giant 18 ft (5 m) tall, one-eyed troll that squats beneath the north end of the bridge. The troll was commissioned by the Fremont Arts Council and was sculpted in 1990 by four Seattle artists. Since then, it has become

an icon of the Fremont neighborhood and is one of its most photographed objects. A photo of the troll is shown in Figure 5.

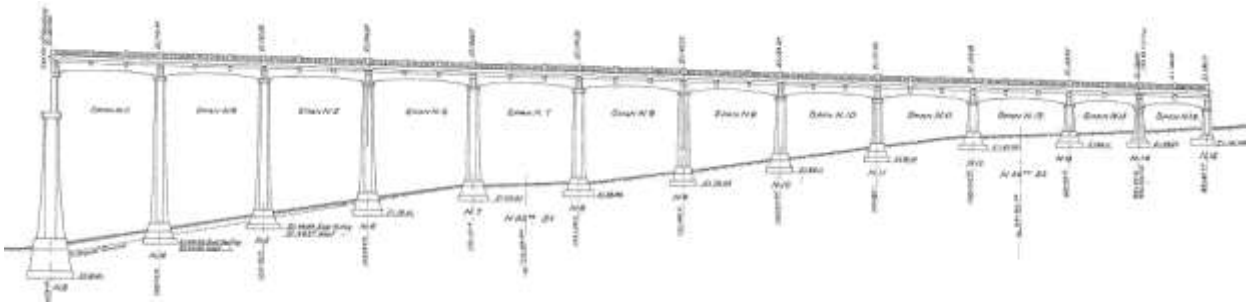

Figure 3 – Layout of the North Approach (1 ft = 0.30 m)

(a) **(b)**

Figure 4 – Typical Solid and Split Columns in the North Approach

Figure 5 – Troll under North Approach

SEISMIC RETROFIT

The seismic retrofit of the Aurora Avenue Bridge has been ongoing in stages since 1998 as part of the WSDOT's Bridge Seismic Retrofit Program, and the most recent stage is retrofitting of the concrete approaches. The 150 ft (45m) south approach and the 700 ft (212 m) north approach structures feature cruciform-shaped concrete columns, varying in height from 13 ft (4 m) to 87 ft (27 m). T.Y. Lin International, a consulting engineering firm specializing in retrofit of existing structures, was hired to perform a seismic evaluation of the structure and determine any vulnerabilities. Among the vulnerabilities, a number of concrete columns were found to be deficient in shear.

Several retrofit options for the Aurora Avenue Bridge were considered, including: external frame strengthening, concrete jacketing, full-height steel column jacketing, and fiber

reinforced polymer (FRP) wrapping. It was determined that the FRP wrapping option best satisfied the WSDOT's desire to maintain the historic character and overall aesthetic appeal of the bridge by keeping the original cruciform shape of the columns. In order to verify the effectiveness of FRP wrapping for improving shear performance in cruciform-shaped columns, a testing program was established.

LITERATURE REVIEW

COLUMN DEFICIENCIES

Many older bridges were designed primarily for gravity loads with little or no consideration of lateral forces from seismic loading. As a result, older columns lack sufficient transverse reinforcement to provide satisfactory performance in a major seismic event. Typically, No. 3 or No. 4 ties at 12 in. (0.3 m) on center were used in columns regardless of the column cross-sectional dimensions. The ties were anchored by 90-degree hooks with short extensions which become ineffective once the cover concrete spalls. Furthermore, intermediate ties were rarely used. These details result in many older columns being susceptible to shear failure, and the ties provide insufficient confinement to develop the full flexural capacity. The limited level of confinement is also unable to prevent buckling of the longitudinal reinforcement once spalling of the cover concrete occurs.

Another detail commonly used in the pre-1971 columns is splicing of the longitudinal bars at the base of the columns, which is a potential plastic hinging region. Starter bars often extended 20 to 35 times the column longitudinal bar diameter (d_b) from the footing. A lap splice length of $20d_b$ has been shown to be inadequate to transfer the full tensile force of the longitudinal reinforcement to the starter bars of the foundation (Haroun et al., 2005; Iacobucci et

al., 2003; Memon et al., 2005; Seible et al., 1995). Columns with longer lap splice lengths have been shown to perform better. Tests on circular columns with a $35d_b$ lap splice have demonstrated relatively ductile performance, with displacement ductility levels of up to 4 being reported (Coffman et al., 1993; Stapleton et al., 2005). Many existing bridge columns in Washington State include lap splices of the column longitudinal reinforcement with a lap length of $35d_b$ (Endeshaw, 2008).

Shear failures may result from the underestimation of lateral seismic forces as well as inadequate transverse reinforcement for shear. Also, underestimation of the flexural strength caused by very conservative elastic design methods coupled with much less conservative shear strength provisions during the 1950's and 1960's typically results in column shear strength being much less than actual flexural capacity, thereby creating a tendency for a brittle shear response of a column.

COLUMN RETROFITTING

The ability of structures to achieve adequate deformation capacity plays a significant role in the prevention of structural failures in seismic events. Ductile structures dissipate more energy and thereby may be designed for lower lateral loads than brittle structures. The deformation capacity of existing bridges can be enhanced by modifying certain substructure elements and connections. Usually it is the bridge piers which are chosen as an effective system for dissipation of seismic-induced energy, as the design of the bridge superstructure is governed by dead load and live loads and hence it is undesirable to allow any inelastic action to occur in this region. Also, the footings are inaccessible beneath the ground and are generally deemed unfit for any ductile response either. Hence the selection of suitable and properly detailed plastic hinges is

made to occur at the ends of the columns, where moments from lateral response are at a maximum.

To ensure against shear failure in a bridge, the shear strength of the bridge pier should be set higher than the shear corresponding to the maximum feasible flexural strength, taking into account overstrength factors for concrete and steel strengths as well steel strain hardening effects at large deformations. Thus, the design shear forces are not necessarily related to the design horizontal inertia forces specified by design codes and may exceed the latter by substantial margins, depending on the degree of conservatism in the flexural design. This process, known as Capacity Design, also ensures that significant variations in ductility demands from expected values can be accommodated without any loss of resistance to lateral loads.

Several methods for increasing the strength and/or ductility of bridge columns have been used in the past. These methods are aimed at upgrading the seismic performance of bridge columns, which have various typical structural deficiencies, so as to prevent collapse of all or part of the bridge. Methods for enhancing the performance of bridge columns include the use of reinforced concrete jackets containing longitudinal and transverse reinforcement, site-welded thin steel jackets filled with high-strength grout, fiber reinforced polymer wrapping, external hoops tensioned by turnbuckles, active confinement by wrapping with prestressed wire, and containment by a fiberglass/epoxy confinement jacket. Alternative means of effective seismic retrofitting can be achieved by seismic isolation techniques, especially if the superstructure is supported on columns by bearings which can be replaced by isolation devices to significantly reduce the seismic forces. Of these techniques, steel jacketing is the most widely used method to retrofit bridge columns (FHWA, 2006).

Steel Jacketing

Previous research studies (Chai et al. 1991; Priestley and Seible, 1991) have shown that steel jacketing is an effective retrofit technique for seismically-deficient concrete columns. Based on satisfactory laboratory results, steel jackets have been employed to retrofit both circular and rectangular columns around the world. For circular columns, two half-circle steel shells, which have been rolled to a radius equal to the column radius plus ½ in. to 1 in. (13 mm to 25 mm) for clearance, are positioned over the portion of the column to be retrofitted, and the vertical seams are then welded (FHWA, 2006). The space between the jacket and the column is flushed with water and then filled with a high-strength cement grout. To avoid any significant increase in the column flexural strength, a gap of approximately 2 in. (50 mm) is typically provided between the end of the jacket and any supporting member (e.g., footing, cap beam, or girders) since at large drift angles the jacket can act as a compression member as it bears against the supporting members (Chai et al., 1991; FHWA, 2006; Priestley et al., 1996; Endeshaw, 2008).

Fiber Reinforced Polymer Wrapping

Recent developments in the manufacturing of fiber reinforced polymer (FRP) composite materials have made these materials available for a wide range of applications, including seismic retrofit of reinforced concrete columns. Compared to steel and concrete jacketing, FRP wrapping has several advantages, including very high strength-to-weight ratios, a high modulus of elasticity, resistance to corrosion, and ease of application. In addition, unidirectional FRP wrapping can improve column ductility without significant stiffness amplification, thereby maintaining the original dynamic properties of the bridge (Haroun et al., 2005).

Commonly employed FRP composite materials are carbon fiber reinforced polymer (CFRP), glass fiber reinforced polymer (GFRP) and aramid fiber reinforced polymer (AFRP).

Most FRP materials exhibit nearly linear elastic behavior up to failure. In general, CFRP has a higher modulus of elasticity than AFRP or GFRP. In terms of tensile strength, CFRP has the highest strength, followed by AFRP and GFRP. Despite GFRP's lower mechanical properties, it is preferable for many civil engineering applications due to its lower cost (ACI 440, 2006; Xiao et al., 2003). However, the durability of GFRP may be a concern for applications in wet environments, such as that of Western Washington.

The California Department of Transportation (Caltrans) funded several research studies at the University of California at San Diego to develop design guidelines for FRP retrofit systems. The findings and recommendations of these studies are given in *Suggested Revisions to Caltrans Memo to Designers 20-4 to Cover Fiberglass/Epoxy Retrofit of Columns* (SEQAD 1993), ACTT-95/08 (Seible et al., 1995) and Priestley et al., 1996. These documents present similar design equations with only minor differences. The FHWA's *Seismic Retrofitting Manual for Highway Structures* (2006) has adopted these design guidelines for application to circular columns.

Caltrans primarily uses steel jacketing to retrofit deficient columns, with composite fiber wrapping listed as an alternative. Composite material retrofitting is approved only for cases that have been verified through experimental testing. The Caltrans *Memo to Designers 20-4* (1996) limits composite material retrofitting of rectangular columns with cross-sectional aspect ratios or 1.5 or less and a maximum dimension of 3 ft (1 m). Other restrictions include axial dead load not more than 15% of the column capacity, longitudinal reinforcement ratios of 2.5% or less, and a maximum displacement ductility of 3. The guideline also stipulates that rectangular columns with lap splices in a potential plastic hinge region must not be retrofitted with composite fiber unless slippage of reinforcing bars is allowed.

ACTT-95/08 provides design equations to determine the required jacket thickness for each mode of failure (i.e., shear failure, confinement failure and lap splice failure) (Seible et al., 1995). The shear strength of FRP wrapped columns can be calculated using the following equation:

$$V = V_C + V_S + V_{FRP} \qquad \text{(Equation 1)}$$

V_C is the shear strength of the concrete, V_S is the contribution of the transverse reinforcement, and V_{FRP} is the contribution of the FRP to the shear strength of the column. The shear contribution of the FRP can be calculated using Equation 2:

(Equation 2)

t_j is the effective thickness of the FRP, D is the column dimension in the loading direction, and θ is the inclination of the shear crack of principal compression strut. The design stress level for the jacket, f_{jd}, is specified by the FRP manufacturer. The value should also be capped to limit strains in the concrete. When the dilation strain in the concrete exceeds 0.004, the contribution of the concrete to the shear capacity, V_c, decreases due to aggregate interlock degradation (Priestley et al., 1996). As shown in Equation 3, the design stress of the FRP, f_{jd}, should not exceed that associated with developing a strain of 0.004.

$$f_{jd} \le 0.004 E_j \qquad \text{(Equation 3)}$$

E_j is the elastic jacket modulus in the tie direction. After simplifying the previous equations, the required jacket thickness can be calculated as follows:

$$t_j = \frac{\frac{V_o}{\phi} - (V_c + V_s)}{2 f_{jd} D \cot\theta} \qquad \text{(Equation 4)}$$

V_o is taken as 1.5 times the shear force required to develop the onset of flexural yielding in the original column, and ϕ is taken as 0.85 (Seible. et al., 1995).

ACI 440 (2006) uses similar equations but with additional safety factors. The design stress of the FRP, f_{jd}, should not exceed $0.75\varepsilon_{ju}E_j$, where ε_{ju} is the ultimate strain of the FRP and E_j is the modulus of elasticity of the FRP jacket. In addition to the shear strength reduction factor, ϕ, ACI 440 imposes an additional safety factor of 0.95 on the contribution of the FRP to the shear strength, V_{FRP}, to account for loss of strength over time.

EXPERIMENTAL TESTING PROGRAM

TEST SPECIMENS

Prototype Selection and As-Built Details

This section provides details of the design and construction of seven large-scale cruciform-shaped column specimens, consisting of two as-built columns and five columns retrofitted with fiber-reinforced polymer (FRP) jackets. The retrofitted specimens included both solid and split columns. The specimens were constructed to be representative of the cruciform-shaped columns present in the Aurora Avenue Bridge located in Seattle, Washington and were expected to be vulnerable to shear failure.

As-built column details for the test specimens were based on "Bridge 99-560 Approach Span As-Built Plans" provided by the WSDOT. Properties for the materials in the bridge were obtained from the 1931 *Standard Specification for Highway Bridges* (AASHO, 1931). This standard required all concrete to have a minimum compressive strength at 28 days of 3500 psi (24 MPa) and steel reinforcement conforming to ASTM A15-30. Due to the strength gain of concrete with time, it was estimated that the concrete strength of the in-place concrete in the bridge would now be about 5000 psi (34 MPa). Information on ASTM A15-30 steel was found

in “FEMA 356 – Prestandard for the Seismic Rehabilitation of Buildings”, which lists the yield strength of A15, Intermediate Grade steel as 40 ksi (276 MPa).

The experimental tests were conducted on 1/3-scale specimens that generally modeled the dimensions, reinforcement, detailing, and material properties of the columns in the Aurora Avenue Bridge. Details for the solid column specimens were chosen to represent those in the columns in Bent N13 in the as-built plans. Figure 5 shows the column dimensions and reinforcement details for Bent N13. Details for the split column specimens were chosen to represent those in the columns in Bent N11 in the as-built plans. Figure 5 shows the column dimensions and reinforcement details for Bent N11.

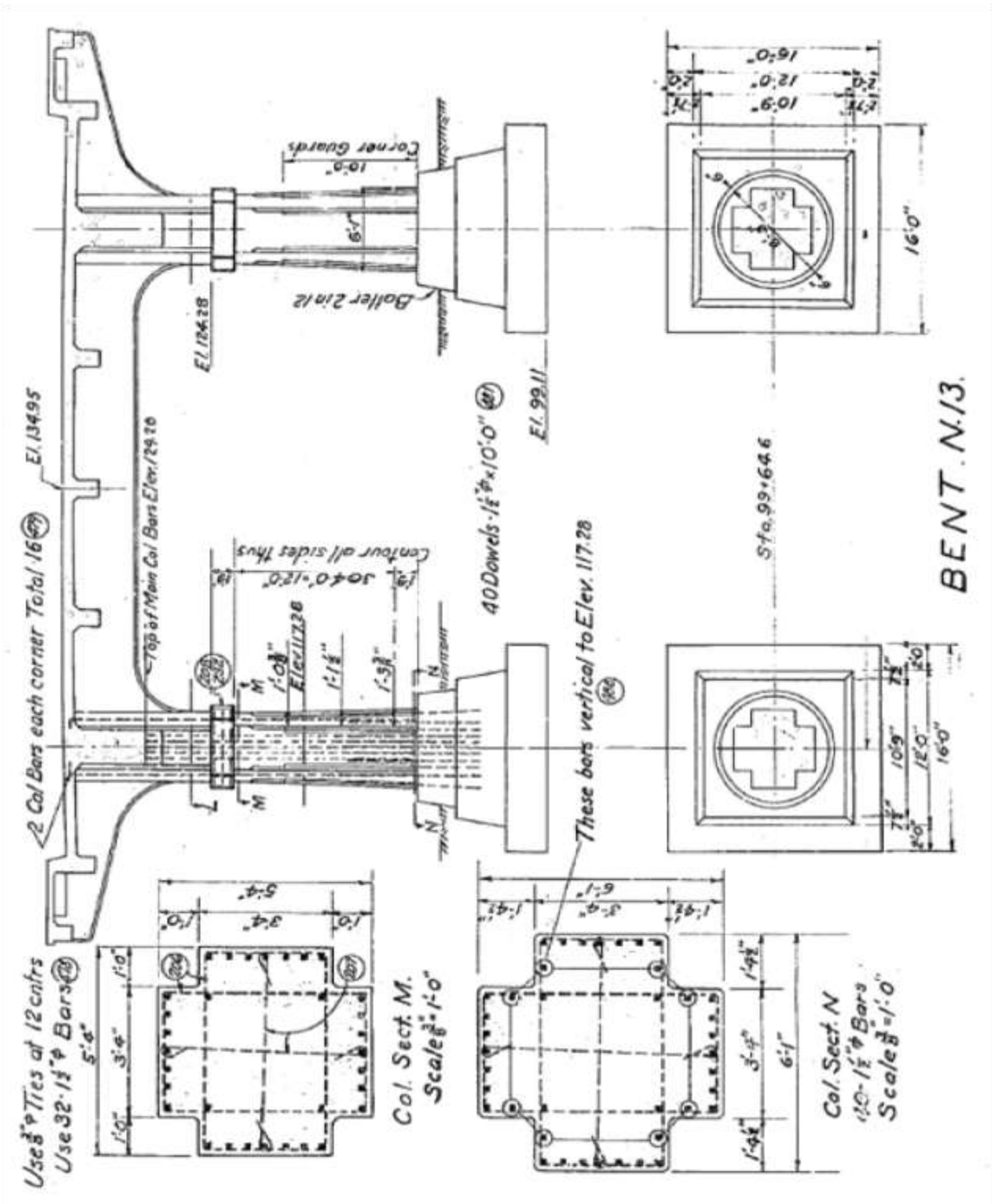

Figure 5 – Solid Column As-Built Details (1 in. = 25.4 mm)

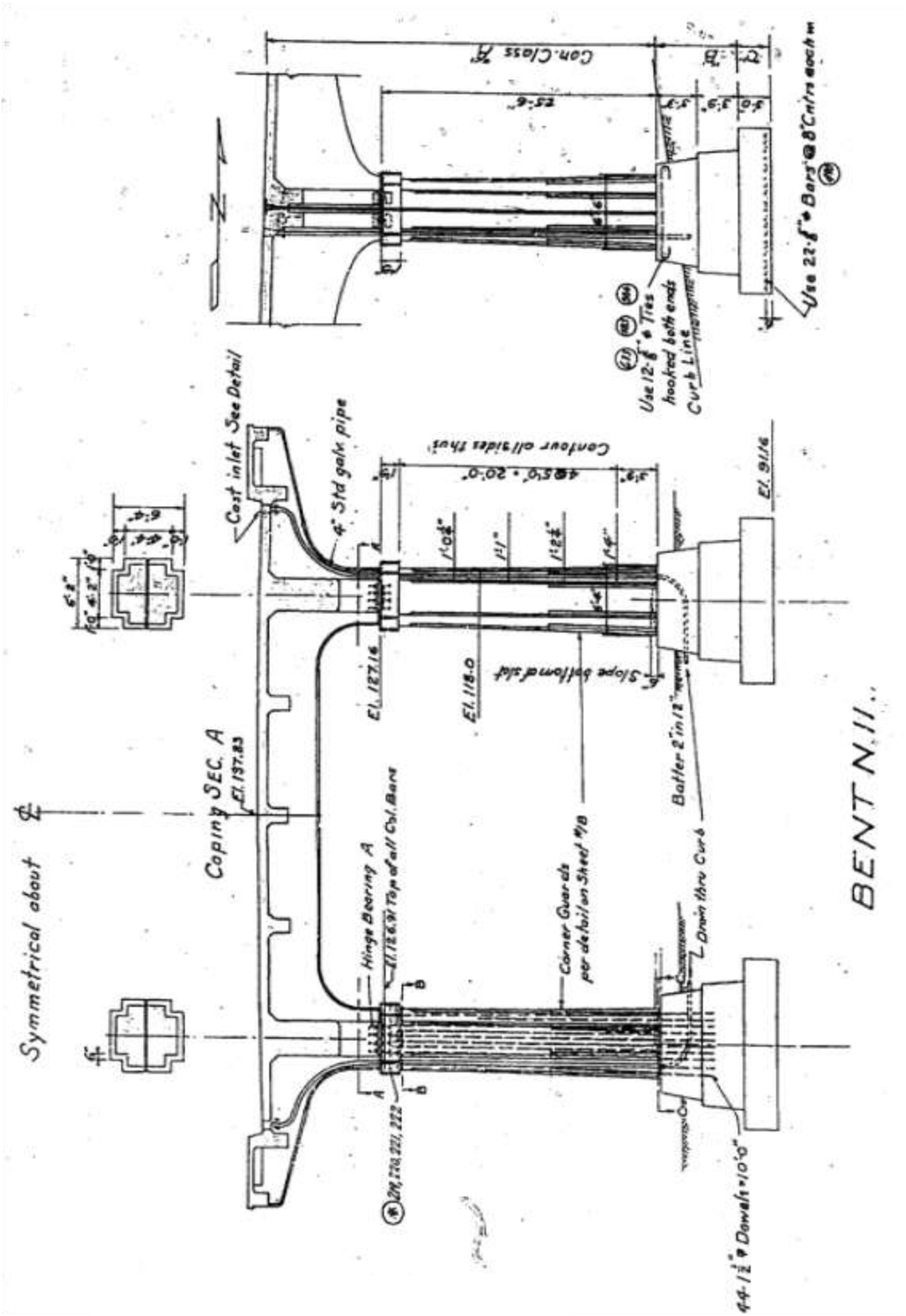

Figure 6 - Split Column As-Built Details (1 in. = 25.4 mm)

The longitudinal steel in the columns of the bridge consists of (40) 1½ in. x 1½ in. (38 mm x 38 mm) square bars in the solid columns and (44) 1½ in. x 1½ in. (38 mm x 38 mm) square bars in the split columns. No equivalent bar diameter is available for the scaled test specimens, so (40) No. 4 rebars were used, which resulted in a 21.5% decrease in the amount of flexural reinforcement in the test columns. The tested yield strength of the longitudinal bars in the column specimens was 48 ksi (331 MPa), 20% higher than the expected yield strength for the reinforcement in the bridge. Taking into account the higher yield strength resulted in longitudinal steel in the column specimens that was effectively only 6% less than the equivalent steel in the columns of the bridge. Because it was determined shear failure would govern the column capacity, this distortion in the model column was deemed acceptable.

The transverse steel in the bridge columns consisted of No. 3 ties spaced at 12 in. (0.3 m) on center. An equivalent area of reinforcement in the test columns would be 1/8-in. (3-mm) diameter ties spaced at 4 in. (0.1 m) on center. Installation of strain gages on 1/8-in. (3-mm) diameter bars would be difficult, so the size of the transverse steel in the test columns was increased to ¼-in. (6-mm) diameter bar in order to obtain accurate strain gage measurements. To account for the increased area, A36 wire was used. This resulted in a transverse reinforcement capacity that was higher than in the bridge; however, the contribution to shear strength of the No. 3 ties at 12 in. (0.3 m) on center in the bridge is small in comparison to the overall shear strength of the column, so the distortion in scaling of the ties was judged to not significantly alter the shear strength of the test columns.

The test specimens were constructed by Central Premix Inc. of Spokane, Washington. The columns were supported on a heavily-reinforced footing and a heavily-reinforced loading stub at the top. The footings were designed to provide a rigid support at the base of the columns

and were anchored to a laboratory strong floor through high-strength bolts running through PVC tubes that were cast into the footings.

Figure 7 shows the details of the solid column specimens. Column longitudinal reinforcement consisted of (40) No. 4 Grade 40 bars distributed around the perimeter of the column with (7) bars on each face and (3) bars in each reentrant corner. (2) bars in each reentrant corner were terminated at 3 ft (1 m) above the top of the footing. All other longitudinal reinforcement extended into both the top loading stub and the footing. Unlike the columns in the bridge, no lap splice was provided between the footing and column reinforcement in the test columns to eliminate possible effects from lap splices on column behavior. Transverse reinforcement consisted of ¼-in. (6-mm) diameter, A36 ties and crossties at 4 in. (0.1 m) on center. A cover of ¾ in. (19 mm) was provided for the column reinforcement as compared to 2 in. (51 mm) in the bridge.

Figure 8 shows the details of the split column specimens. Column longitudinal reinforcement consisted of (22) No. 4 Grade 40 bars distributed around the perimeter of each section of the column (44 total) with (6) bars on each face and (3) bars in each reentrant corner. (2) bars in each reentrant corner were terminated at 5 ft 6 in. (1.7 m) above the top of the footing. All other longitudinal reinforcement extended into both the top loading stub and the footing. Unlike the columns in the bridge, no lap splice was provided between the footing and column reinforcement in the test columns. Transverse reinforcement consisted of ¼-in. (6-mm) diameter, A36 ties and crossties at 4 in. (0.1 m) on center. A cover of ¾ in. (19 mm) was provided for the column reinforcement as compared to 2 in. (51 mm) in the bridge.

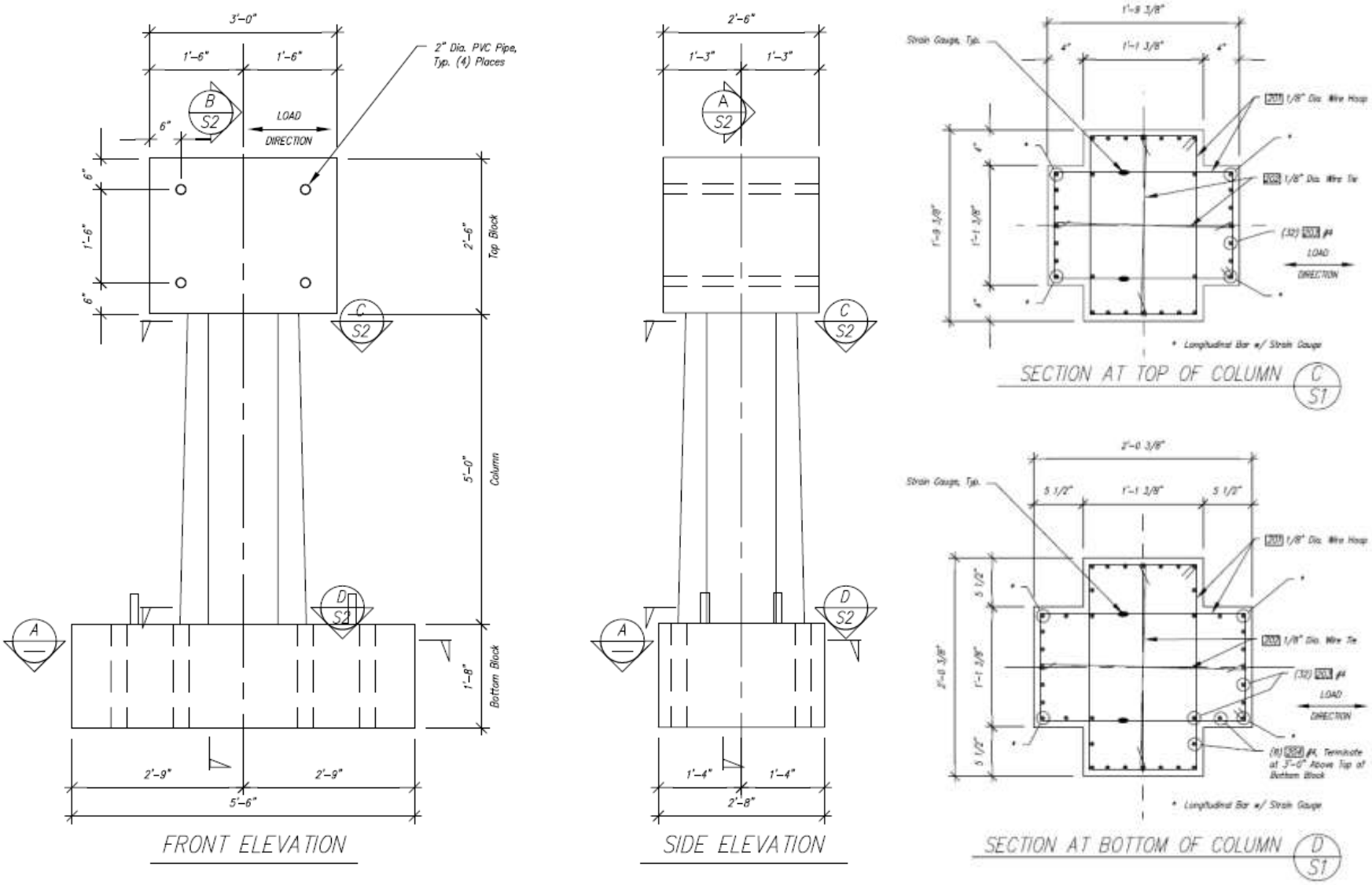

Figure 7 – Solid Column Specimen Details (1 in. = 25.4 mm)

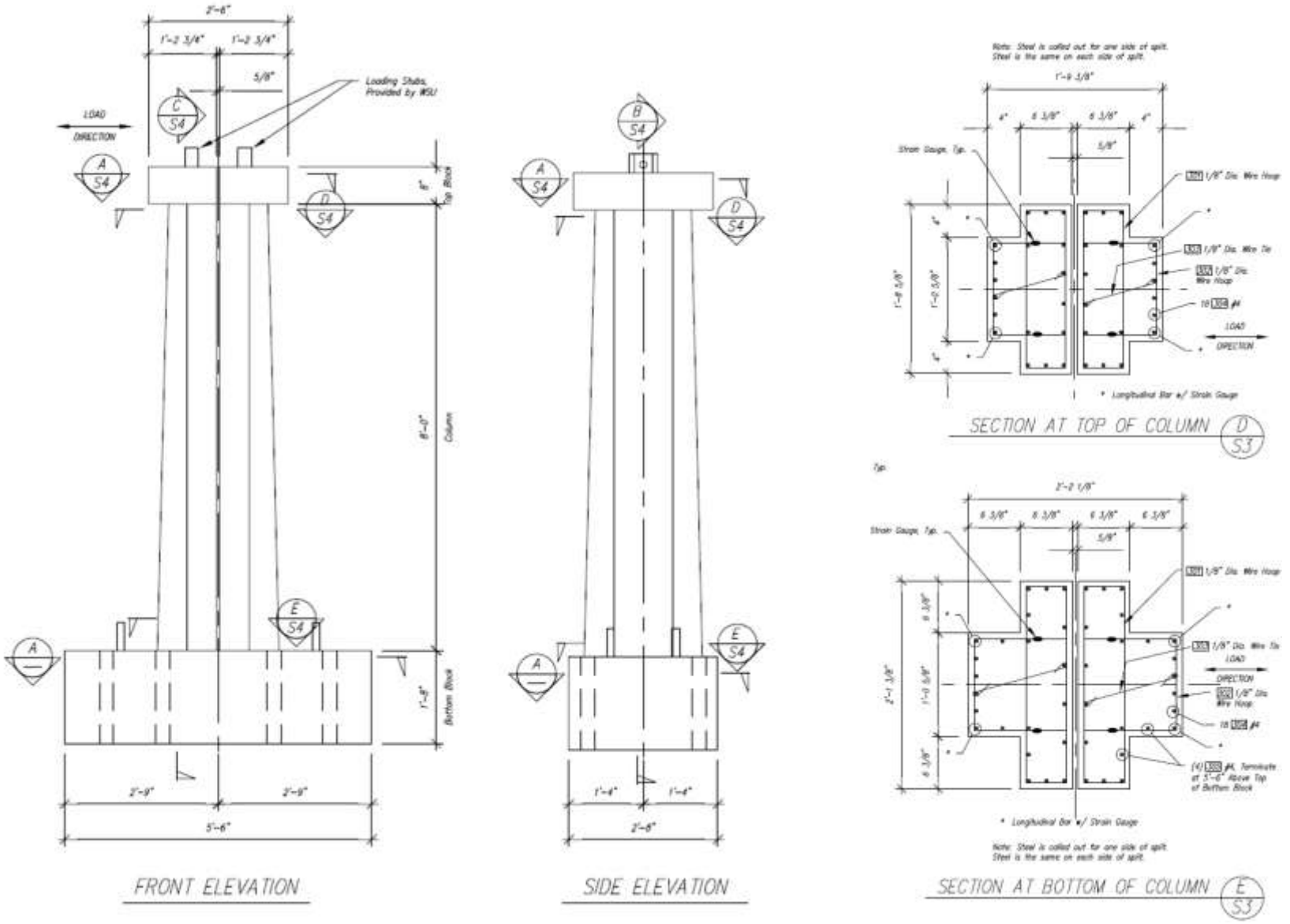

Figure 8 – Split Column Specimen Details (1 in. = 25.4 mm)

A heavily-reinforced loading stub was constructed at the top of the solid columns. The loading stub contained (30) No. 5 Grade 60 straight bars with 90º hooks running in the horizontal direction and (8) No. 5 Grade 60 hoops and (16) No. 5 Grade 60 crossties in the vertical direction. (4) 3-in. (76 mm) diameter standard steel pipes were cast into the load stub to connect the load stub to the load frame. (3) No. 6 Grade 60 hairpins were provided between each of the four steel pipes to resist the design shear and the torsion force developed at the four steel pipe locations due to the column top moment and applied shear forces, as shown in Figure 9. These hairpins were provided in both the horizontal and vertical directions for a total of (12) hairpins, which provided a lateral tension capacity of 158 kips (703 kN) at each bend. This was considered to be adequate to resist the worst possible loading case shown in Figure 9, associate with a shear force of 120 kips (534 kN) and an equivalent moment of 427 k-ft (579 kN-m) at the center of the load stub, producing a tension force, T, of 98 kips (436 kN) at each bend.

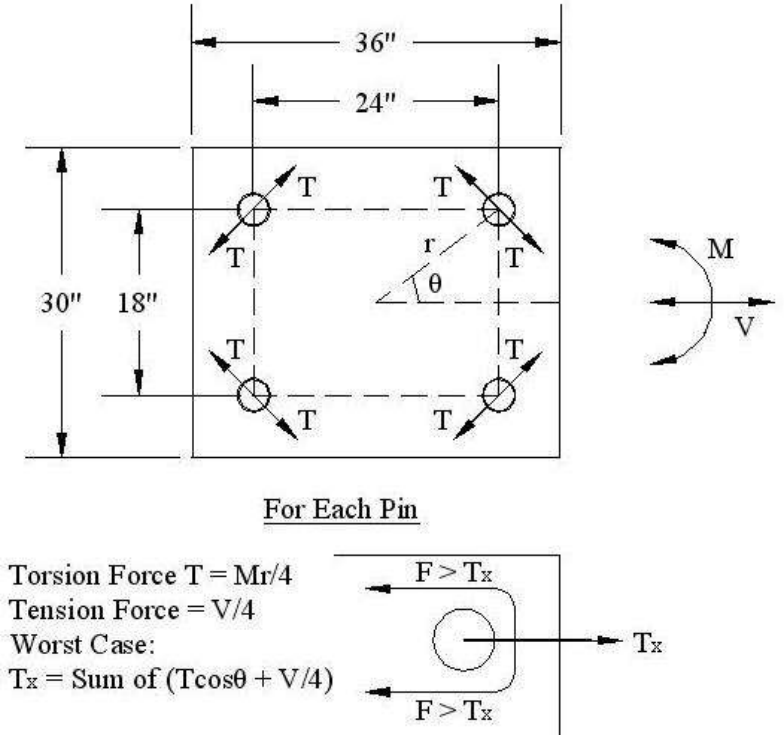

Figure 9 – Torsion Design in Top Loading Stub (1 in. = 25.4 mm)

Retrofit Details

Two solid column specimens were tested without any retrofitting to reveal vulnerabilities present in the existing columns and to establish benchmarks for evaluating the effectiveness of the applied retrofit measures. All other columns were wrapped with two layers of 0.014-in. (0.36-mm) thick commercially-available FRP fabric with primary fibers oriented in the horizontal direction. This thickness of FRP was determined using the shear design procedures presented earlier (Equation 4). One retrofitted column was tested without reentrant corner anchorage to evaluate whether such anchorage was necessary to fully engage the FRP jacket. Reentrant corner anchorage was provided for the other four retrofitted columns using two different anchorage methods. A summary of the test specimens is given in Table 1.

Table 1 – Specimen Test Parameters

Specimen	Column Type	Test Parameter
Column 1	Solid	As-built
Column 2	Solid	FRP jacket without reentrant corner anchorage and no hinge confinement
Column 3	Solid	FRP jacket with angle and steel inserts for corner anchorage and no hinge confinement
Column 4	Solid	FRP jacket with FRP inserts for corner anchorage and confinement of top and bottom hinges
Column 5	Solid	As-built - repeat of Column 1
Column 6	Split	FRP jacket with FRP inserts for corner anchorage, cored and grouted split region, and confinement of bottom hinge
Column 7	Split	Repeat of Column 6

A dry lay-up method in accordance with the manufacturer's recommendations was used to install the FRP wrap on Columns 2 and 3. To avoid stress concentrations in the FRP jacket, the corners of the columns were rounded to a minimum ¾-in (19 mm) radius before the FRP wrap was applied. The FRP application procedure consisted of first coating the column with a layer of epoxy followed by applying the dry FRP fabric in the arrangement shown in Figure 10. After the first layer of FRP fabric was in place, a second layer of epoxy was applied to the column. This process was repeated for the second layer of FRP wrap. A wet lay-up method was used to install the FRP wrap on Columns 4, 6 and 7 in accordance with recommendations from the FRP anchorage manufacturer. This procedure was similar to the dry lay-up except that no epoxy was applied to the column prior to installing the FRP fabric. Instead, the dry FRP fabric was first saturated with epoxy and then applied to the column. Also, no additional epoxy was applied in between FRP layers except to smooth out irregularities around the corner anchorages.

The reentrant corner anchorage for Column 3 consisted of a 3/8-in. (10-mm) thick steel bent plate with 3/16-in. (5-mm) stiffener plates at 2 in. (51 mm) on center. Figure 11 shows the corner anchorage as a quarter-section of HSS tube; however, this was later changed to a bent plate due to residual stresses present in the HSS section which caused it to warp when cut. 7/16-in. (11-mm) diameter anchor bolts holes were drilled through the FRP wrap extending 3⅜ in. (86 mm) into the concrete column. These anchor bolt holes were staggered at 4 in. (0.1 m) on center up each face of the reentrant corners. The steel plate was predrilled with ½-in. (13-mm) diameter holes at 4 in. (0.1 m) on center and anchored to the column using A 193 B7 threaded rod anchors with 3⅜-in. (86-mm) embedment and epoxy adhesive as shown in Figure 10. The reentrant corners for this specimen were also reinforced with two additional layers of FRP oriented at 45º from the horizontal and filled with thickened epoxy resin to a minimum 1-in. (25-mm) radius.

The reentrant corner anchorage for Column 4 consisted of ½-in. (13-mm) diameter FRP anchors as shown in Figure 11. These anchors were installed at 4 in. (0.1 m) on center up each face of the reentrant corners. The anchors were designed assuming they were effective only in tension (Ozbakkaloglu et al. 1996). Shear strength of the FRP anchors was neglected, and thus anchors were proportioned to carry the full anchorage demand in tension on one face of the reentrant corner. Prior to installation of the first layer of FRP, 7/16-in. (11-mm) diameter anchor holes extending 5 in. (0.13 m) into the concrete column were drilled and filled with epoxy and the reentrant corner of the column was filled with epoxy to a minimum ¾-in. (19-mm) radius. After installation of the first FRP jacket layer, the dry FRP anchors were soaked in epoxy and then pushed through a small cut in the FRP jacket. The end fibers of the FRP anchors were then splayed out and laid flat onto the surface of the FRP jacket as shown in Figure 12. After the FRP anchors were installed, a coating of epoxy was applied over the top of the anchors to fill any voids between anchor locations. The second FRP jacket layer was then applied. Following installation of the FRP jacket, a ¼-in. (6-mm) thick by 6-in. (0.15-m) tall A36 steel collar was installed at the top and bottom of the column and filled with high-strength non-shrink grout. A 1-in. (25-mm) gap was provided between the collars and the footing and top loading blocks.

Retrofit details for Columns 6 and 7 were similar to those used for Column 4 except that a steel collar was installed only at the bottom of the column.

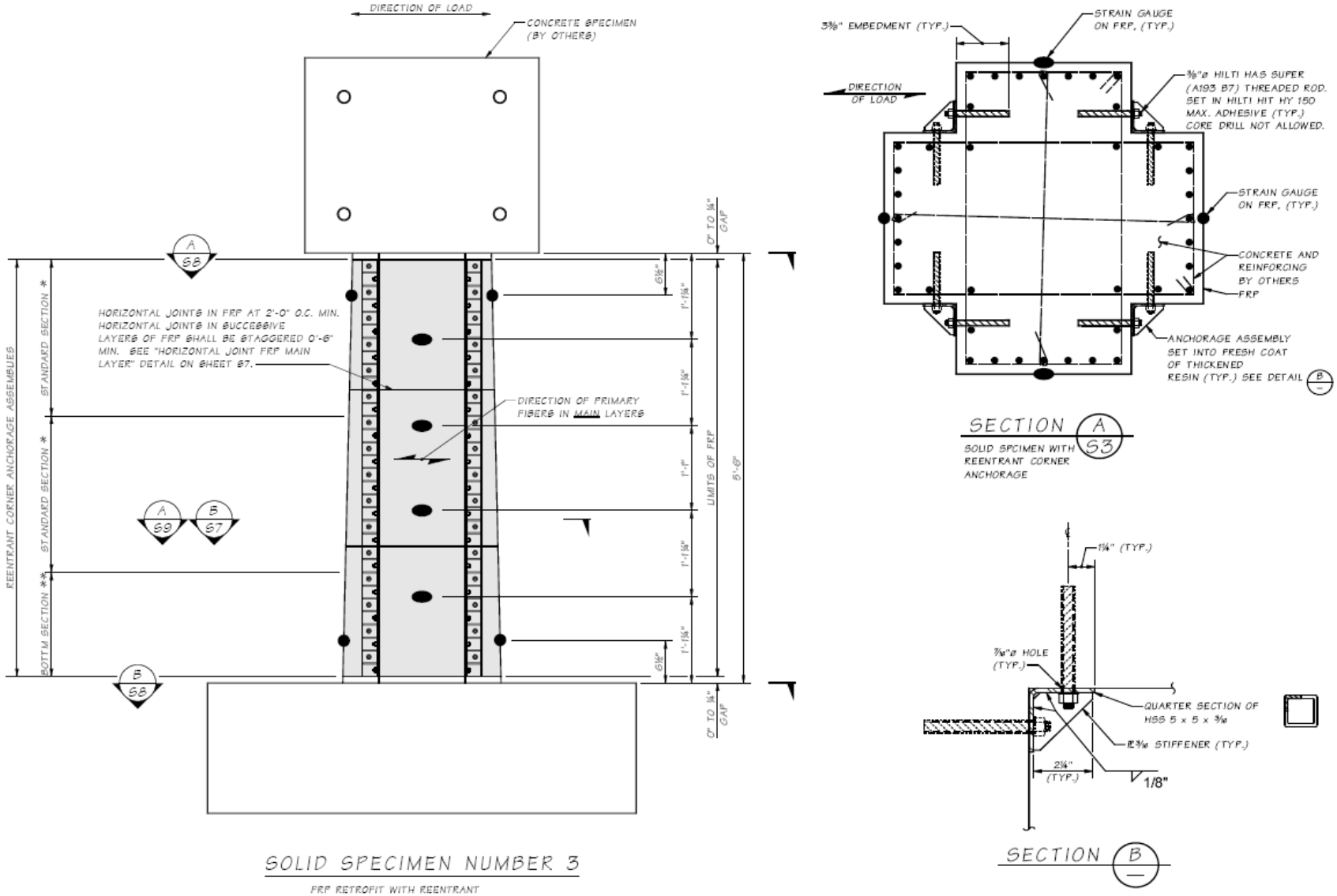

Figure 10 – Steel Bent Plate with Anchor Bolts Retrofit Details (1 in. = 25.4 mm)

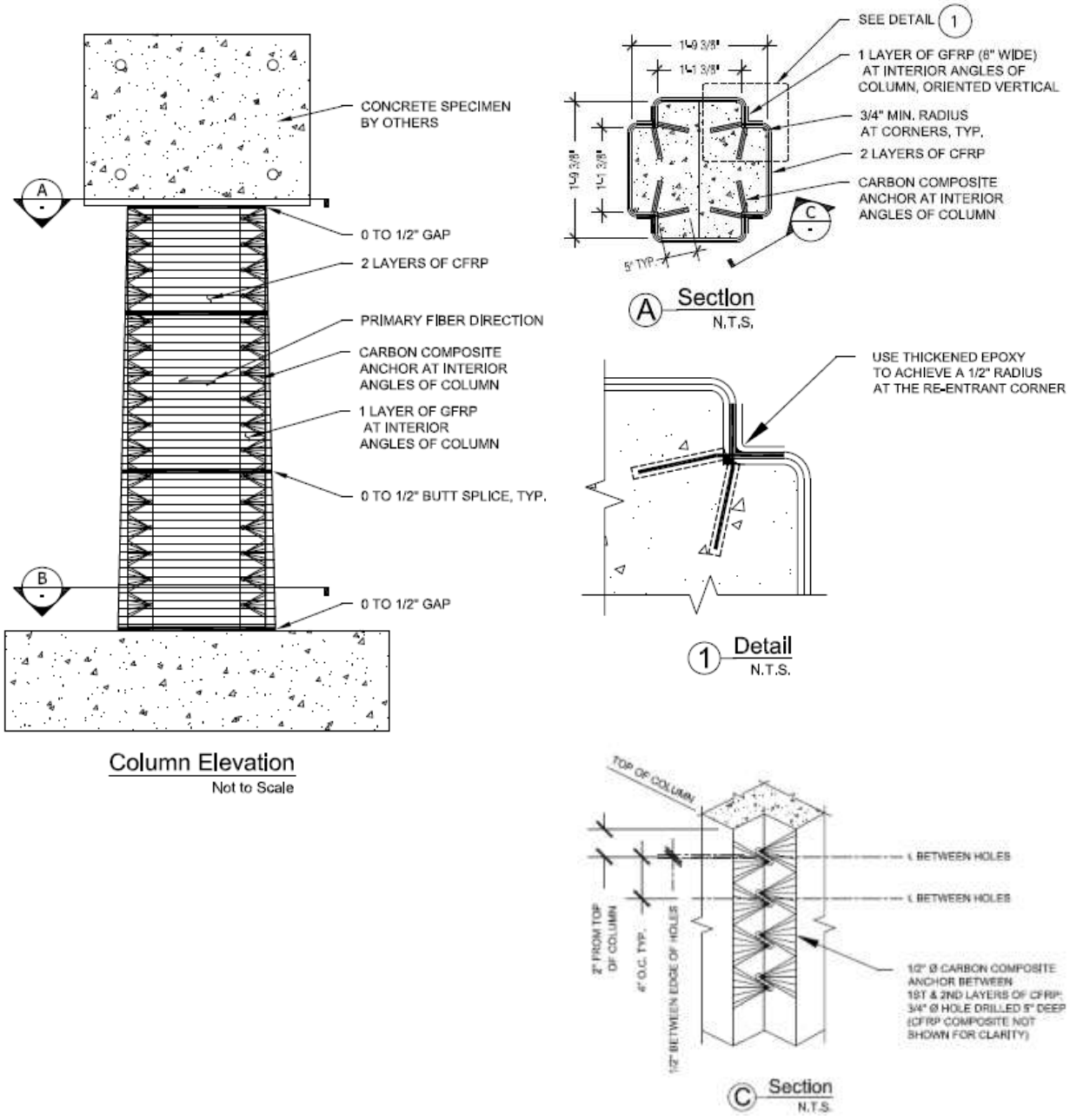

Figure 11 – FRP Anchor Retrofit Details (1 in. = 25.4 mm)

Figure 12 – FRP Anchor Installation

The retrofit details for Columns 6 and 7 are shown in Figure 13, except that FRP anchors were used, similar to those in Column 4. A goal of the retrofitting for the split columns was to provide for full composite action of the two split sections. 2-in. (50-mm) cores were provided at 4-in. (100-mm) centers over the full height of the split, and the gap in the split along with the cores were filled with high-strength grout. Through-bolts across the interface were originally planned for Column 7; however, test results for Column 6 showed that the through bolts were not needed to provide composite action and were not used. Following installation of the FRP jacket, a ¼-in. (6-mm) thick by 6-in. (0.15-m) tall A36 steel collar was installed at the bottom of the column and filled with high-strength non-shrink grout. A 1-in. (25-mm) gap was provided between the collar and the footing.

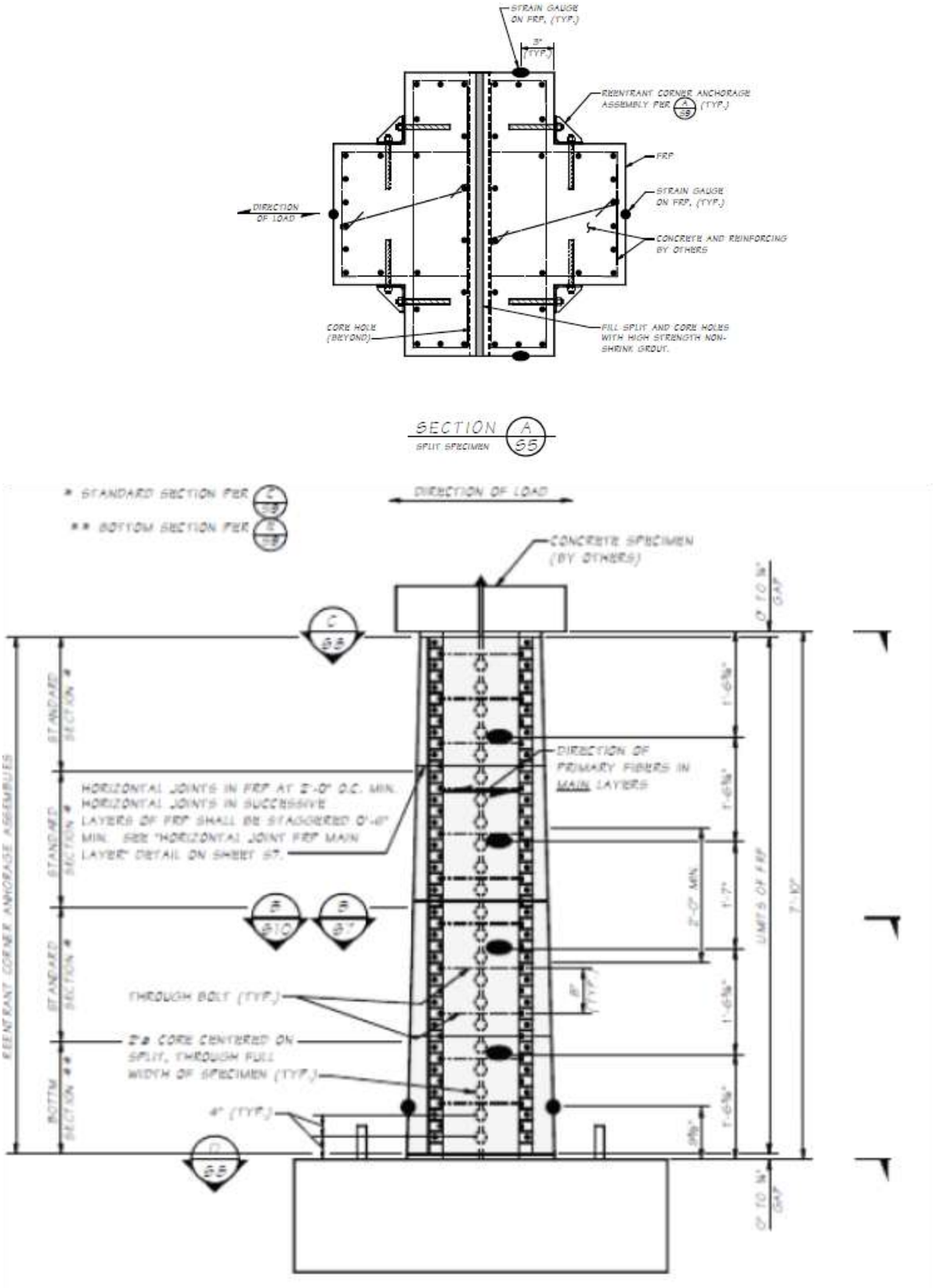

Figure 13 – Retrofit Details for the Split Columns (1 in. = 25.4 mm)

Material Properties

The concrete used in the construction of the column specimens had an average measured compressive strength of 4100 psi (28 MPa) at the time of testing. The grout used for the retrofit collars and to fill the split interface had an average measured compressive strength of 5700 psi (39 MPa) at 7 days. The Grade 40 No. 4 longitudinal bars in the columns had an average measured yield strength of 48 ksi (330 MPa). The A36 ¼-in. (6-mm) diameter transverse ties had an average measured yield strength of 62 ksi (430 MPa). The cured FRP composite used to jacket the columns had a specified ultimate strength of 150 ksi (1035 MPa) and a specified elastic modulus of 10,100 ksi (69,600 MPa). The specified ultimate strength of the cured FRP anchors was 108 ksi (745 MPa). Finally, the A36 steel used in the retrofit collars had an average measured yield strength of 42 ksi (290 MPa).

TEST SETUP AND LOADING PROCEDURES

The test setup for the solid column specimens was adapted from testing performed at the University of California at San Diego (Verma et al, 1993). Figure 14 shows the overall test setup for the solid columns. A stiff loading frame connected the column loading stub to a horizontal double-acting actuator aligned at the point of zero moment, inducing double bending in the column specimen. Moment was introduced into the top of the specimen through large bolts that passed through tubes cast into the loading stub. The footing was bolted to the strong floor to prevent overturning of the specimen. Sliding of the footing base was prevented by two stiff brackets bolted to the floor. Loading frame eccentricity was compensated for using a load-balancing system consisting of a load-follower jack which counteracted the extra bending

moment transmitted to the loading stub due to the self-weight of the large loading arm and half of the weight of the actuator.

Figure 15 shows the overall test setup for the split column specimens. This test setup was designed to subject the column specimens to single bending without restricting potential movement between the two halves of the split columns. The actuator was attached to the top of the column through specially designed pin assemblies and a rigid loading arm. The footing was bolted to the strong floor to prevent any overturning from occurring. Sliding of the footing base was prevented by two braces which were bolted to the floor.

Loading of the test specimens was slowly applied in a quasi-static manner. Horizontal loads were applied under displacement control based on a pattern of progressively increasing displacements, referenced to the horizontal displacement to cause first yield (Δ_y) in the column. Displacements were applied at a rate of 0.005 in./s (0.13 mm/s) for three complete cycles at displacement levels of ±0.33, ±0.67 and ±1 times Δ_y, then increased to a rate of 0.01 in./s (0.26 mm/s) for three complete cycles at displacement levels of ±1.5, ±2, ±3, ±4, ±5, ±6, ±8, ±10, ±12, ±14, ±16, ±18 and ±20 times Δ_y, unless failure occurred first. Failure was defined as a 20% drop in peak lateral load for each specimen. Δ_y was theoretically determined from moment-curvature analyses of the columns prior to testing.

Load cells and displacement potentiometers measured column displacements and applied loads during testing. Strain gages were used to measure strains in the column longitudinal reinforcement at the points of peak moments, in the transverse tie reinforcement at various points over the column height, in the FRP jacket both parallel and perpendicular to the applied loading (measuring FRP strains due to shear and FRP strains due to flexural bulging, respectively), and

circumferential strains in the steel ring of the retrofit collar. Data were collected at 1-second intervals during testing.

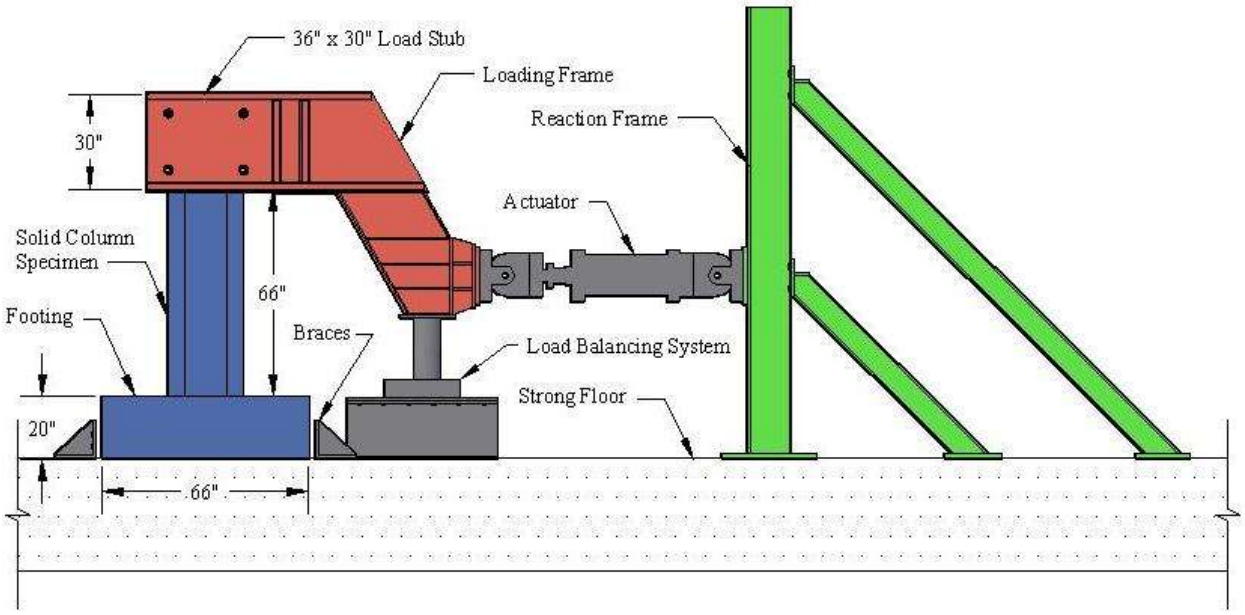

Figure 14 – Test Setup for the Solid Columns (1 in. = 25.4 mm)

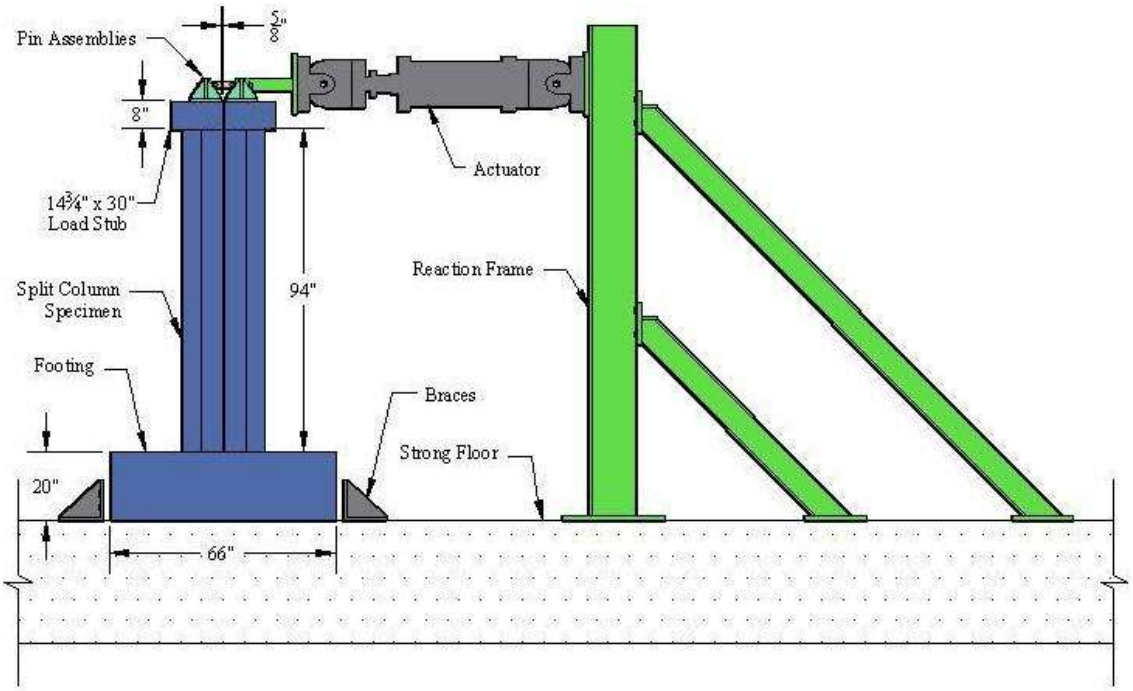

Figure 15 – Test Setup for the Split Columns (1 in. = 25.4 mm)

TEST RESULTS AND DISCUSSION

This section presents the experimental results from cyclic tests of seven 1/3-scale cruciform-shaped columns. Discussion of the test results for the as-built solid columns is provided first, followed by discussion of the test results for the retrofitted solid columns and a comparison of the as-built and retrofitted column results. Discussion of the test results for the retrofitted split columns is then presented. Column performance is assessed with respect to the overall hysteretic behavior, shear strength, failure mode and any observable characteristics such as crack patterns. Other aspects considered for the case of the as-built columns are the lateral tie strains and longitudinal bar strains at the top and bottom of the column. For the retrofitted columns, in addition to the above aspects, FRP jacket strains corresponding to the shear and confinement effects are also considered.

AS-BUILT SOLID COLUMNS

Columns 1 and 5 were designed to be representative of typical as-built conditions in the solid columns of Bent 13 of the Aurora Avenue Bridge. Based on predictions of column performance prior to testing, an initially stable flexural response followed by shear failure with limited ductility was expected. The performance of as-built columns was intended to reveal the vulnerabilities in the existing columns and to establish benchmarks for evaluating the effectiveness of the applied retrofit measures.

Column 1

Figure 16 shows the overall hysteretic performance of Column 1 in terms of the lateral force vs. actuator displacement. The displacements shown in the figure include unintentional displacements due to gaps between the steel pipes cast into the load stub and the steel loading rods

used to connect the loading frame. These gaps were intended to provide construction tolerances for placing the loading rods, but also resulted in flat spots in the hysteresis curves. i.e., displacements under zero lateral force. These unintended displacements were later removed from the data for the purpose of comparing results with other tests. Shims between the steel pipes in the load stub and the loading pins were also installed in later tests to minimize these unintended displacements.

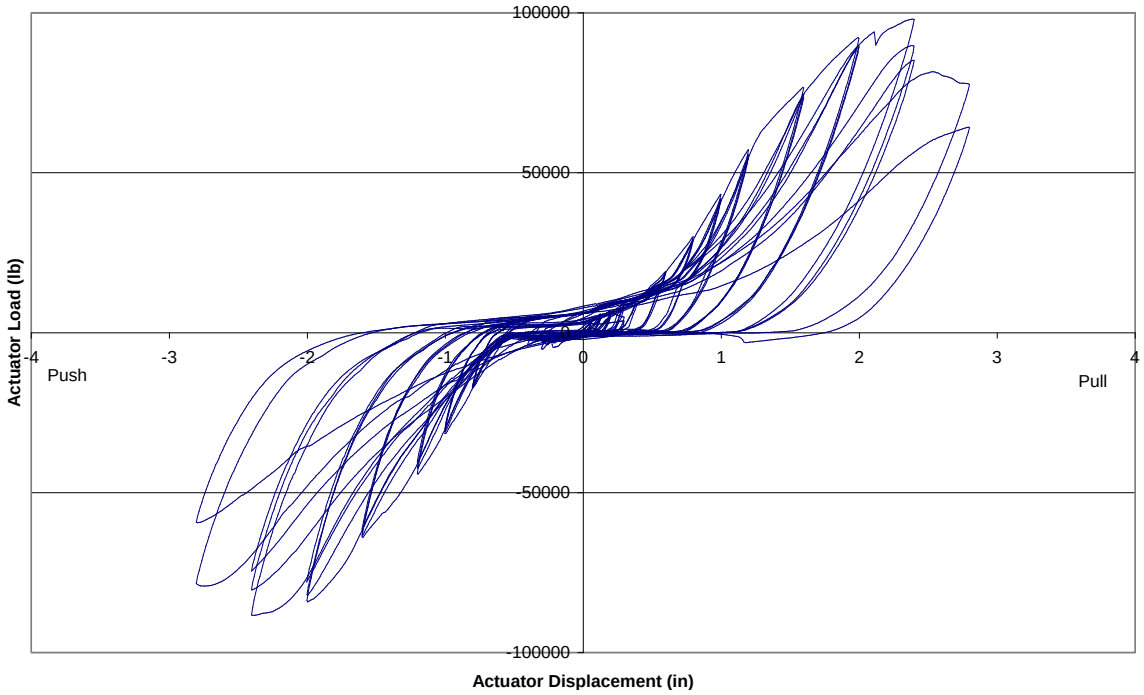

Figure 16 – Column 1 Lateral Load vs. Displacement Hysteresis Curves (1 kip = 4.45 kN, 1 in. = 25.4 mm)

Column 1 exhibited moderate energy dissipation capacity but little ductility. The stiffness of the column showed minor degradation up to a displacement level of 1.2 in. (30 mm), with a loss in stiffness at later displacement levels up to the peak load. The peak lateral load achieved was 98 kips and occurred at a lateral displacement of 2.4 in. (61 mm). The column exhibited a significant decrease in lateral stiffness and strength at a displacement level of 2.8 in. (71 mm), and the applied

load dropped below 80% of the peak load during the first cycle at this displacement. The test was stopped after the second cycle at a displacement level of 2.8 in. (71 mm).

Figure 17 shows Column 1 at the beginning of the test. Yielding of the longitudinal bars first occurred at lateral force level of 27 kips (120 kN) followed by flexural cracking at the top and bottom of the column. Early shear cracks formed at a lateral force level of about 65 kips (290 kN). Yielding of the transverse reinforcement first occurred at a lateral force level of 88 kips (390 kN) followed by the opening of large shear cracks near the end of the test. The final failure mode for the column was a shear failure. Figure 18 shows the large shear cracks present near the end of testing.

Figure 19 shows transverse tie strains with time alongside a plot of the column load with time. Very small tie strains were observed up to a displacement level of 1.6 in. (41 mm). During the first cycle at a displacement level of 1.6 in. (41 mm), the peak lateral force achieved was 65 kips (290 kN) and the first shear cracks appeared in the column. Strain gage 2, located slightly above the column mid-height, recorded strain values near yielding. Very large tie strains were observed beyond the third cycle at a displacement of 2.4 in. (61 mm), corresponding to the opening of large shear cracks in the column.

Figures 20 and 21 show the strains in the longitudinal bars at the top and bottom of the column, respectively. Approximately a linear strain profile was observed in the top strain gages up to the first yield at a displacement level of 1.6 in. (41 mm). Very large strains in excess of 15,000 με were observed during cycling at a displacement level of 2.4 in. (61 mm), Strains in the bottom strain gages reached first yield at a displacement level of about 0.8 in. (20 mm). Strains stayed nearly constant up to a displacement level of 1.6 in. (41 mm) and then increased rapidly to strains in excess of 5,000 με for the remainder of the test.

Figure 17 – Column 1 Test Setup

Figure 18 – Column 1 Shear Cracking Near the End of Testing

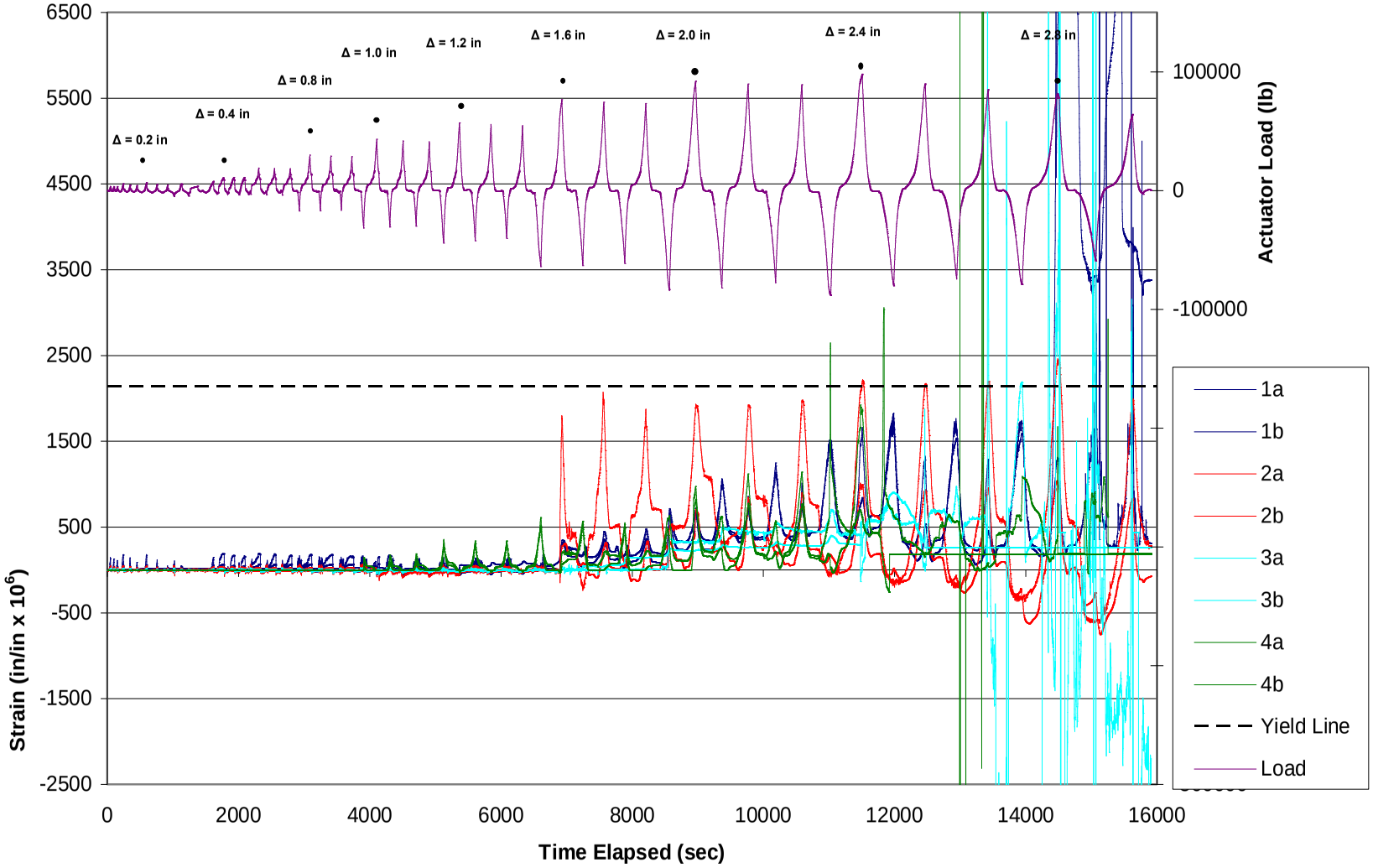

Figure 19 – Column 1 Transverse Strain Gage Data (1 kip = 4.45 kN, 1 in. = 25.4 mm)

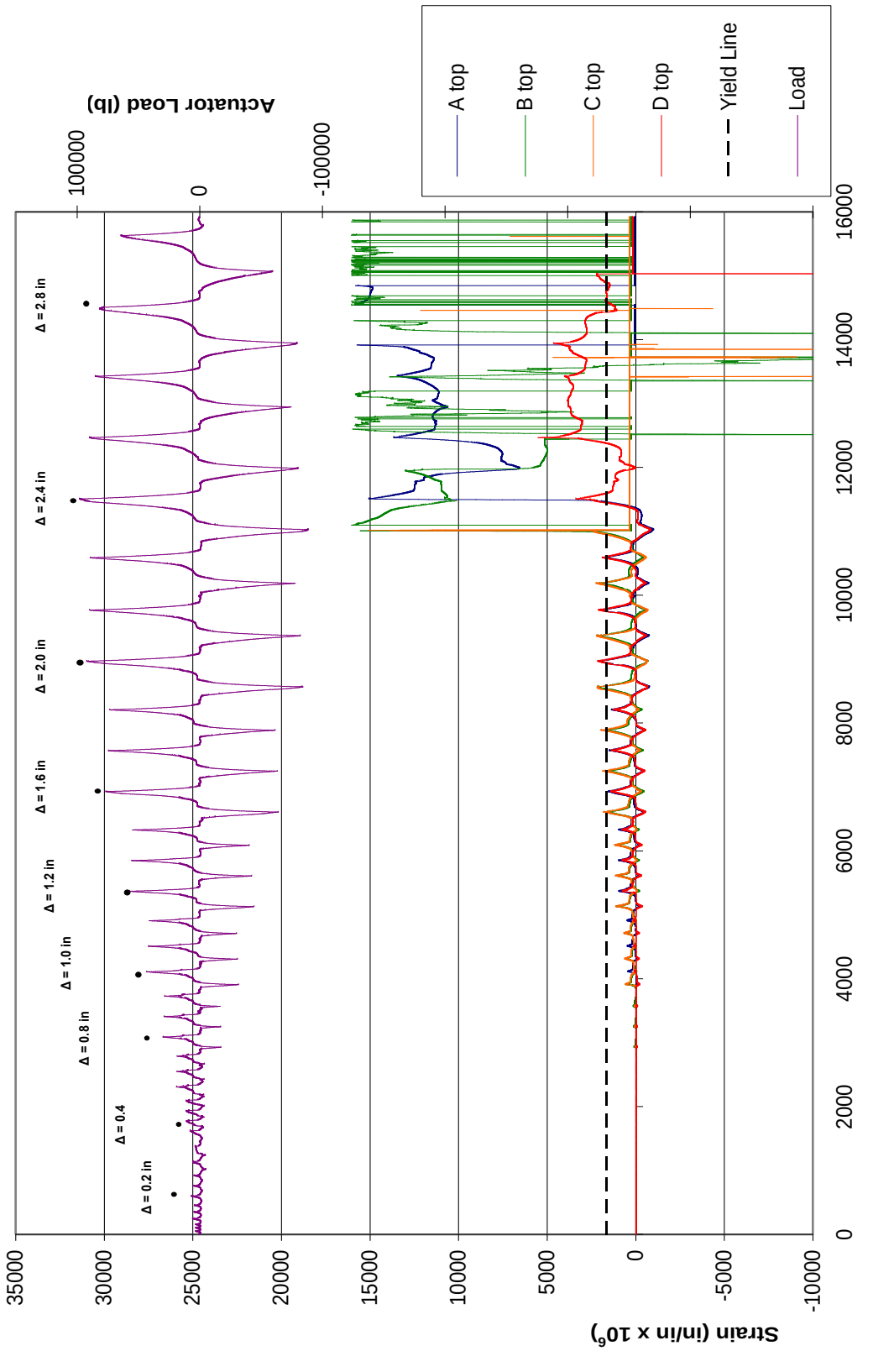

Figure 20 – Column 1 Longitudinal Bar Strain Gage Data at the Top of the Column (1 kip = 4.45 kN, 1 in. = 25.4 mm)

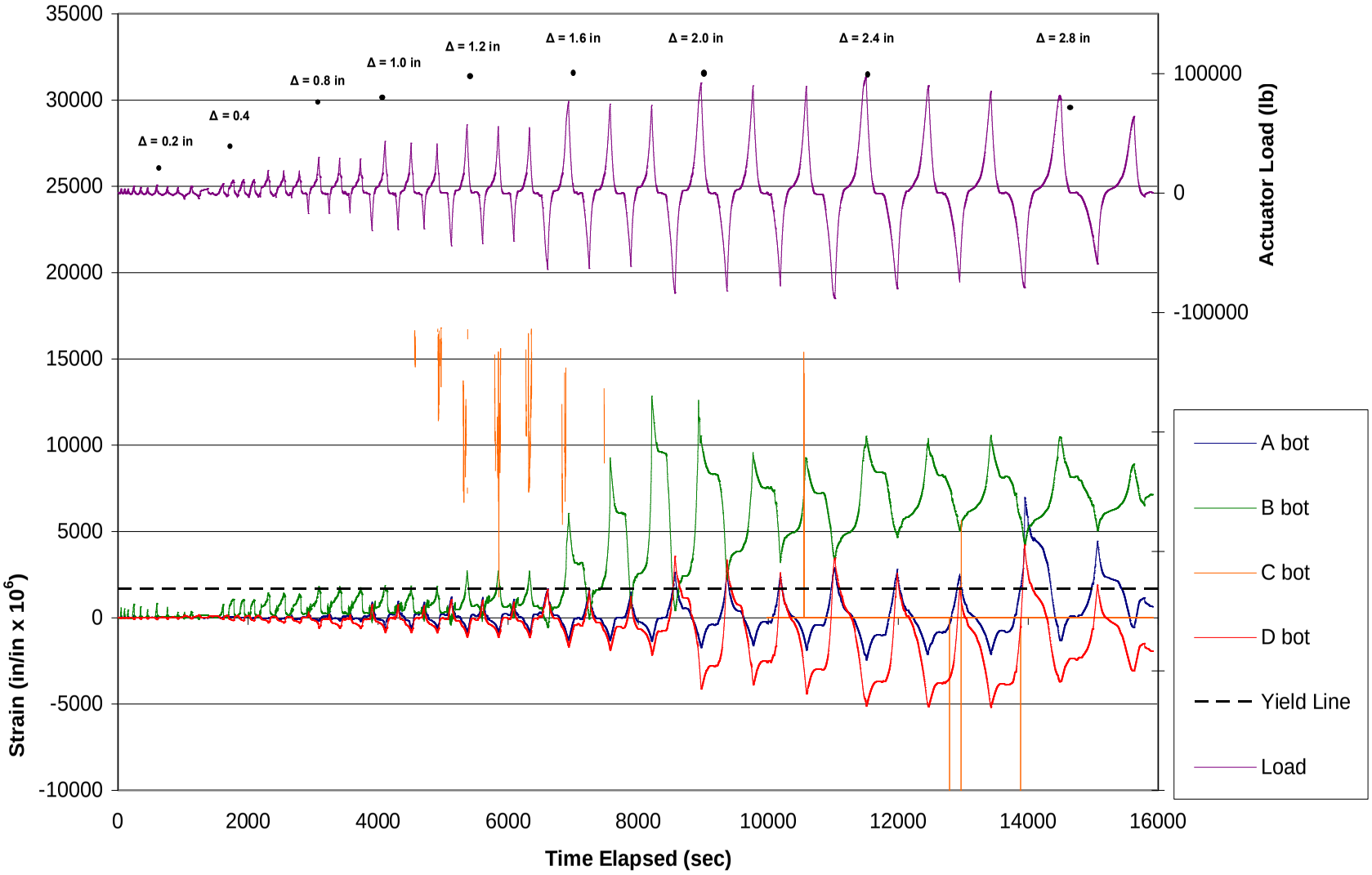

Figure 21 – Column 1 Longitudinal Bar Strain Gage Data at the Bottom of the Column (1 kip = 4.45 kN, 1 in. = 25.4 mm)

Column 5

Column 5 was identical to Column 1 except that shims were installed between the column top block and the loading frame to remove unintended actuator deflection and rotation. The purpose of this test was to determine if the presence of shims would impact the flexural response of the column as well as to provide a measure of the consistency in results from two nominally identical column specimens.

Figure 22 shows the overall hysteretic performance of Column 5 in terms of the lateral force vs. actuator displacement. The column exhibited moderate energy dissipation capacity but little ductility. The stiffness of the column showed minor degradation up to a displacement level of 1.2 in. (30 mm), followed by a loss in stiffness at later displacement levels up to the peak load. The peak lateral load achieved was 102 kips (453 kN) and occurred at a lateral displacement of 2.0 in. (51 mm). The column exhibited a significant decrease in lateral stiffness and strength at a displacement level of 2.0 in. (51 mm), and the applied load dropped below 80% of the peak load during the third cycle at this displacement. The test was stopped after the third cycle at a displacement level of 2.4 in. (61 mm).

Yielding of the longitudinal bars in Column 5 first occurred at a lateral force level of 49 kips (218 kN) followed by flexural cracking at the top and bottom of the column. Early shear cracks formed at a lateral force level of about 73 kips (325 kN). Yielding of the transverse reinforcement first occurred at a lateral force level of 93 kips (414 kN) followed by the opening of large shear cracks near the end of the test. The final failure mode for the column was a shear failure. Figure 23 shows the large shear cracks present near the end of testing.

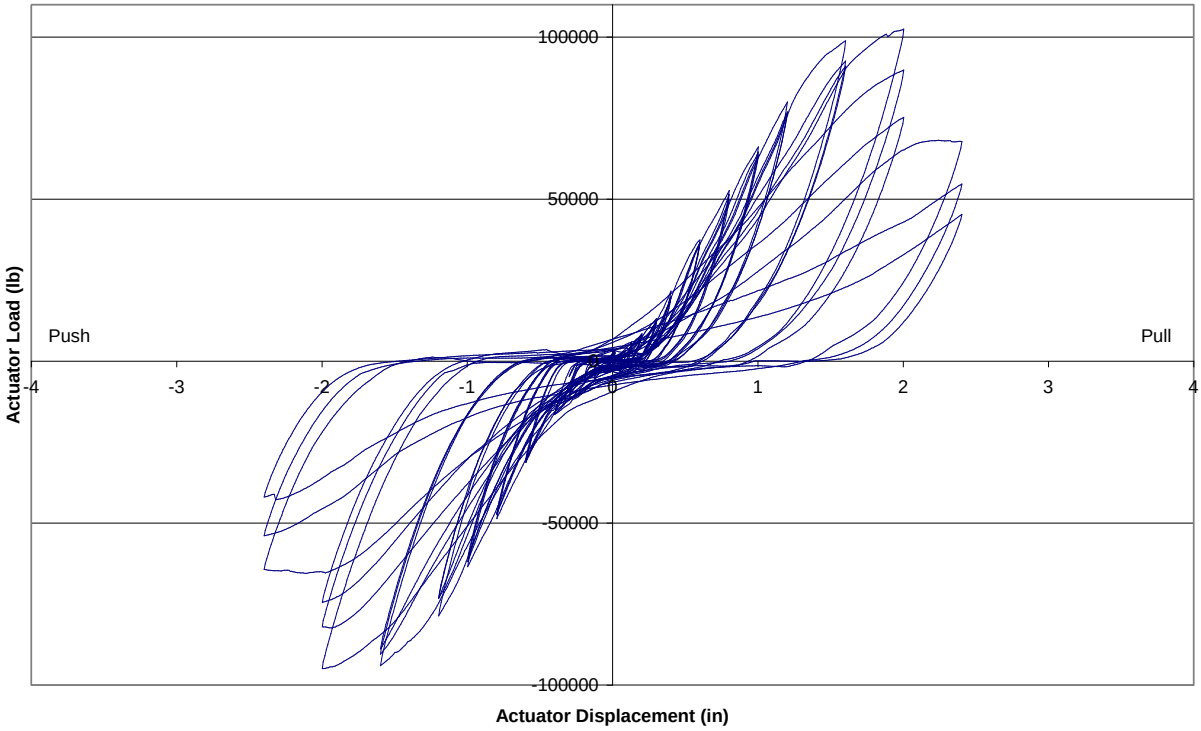

Figure 22 – Column 5 Lateral Load vs. Displacement Hysteresis Curves (1 kip = 4.45 kN, 1 in. = 25.4 mm)

Figure 23 – Column 5 Shear Cracking Near the End of Testing

Figure 24 shows transverse tie strains with time alongside a plot of the column load with time. Almost negligible tie strains were observed up to a displacement level of 1.2 in. (30 mm). Tie strains increased linearly up to the yield point at a displacement level of 2.0 in. (51 mm) and then decreased linearly until the end of the test.

Figures 25 and 26 show the strains in the longitudinal bars at the top and bottom of the column, respectively. A linear strain profile was observed in the top strain gages up to the first yield at a displacement level of 1.0 in. (25 mm). Strains stayed nearly constant until the first cycle at a displacement level of 1.6 in. (41 mm), after which very large strains in excess of 15,000 με were observed. Strains in the bottom strain gages reached first yield at a displacement level of about 0.8 in. (20 mm). Strains stayed nearly constant up to a displacement level of 1.2 in. (30 mm) and then increased rapidly to strains in excess of 10,000 με for the remainder of the test.

Summary of As-Built Solid Column Performance

Tests on Columns 1 and 5 representing as-built conditions resulted in shear failures at a displacement level of approximately 2.0 in. (61 mm), accompanied with severe strength, stiffness and physical degradation. The as-built columns achieved an average peak shear load of approximately 100 kips, about 16% higher than the shear force corresponding to the theoretical ideal flexural strength of the columns. The overall response of the two columns was similar with early shear cracks forming at a lateral force level of approximately 70 kips (311 kN) followed by flexural cracks forming at the top and bottom of the column. Yielding of the transverse reinforcement occurred at a lateral force level of approximately 90 kips (400 kN) followed by the opening of large shear cracks. The final failure mode for both columns was a shear failure with little ductility.

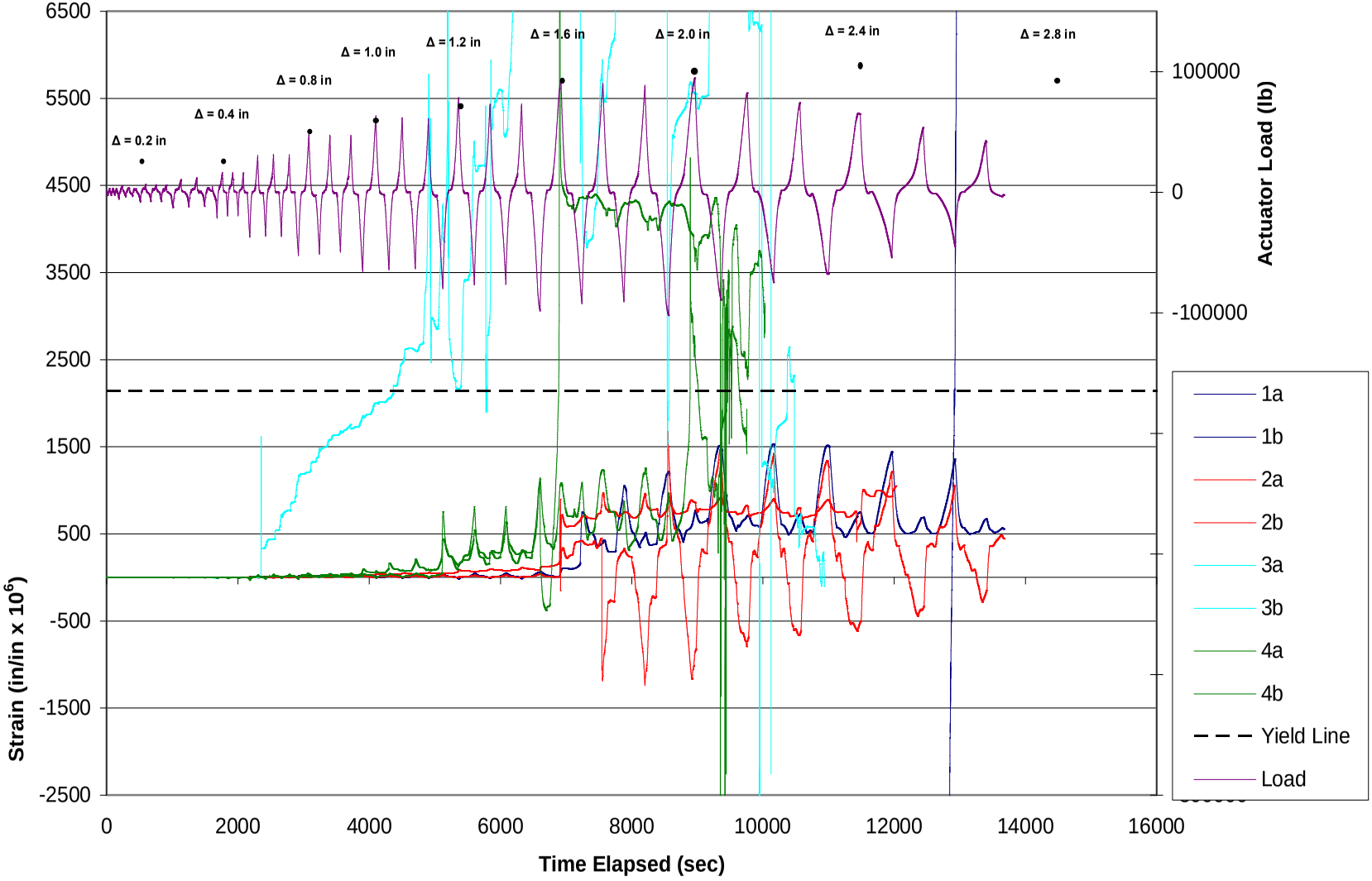

Figure 24 - Column 5 Transverse Strain Gage Data (1 kip = 4.45 kN, 1 in. = 25.4 mm)

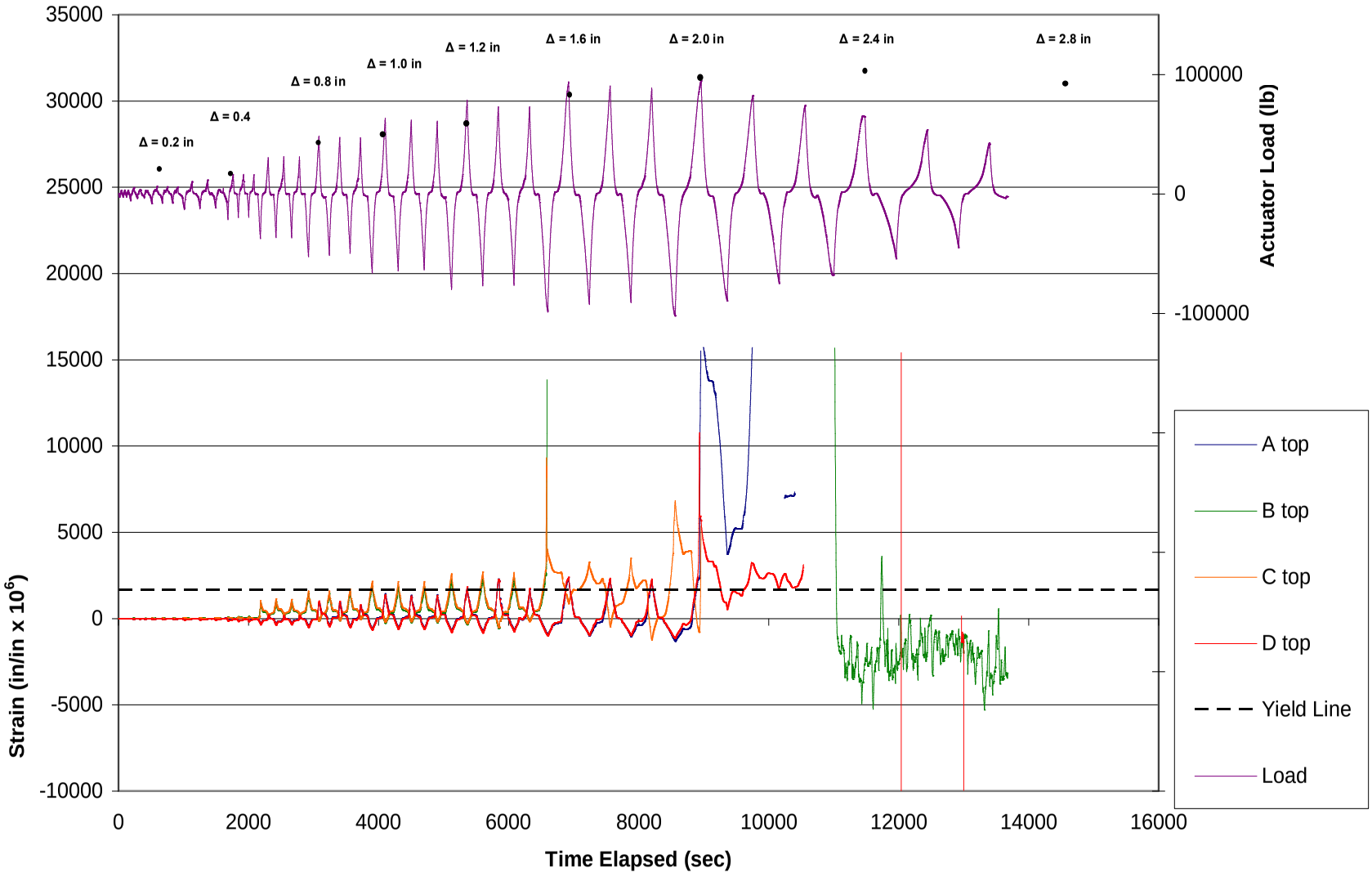

Figure 25 – Column 5 Longitudinal Bar Strain Gage Data at the Top of the Column (1 kip = 4.45 kN, 1 in. = 25.4 mm)

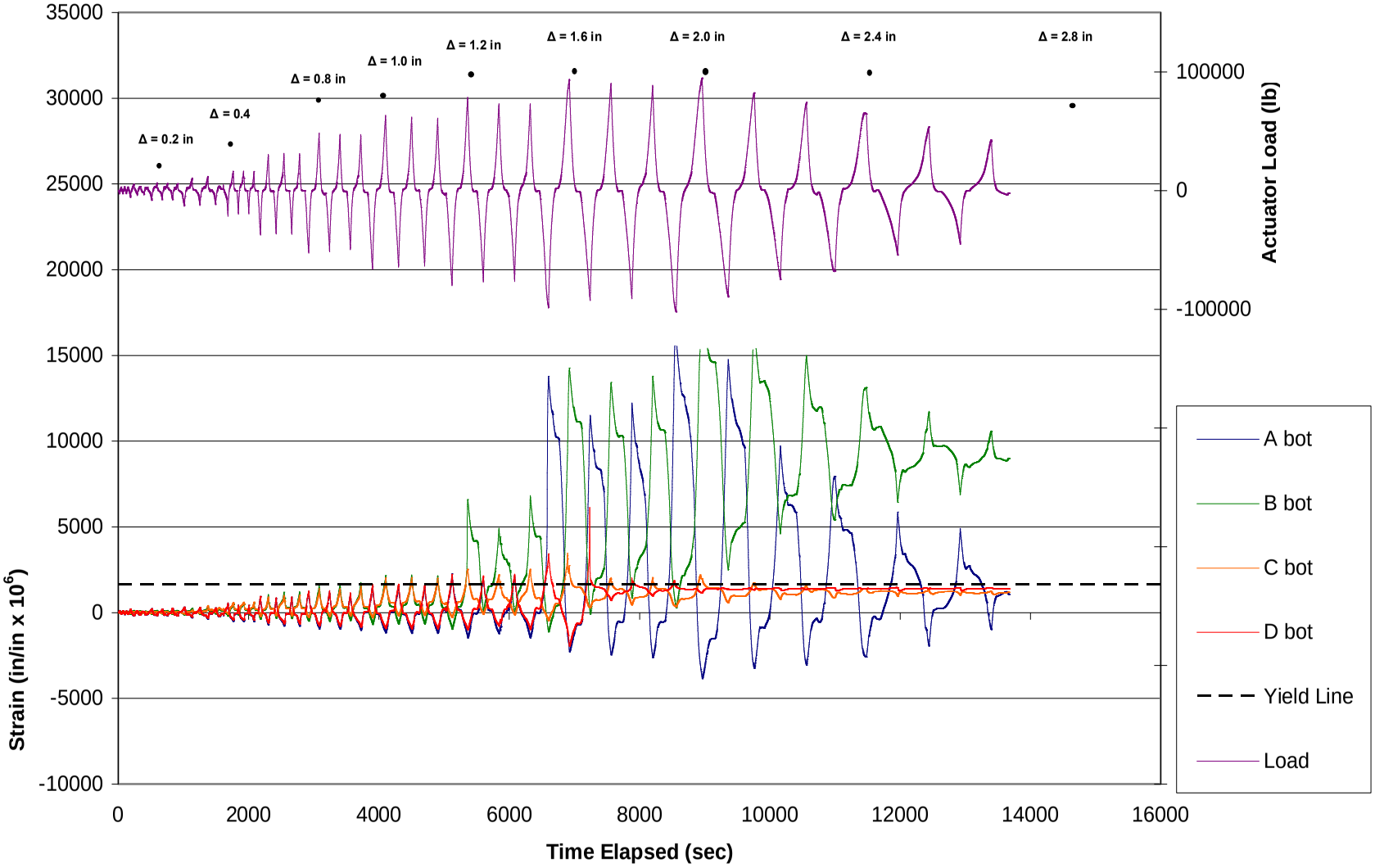

Figure 26 – Column 5 Longitudinal Bar Strain Gage Data at the Bottom of the Column (1 kip = 4.45 kN, 1 in. = 25.4 mm)

RETROFITTED SOLID COLUMNS

Columns 2, 3 and 4 were identical to the as-built Columns 1 and 5 except that they were retrofitted with an FRP jacket. Column 2 was tested without reentrant corner anchorage to evaluate whether such anchorage was necessary to achieve the required strength from the FRP jacket. Reentrant corner anchorage was provided for Columns 3 and 4 using two different anchorage methods. Column 4 also contained steel retrofit collars at the top and bottom of the column.

Column 2

Figure 27 shows the overall hysteretic performance of Column 2 in terms of the lateral force vs. actuator displacement. The column exhibited slightly improved energy dissipation capacity and ductility as compared with those for the as-built columns. The peak lateral load achieved was 101 kips (450 kN) and occurred at a lateral displacement of 2.0 in. (51 mm). The flexural response of the column remained stable through three cycles at a displacement level of 2.0 in. (51 mm), with only a minor degradation in stiffness. However, the column underwent a significant decrease in lateral stiffness and strength while cycling at a displacement level of 2.4 in. (61 mm), and the applied load dropped below 80% of the peak load during the second cycle at this displacement. The test was stopped after completing the first cycle at a displacement level of 2.8 in. (71 mm).

Yielding of the longitudinal bars in Column 2 first occurred at a lateral force level of 48 kips (214 kN) followed by flexural cracking at the top and bottom of the column. No shear distress was observed in the column up to the peak lateral load of 101 kips (450 kN). After cycling several times near 100 kips (450 kN), the FRP jacket began to pull away from the

reentrant corners at the top and bottom of the column, most noticeably at the top. With continued cycling, the pullout of the FRP began to extend down the column, resulting in a significant decrease in the peak lateral load. Figure 28 shows the pullout of the FRP jacket from the reentrant corners. Yielding of the transverse reinforcement first occurred at a lateral force level of 88 kips (390 kN) during the second cycle at a displacement level of 2.0 in. (51 mm). After removing the FRP jacket at the end of testing, it was evident that the final failure mode for the column was a shear failure. Inspection of the specimen after testing showed that the pullout of FRP from the reentrant corners was likely due to spalling of the cover concrete from flexural hinging rather than debonding of the FRP jacket from the concrete.

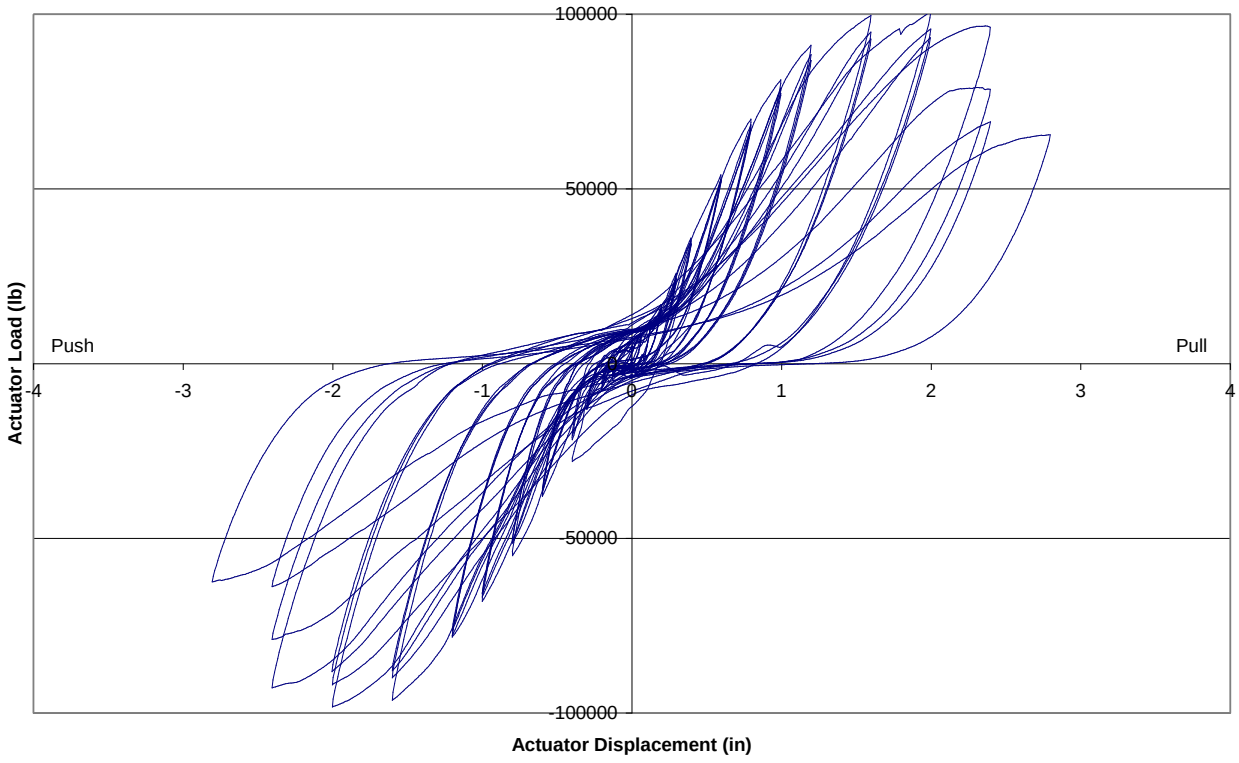

Figure 27 – Column 2 Lateral Load vs. Displacement Hysteresis Curves (1 kip = 4.45 kN, 1 in. = 25.4 mm)

Figure 28 – Column 2 Pullout of FRP Jacket from Reentrant Corners

Figure 29 shows a plot of the transverse tie strains with time. Almost negligible tie strains were observed up to a displacement level of 0.8 in. (20 mm). A linear strain profile was then observed up to the first yield of the transverse reinforcement during the second cycle at a displacement level of 2.0 in. (51 mm). Very large tie strains were observed during further testing as the FRP jacket pulled away from the reentrant corners.

Figures 30 and 31 show the strains in the longitudinal bars at the top and bottom of the column, respectively. A linear strain profile was observed in the top strain gages up to the first yield at a displacement level of 1.0 in. (25 mm). After yielding, strains stayed nearly constant until the first cycle at a displacement level of 1.6 in. (41 mm), after which very large strains in excess of 15,000 με were observed. Strains in the bottom strain gages reached first yield at a displacement level of about 0.6 in. (15 mm), much earlier than the top strain gages. Strains stayed nearly constant up to a displacement level of 1.2 in. (30 mm) and then increased rapidly to

strains in excess of 10,000 με until a displacement level of 2.0 in. (51 mm). At a displacement level of 2.0 in. (51 mm), strains dropped significantly as the FRP jacket began to pull away from the reentrant corners.

Figures 32 and 33 show the strains with time for the FRP jacket strain gages parallel and perpendicular to the applied load, respectively. Almost negligible strains were observed in the parallel FRP strain gages up to a displacement level of 0.8 in. (20 mm). A linear strain profile was then observed up to the peak strain value of 2300 με during the first cycle at a displacement level of 2.4 in. (61 mm). Afterwards, strains decreased rapidly as the FRP jacket pulled away from the reentrant corners. All measured strains were well below the FRP jacket ultimate strain capacity of around 19,000 με.

Negligible strains were observed in the perpendicular FRP gages near the top and bottom of the column up to a displacement level of 2.0 in. (51 mm). Strain readings spiked sharply during the first cycle at a displacement level of 2.0 in. (51 mm) at a peak strain of 2600 με corresponding with the beginning of pullout of the FRP jacket from the reentrant corners. Strains decreased with further testing.

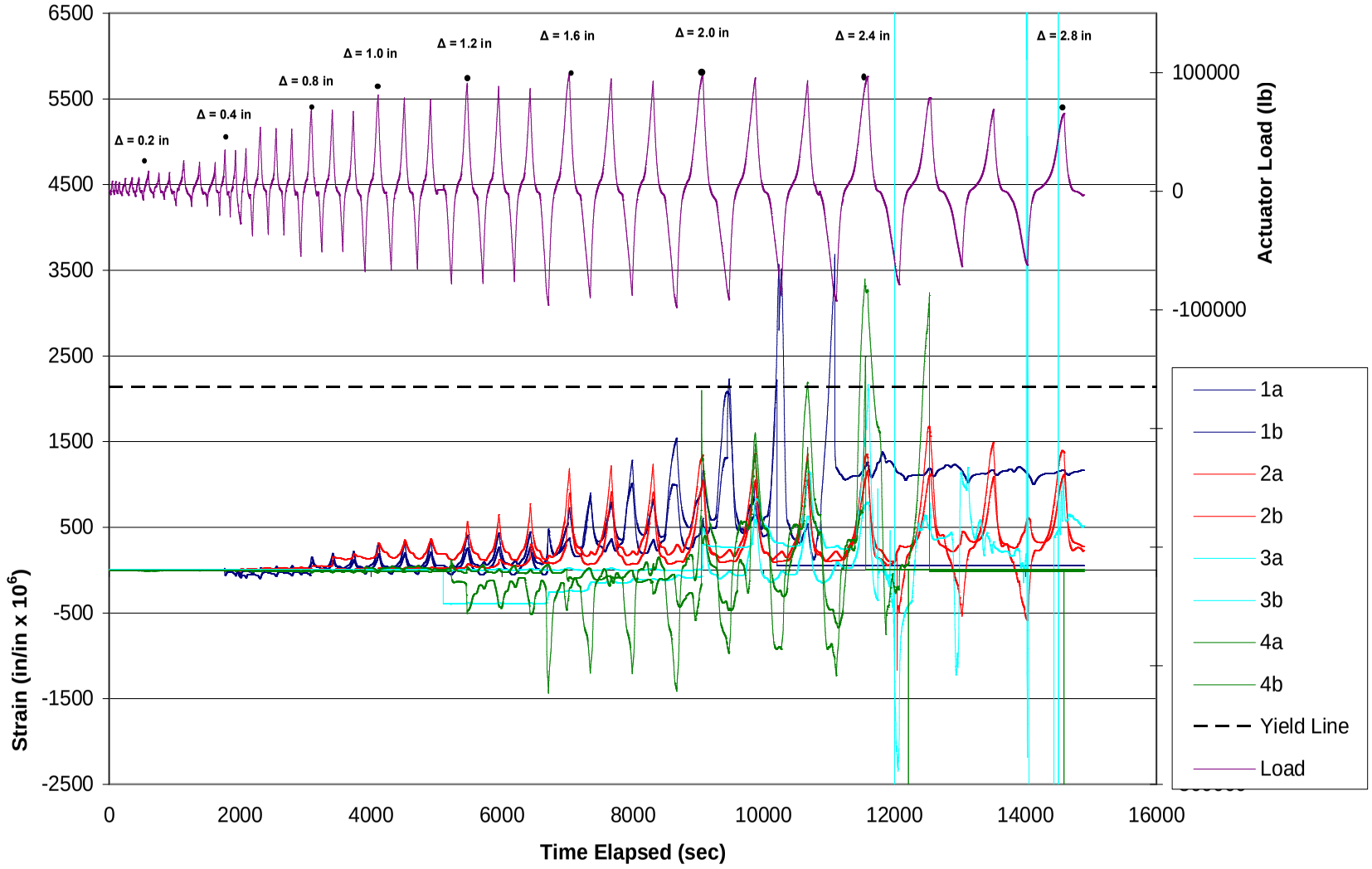

Figure 29 – Column 2 Transverse Strain Gage Data (1 kip = 4.45 kN, 1 in. = 25.4 mm)

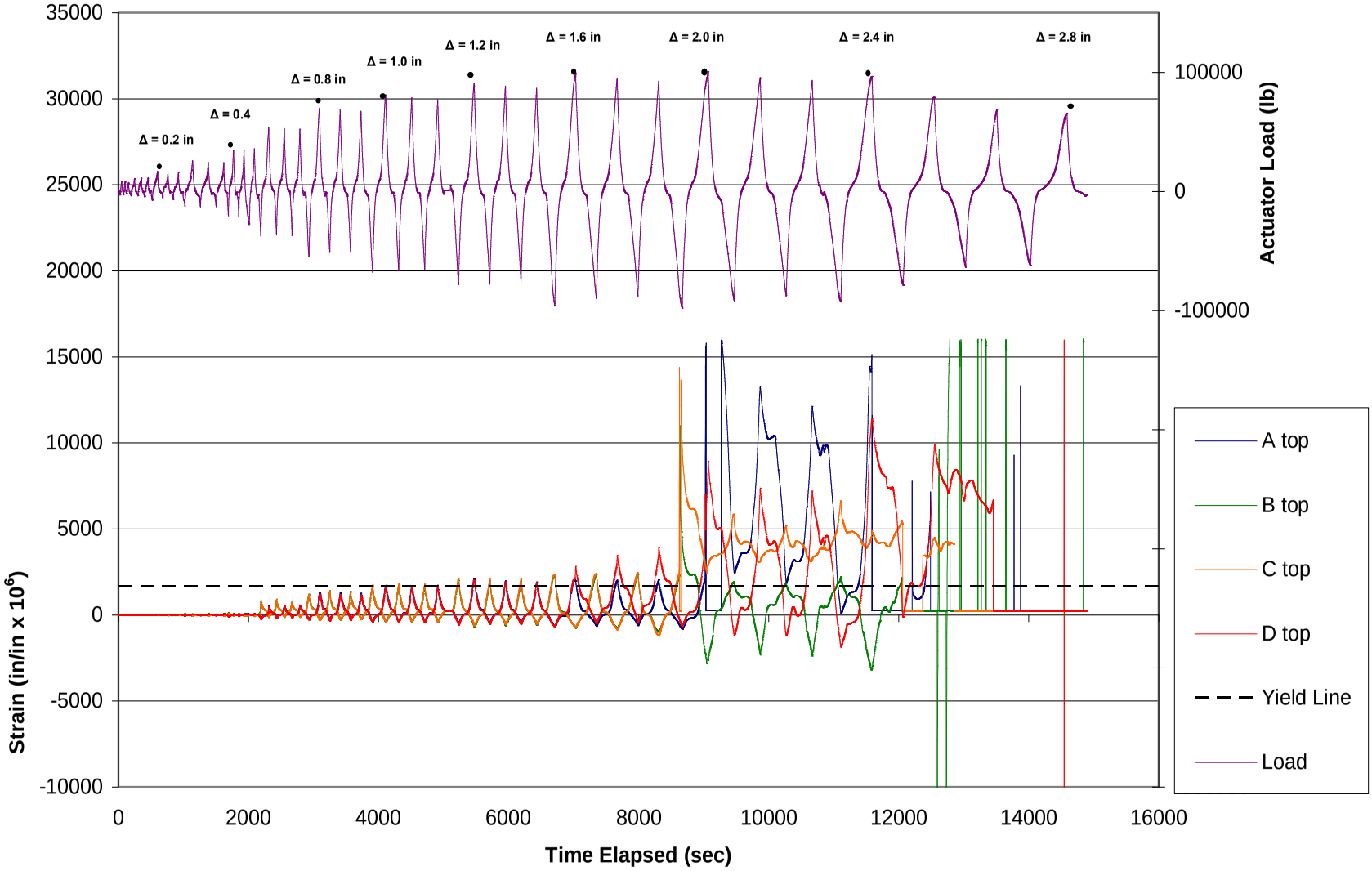

Figure 30 – Column 2 Longitudinal Bar Strain Gage Data at the Top of the Column (1 kip = 4.45 kN, 1 in. = 25.4 mm)

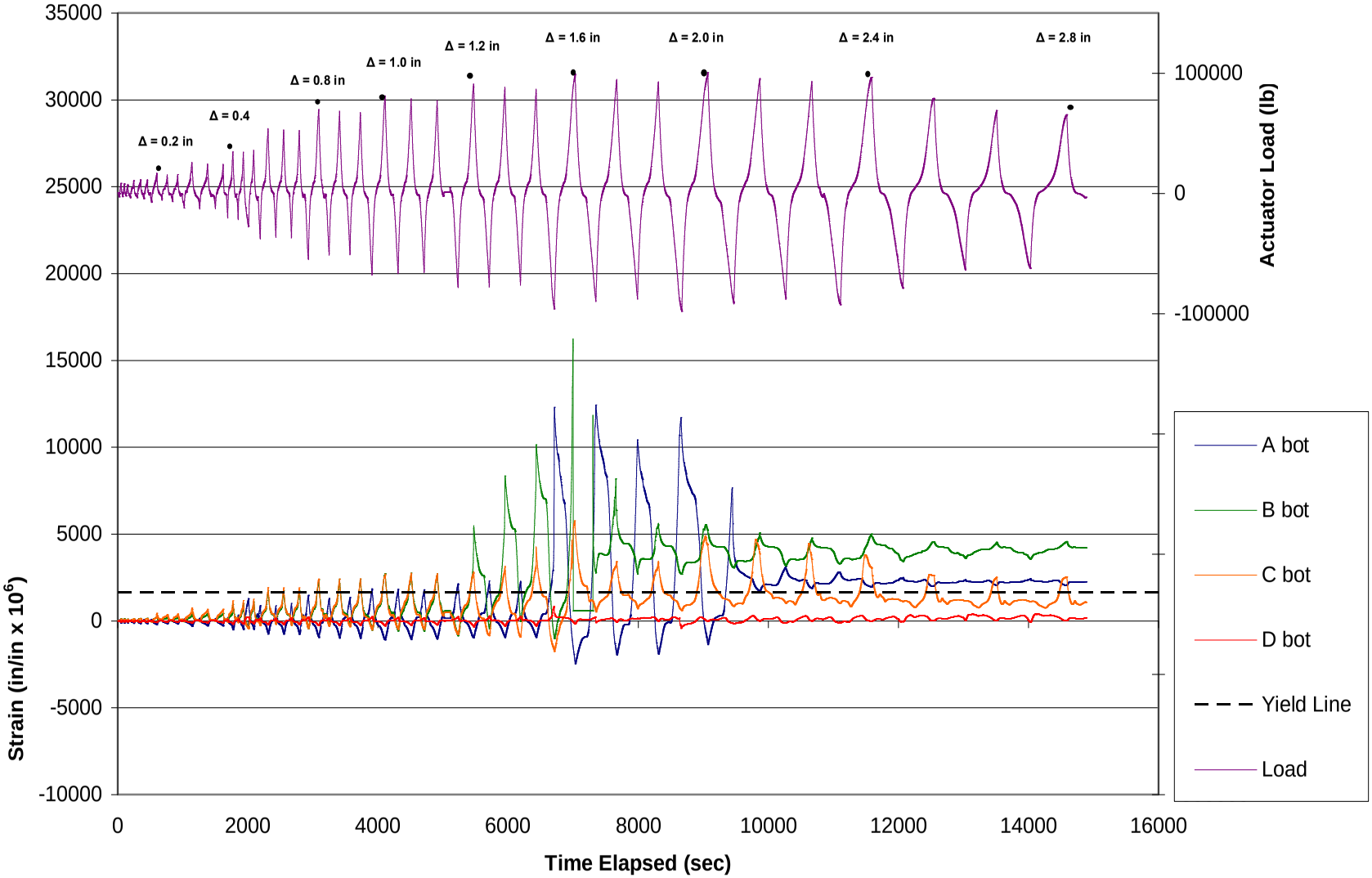

Figure 31 – Column 2 Longitudinal Bar Strain Gage Data at the Bottom of the Column (1 kip = 4.45 kN, 1 in. = 25.4 mm)

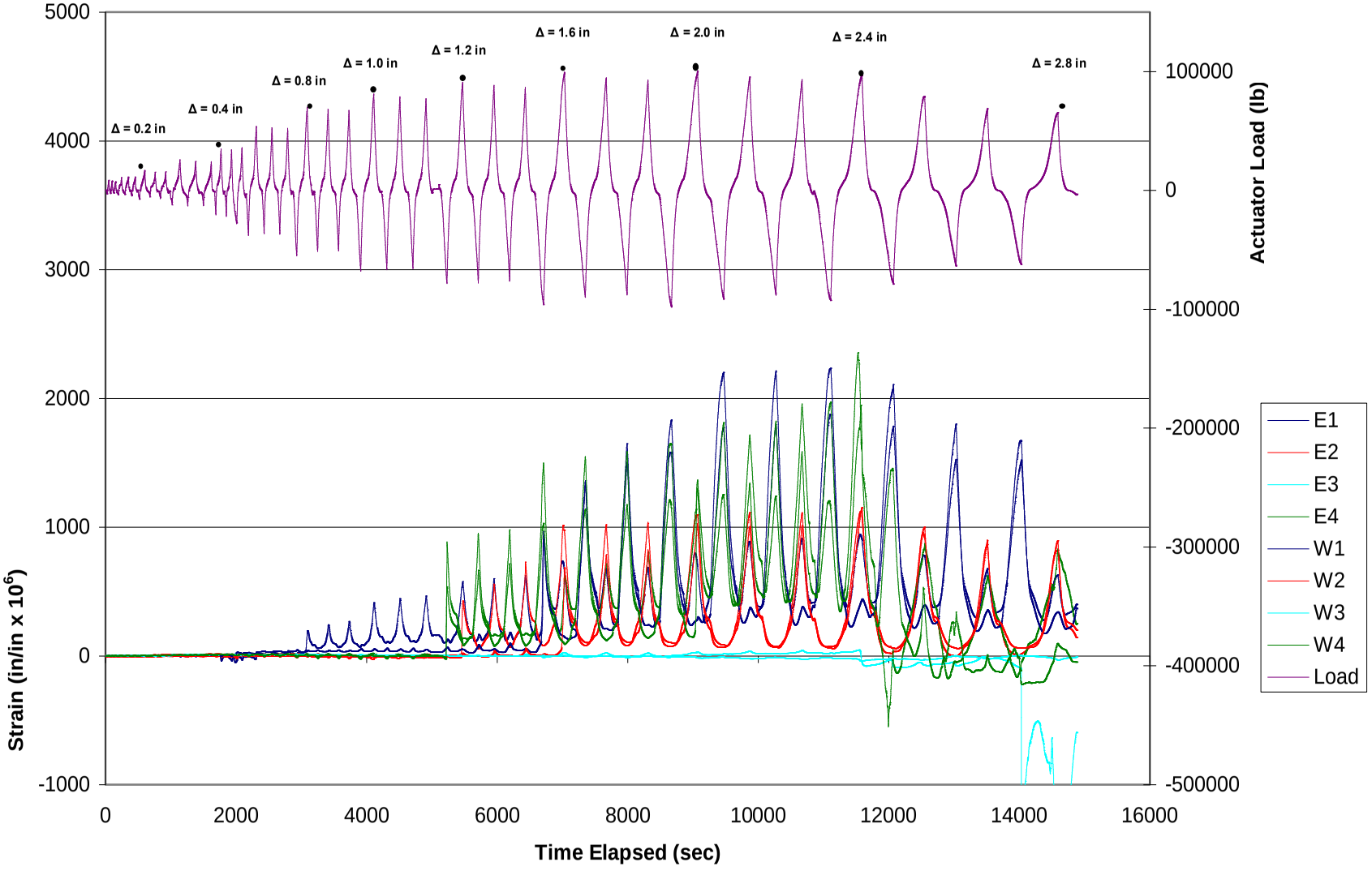

Figure 32 – Column 2 Parallel FRP Jacket Strain Gage Data (1 kip = 4.45 kN, 1 in. = 25.4 mm)

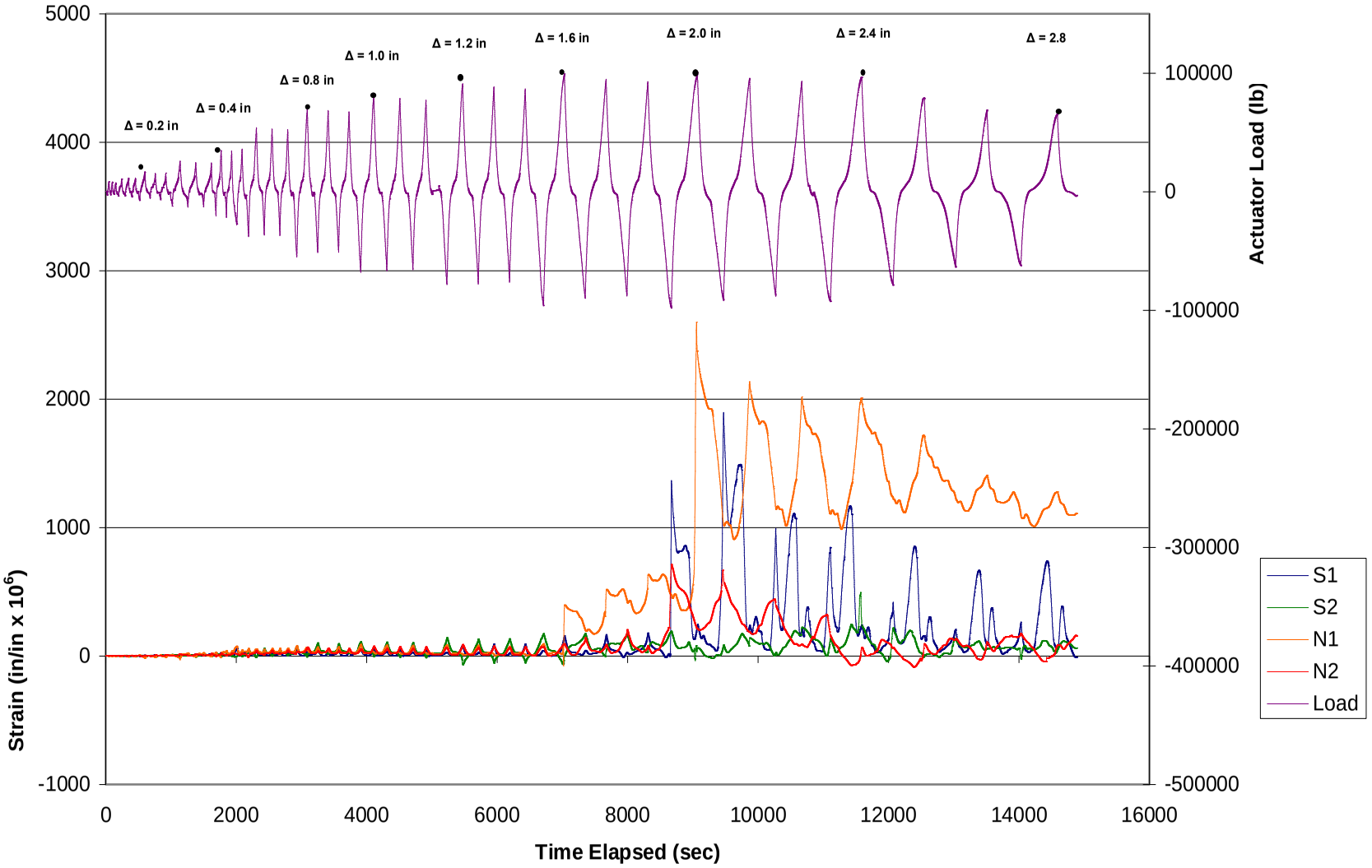

Figure 33 – Column 2 Perpendicular FRP Jacket Strain Gage Data (1 kip = 4.45 kN, 1 in. = 25.4 mm)

Column 3

Column 3 was identical to Column 2 except that the FRP jacket was anchored in the reentrant corners of the column with steel bent plates and epoxy anchors installed over the full-height of the column. The reentrant corner anchorage was designed to develop the full strength of the FRP jacket and thus prevent the column from failing in shear.

Figure 34 shows the overall hysteretic performance of Column 3 in terms of the lateral force vs. actuator displacement. The FRP jacket with reentrant corner anchorage exhibited a significant improvement in the overall seismic performance from the as-built columns. The peak lateral load achieved was 105 kips (470 kN) and occurred at a lateral displacement of 2.4 in. (61 mm). The flexural response of the column remained stable through three cycles at a displacement level of 2.4 in. (61 mm), with only minor degradation in stiffness. The column underwent a decrease in lateral stiffness and strength while cycling at a displacement level of 2.8 in. (71 mm), and the applied load dropped below 80% of the peak load during the third cycle at this displacement. The test was stopped after completing the first cycle at a displacement level of 3.2 in. (81 mm).

Figure 35 shows Column 3 at the beginning of the test. The response of the column was nearly identical to that of Column 2 through the early part of testing, with yielding of the longitudinal bars first occurring at a lateral force level of 50 kips (220 kN) followed by flexural cracking at the top and bottom of the column. Yielding of the transverse reinforcement first occurred at a lateral force level of 100 kips (445 kN) during the first cycle at a displacement level of 2.0 in. (51 mm). While cycling at a displacement level of 2.8 in. (71 mm), bulging began in the plastic hinge regions at the top and bottom of the column, although more pronounced at the top. With continued cycling, the bulging increased, resulting in a decrease in the peak lateral

loads. Figure 36 shows the bulging of the FRP jacket at the top of the column. During the first cycle at a displacement level of 3.2 in. (81 mm), the epoxy anchors at the top of the column failed and the load displacement curve peaked before reaching a lateral displacement of 3.2 in. (81 mm), producing failure in the column. No shear distress was observed in the column throughout the test, and the final failure mechanism was development of plastic hinges at the top and bottom of the column. The failure of the epoxy anchors at the top of the column near the end of testing was likely due to crushing and degradation of the concrete under the FRP jacket in the plastic hinge region.

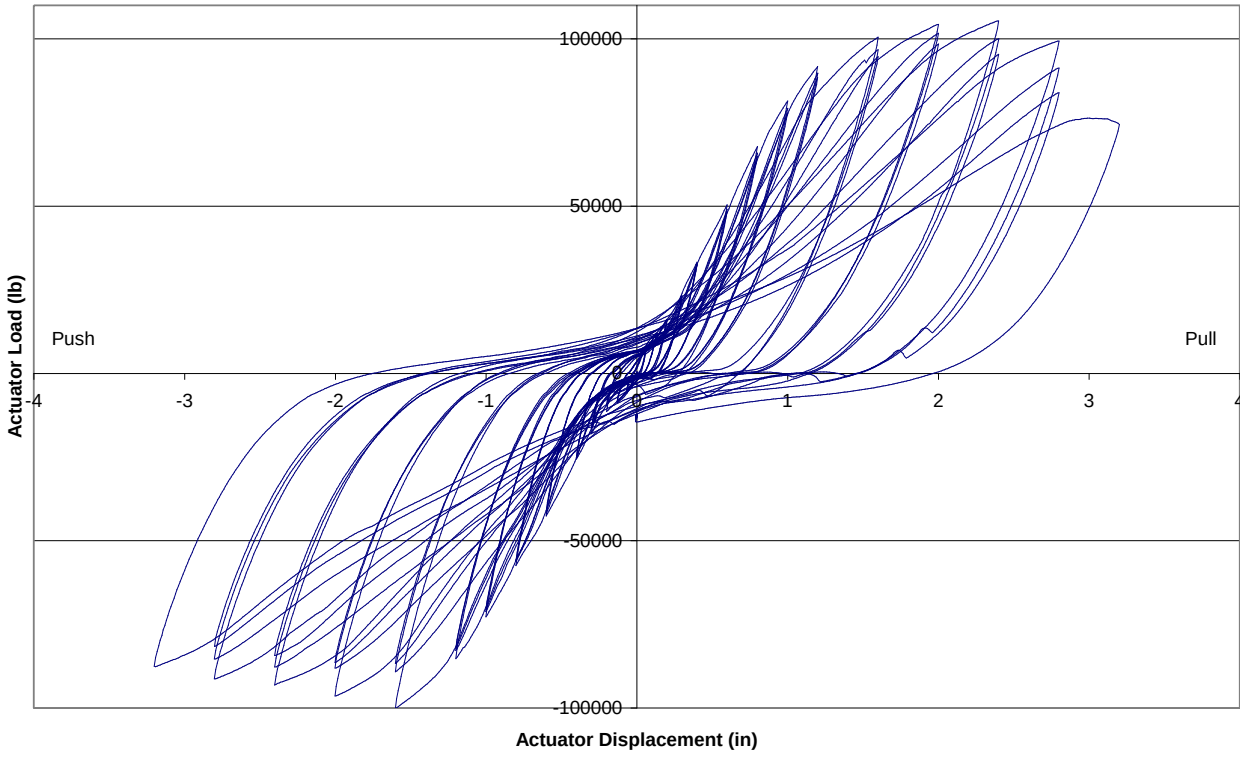

Figure 34 – Column 3 Lateral Load vs. Displacement Hysteresis Curves (1 kip = 4.45 kN, 1 in. = 25.4 mm)

Figure 35 – Column 3 Test Setup

Figure 36 – Column 3 Bulging of FRP Jacket at the Top of the Column

Figure 37 shows a plot of the transverse tie strains with time. Almost negligible tie strains were observed up to a displacement level of 1.0 in. (25 mm). First yield of the transverse reinforcement occurred during the first cycle at a displacement level of 2.0 in. (51 mm). The observed tie strains were nearly constant for the remainder of the test.

Figures 38 and 39 show the strains in the longitudinal bars at the top and bottom of the column, respectively. A linear strain profile was observed in the top strain gages up to the first yield at a displacement level of 1.0 in. (25 mm). After yielding, strains stayed nearly constant until the first cycle at a displacement level of 1.6 in. (41 mm), after which very large strains in excess of 10,000 με were observed for the remainder of the test. Strains in the bottom strain gages reached first yield at a displacement level of about 0.8 in. (20 mm), much earlier than the top strain gages. Strains increased linearly up to a displacement level of 1.2 in. (30 mm) and then increased rapidly to strains in excess of 10,000 με for the remainder of the test.

Figures 40 and 41 show the strains in the FRP jacket for strain gages parallel and perpendicular to the applied load, respectively. Almost negligible strains were observed in the parallel FRP strain gages up to a displacement level of 0.8 in. (20 mm). A linear strain profile was then observed up to the peak strain value of 2200 με during the second cycle at a displacement level of 2.8 in. (71 mm). Afterwards, strains remained nearly constant for the remainder of the test. All measured strains were well below the FRP jacket ultimate strain capacity of around 19,000 με.

Almost negligible strains were observed in the perpendicular FRP gages near the top and bottom of the column up to a displacement level of 1.6 in. (41 mm). A linear strain profile was then observed for the remainder of the test, with a peak strain of 3900 με being observed at a lateral displacement of 3.2 in. (81 mm).

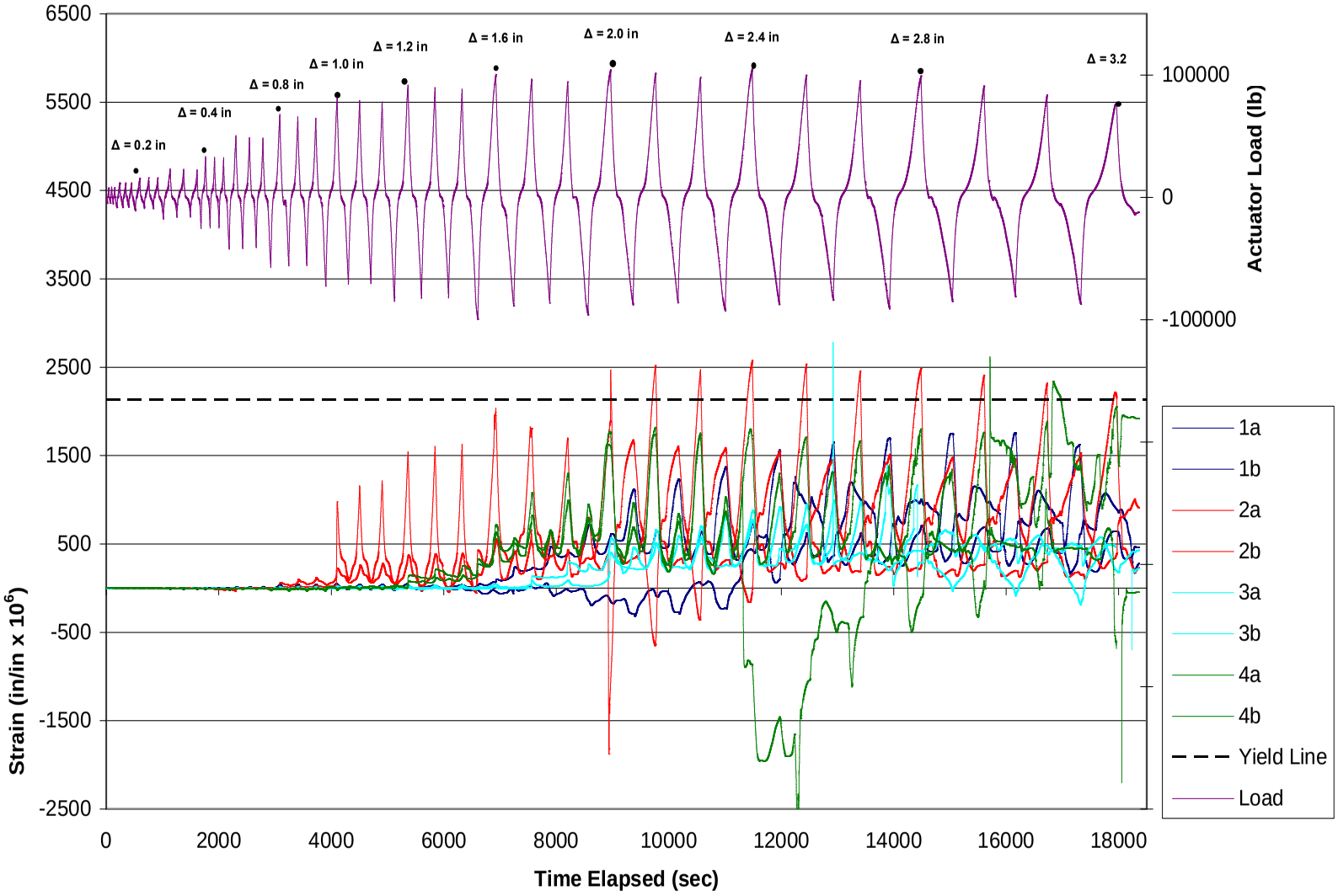

Figure 37– Column 3 Transverse Strain Gage Data (1 kip = 4.45 kN, 1 in. = 25.4 mm)

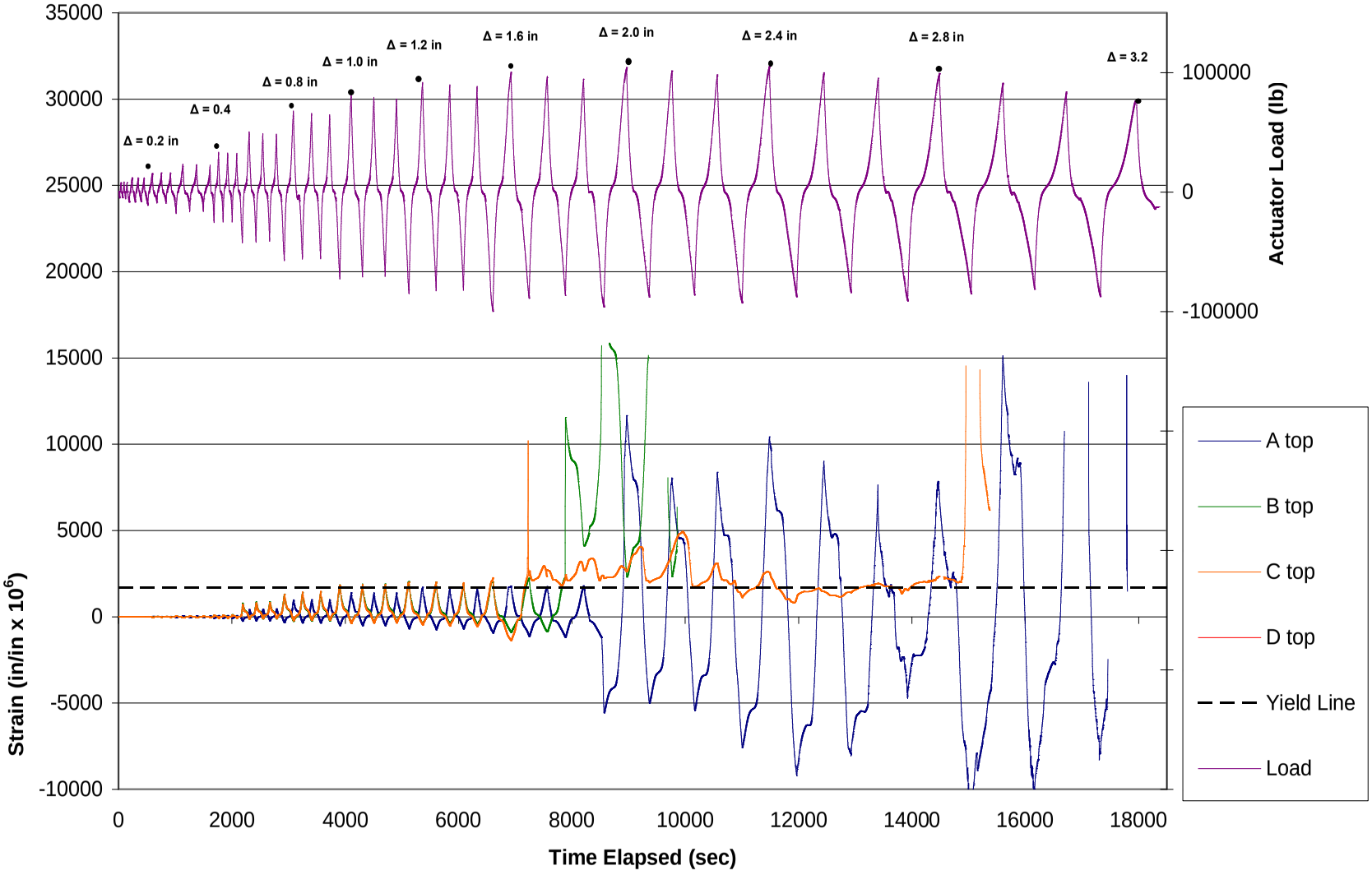

Figure 38 – Column 3 Longitudinal Bar Strain Gage Data at the Top of the Column (1 kip = 4.45 kN, 1 in. = 25.4 mm)

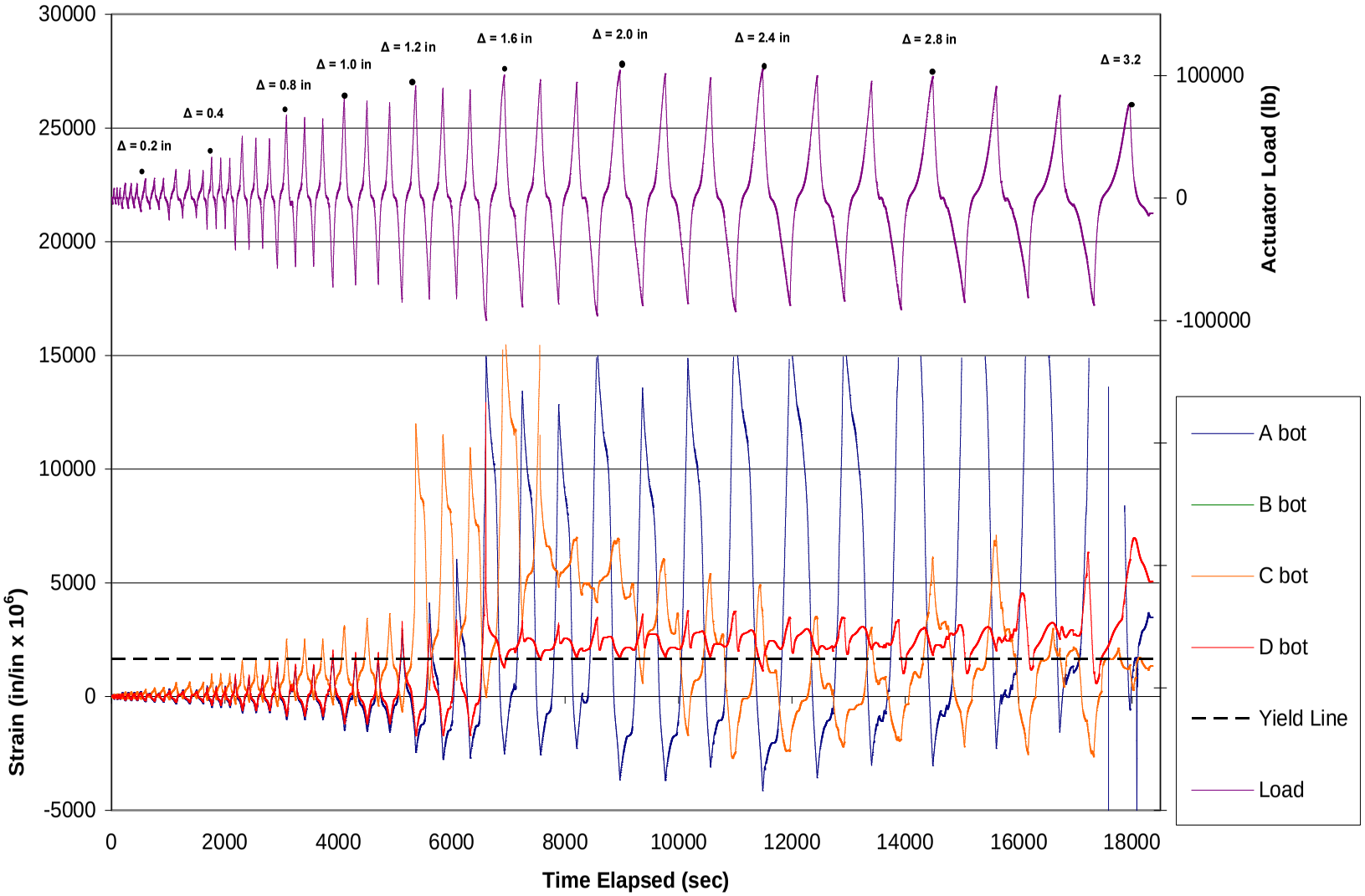

Figure 39 – Column 3 Longitudinal Bar Strain Gage Data at the Bottom of the Column (1 kip = 4.45 kN, 1 in. = 25.4 mm)

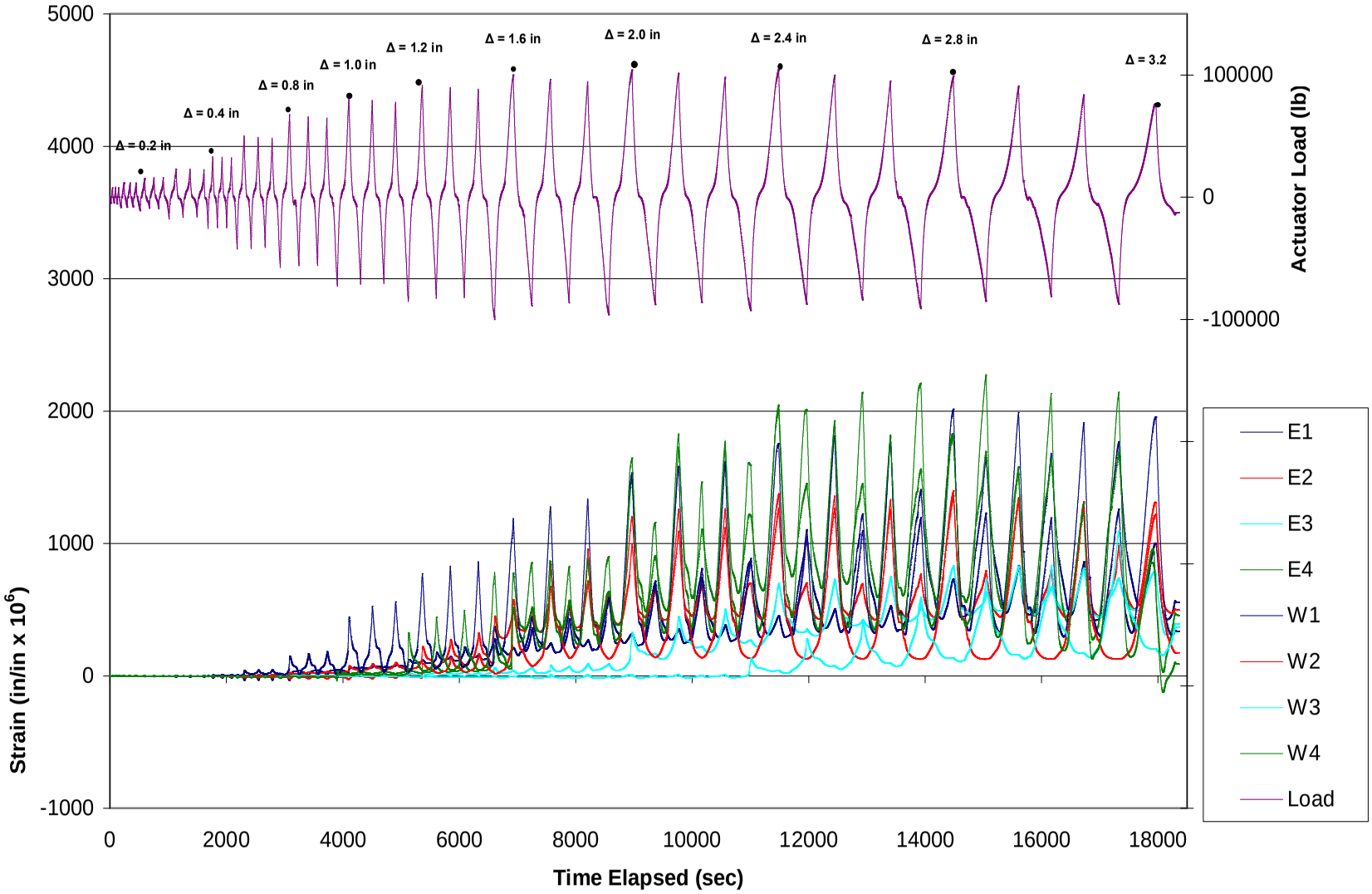

Figure 40 – Column 3 Parallel FRP Jacket Strain Gage Data (1 kip = 4.45 kN, 1 in. = 25.4 mm)

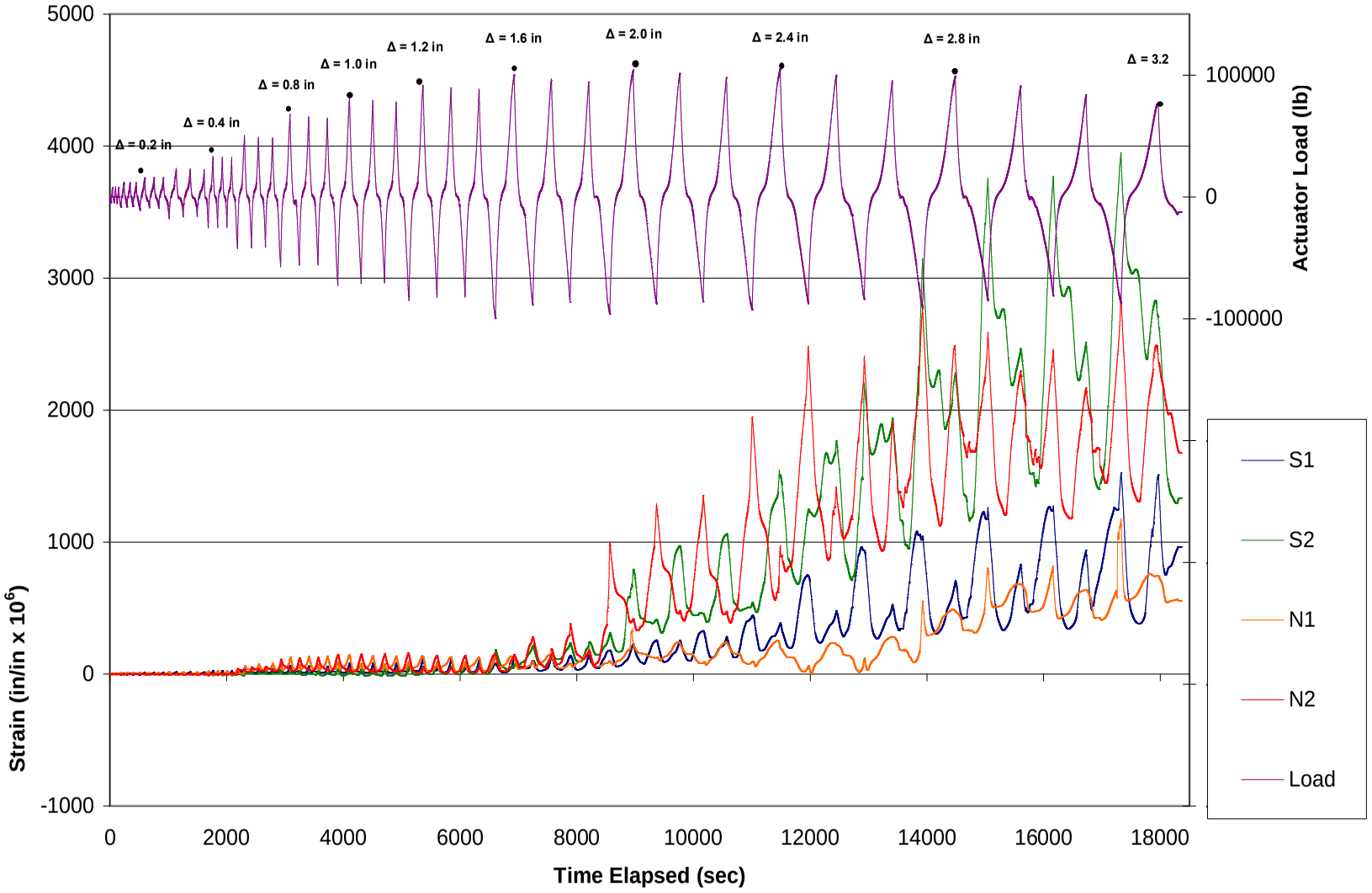

Figure 41 – Column 3 Perpendicular FRP Jacket Strain Gage Data (1 kip = 4.45 kN, 1 in. = 25.4 mm)

Column 4

Column 4 was identical to Column 2 except that the FRP jacket was anchored in the reentrant corners of the column with FRP anchors for the full-height of the column and steel collars for confinement were provided in the plastic hinge zones at the top and bottom of the column. The reentrant corner anchorage was designed to develop the full strength of the FRP jacket and thus prevent the column from failing in shear. The steel collars were designed to prevent bulging of the FRP jacket in the plastic hinge zones that occurred during testing of Column 3 and thereby improve the flexural response of the column at large displacements.

Figure 42 shows the overall hysteretic performance of Column 4 in terms of the lateral force vs. actuator displacement. The FRP jacket with reentrant corner anchorage and plastic hinge zone confinement exhibited a significant improvement in the overall seismic performance from the as-built columns and the retrofitted columns without collars. The peak lateral load achieved was 113 kips (503 kN) and occurred at a lateral displacement of 2.8 in. (71 mm). The flexural response of the column remained stable through three cycles at a displacement level of 3.2 in. (81 mm), with only a minor degradation in stiffness. The column underwent a decrease in lateral stiffness and strength while cycling at a displacement level of 3.6 in. (91 mm); however, the applied load remained slightly above 80% of the peak load through the third cycle at this displacement. The peak load dropped rapidly during the first cycle at a displacement level of 4.0 in. (0.1 m), and the test was stopped after completing the second cycle at this displacement level.

The response of Column 4 was nearly identical to that of Column 2 through the early part of testing with yielding of the longitudinal bars first occurring at a lateral force level of 55 kips (245 kN) followed by flexural cracking at the top and bottom of the column. Strains in the transverse reinforcement were small throughout the test and did not come close to the yield

strain. FRP jacket strains were slightly lower than those for Column 3 parallel to the applied load, and strains on the steel collar were almost negligible throughout the test. The applied lateral load remained nearly constant even after development of plastic hinges at the top and bottom of the column up to a displacement level of 3.6 in. (91 mm). While cycling at a displacement level of 3.6 in. (91 mm), several of the vertical reinforcing bars fractured, resulting in significant decrease in the lateral stiffness and strength. Figure 43 shows the fractured longitudinal steel which was caused by low-cycle fatigue due to the stress reversals in the plastic hinge region. The final failure mode for the column was flexural hinging leading to fracture of the longitudinal rebar with no distress observed in the FRP jacket and steel collar at the end of testing. Figure 44 shows the column at the end of testing and illustrates the significant rotation of the plastic hinge regions.

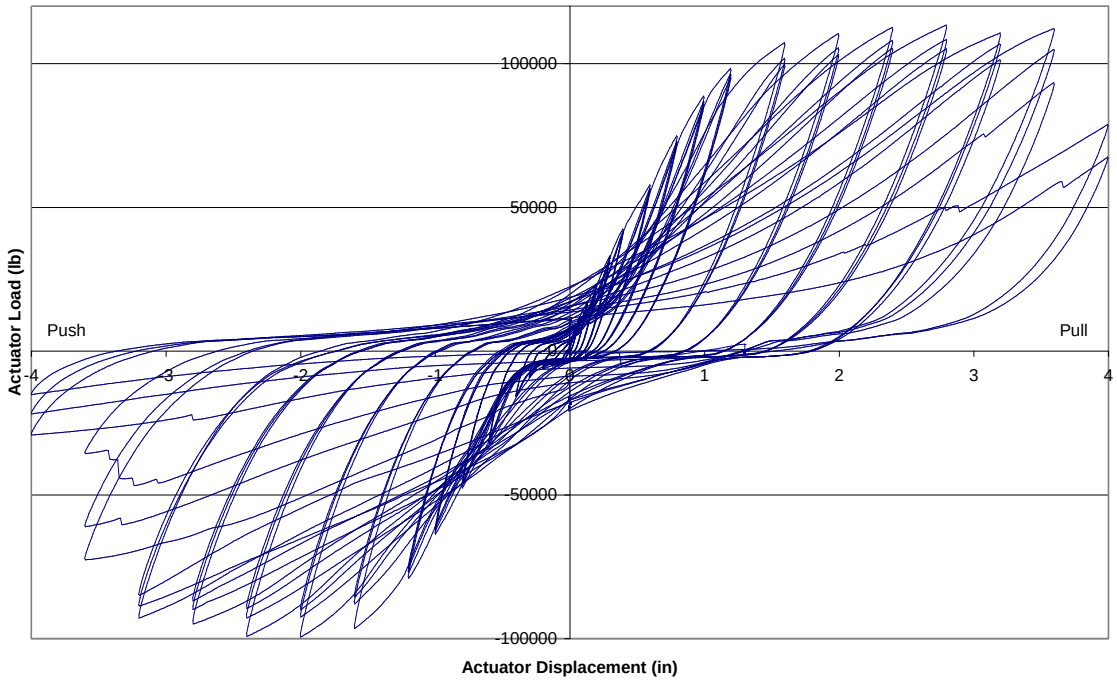

Figure 42 – Column 4 Lateral Load vs. Displacement Hysteresis Curves (1 kip = 4.45 kN, 1 in. = 25.4 mm)

Figure 43 – Column 4 Longitudinal Rebar Fracture

Figure 44 – Column 4 Near the End of Testing

Figure 45 shows a plot of the transverse tie strains with time. Almost negligible tie strains were observed up to a displacement level of 1.2 in. (30 mm). A linear strain profile was then observed up to peak strain of about 700 με at a displacement level of 1.6 in. (41 mm). The observed tie strains were nearly constant for the remainder of the test. The peak strain observed for the transverse ties was far below the yield strain.

Figures 46 and 47 show the strains in the longitudinal bars at the top and bottom of the column, respectively. First yield was observed in the top strain gages at a displacement level of 1.0 in. (25 mm). Very large strains in excess of 10,000 με were observed until a displacement level of 2.8 in. (71 mm), after which strains near the yield strain were observed for the remainder of the test. Strains in the bottom strain gages reached first yield at a displacement level of about 0.8 in. Strains increased linearly up to a displacement level of 1.2 in. (30 mm) and then increased rapidly to strains in excess of 10,000 με. Very large strains were observed up to a displacement level of 3.2 in. (81 mm), after which strains near the yield strain were observed for the remainder of the test.

Figures 48 and 49 show the strains in the FRP jacket for strain gages parallel to the applied load and in the steel collar for strain gages perpendicular to the applied load. Almost negligible strains were observed in the parallel FRP strain gages up to a displacement level of 0.6 in. (15 mm). A peak strain value of 2200 με was observed at a displacement level of 2.4 in. (61 mm). Afterwards, strains remained nearly constant up to a displacement level of 3.6 in. (91 mm) and then decreased linearly for the remainder of the test. All measured strains were well below the FRP jacket ultimate strain capacity of around 19,000 με.

Very small strains were observed in the steel collar strain gages placed perpendicular to the loading direction throughout the test and were well below the steel collar yield strain of 1300 με.

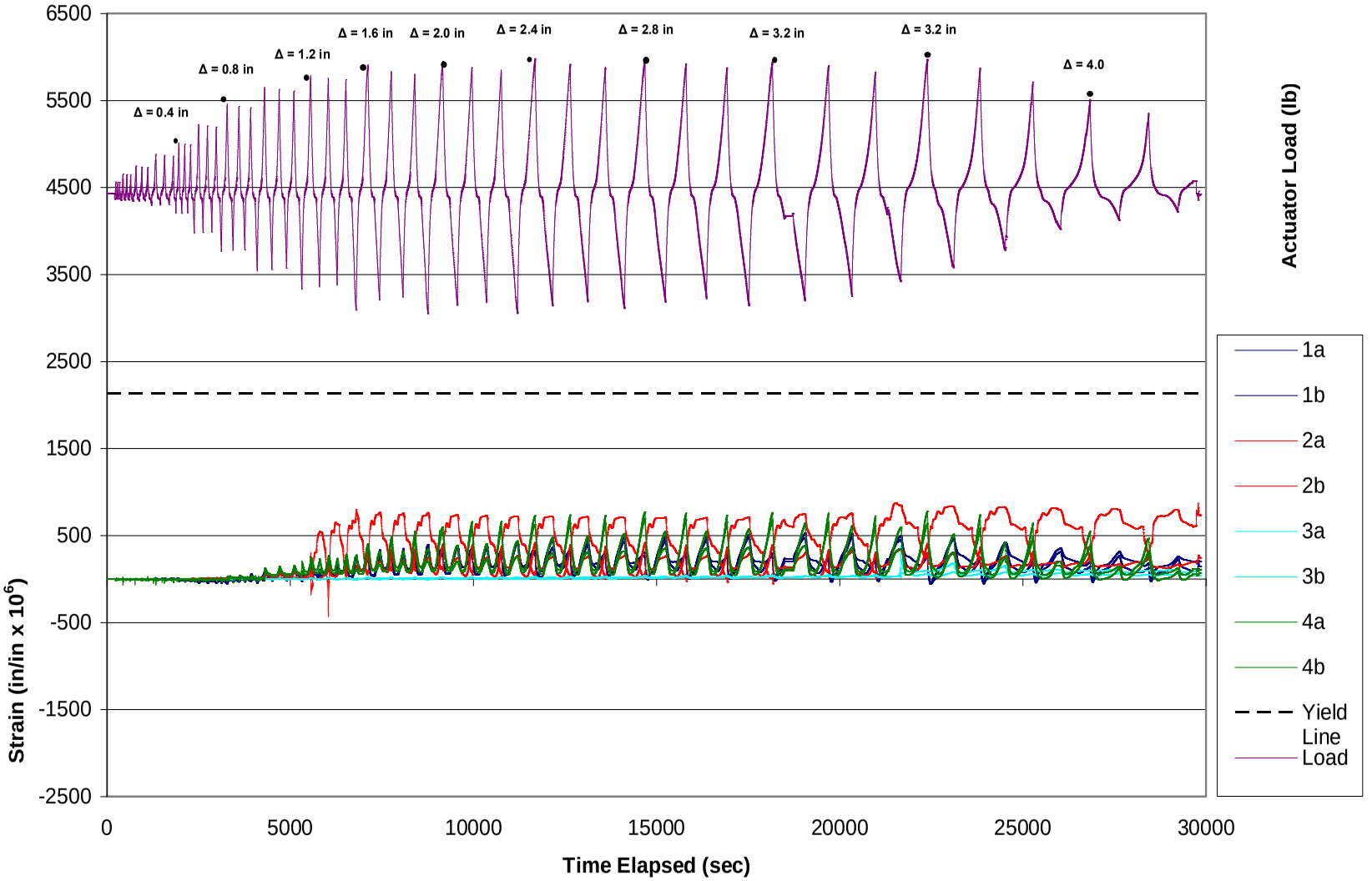

Figure 45 Column 4 Transverse Strain Gage Data (1 kip = 4.45 kN, 1 in. = 25.4 mm)

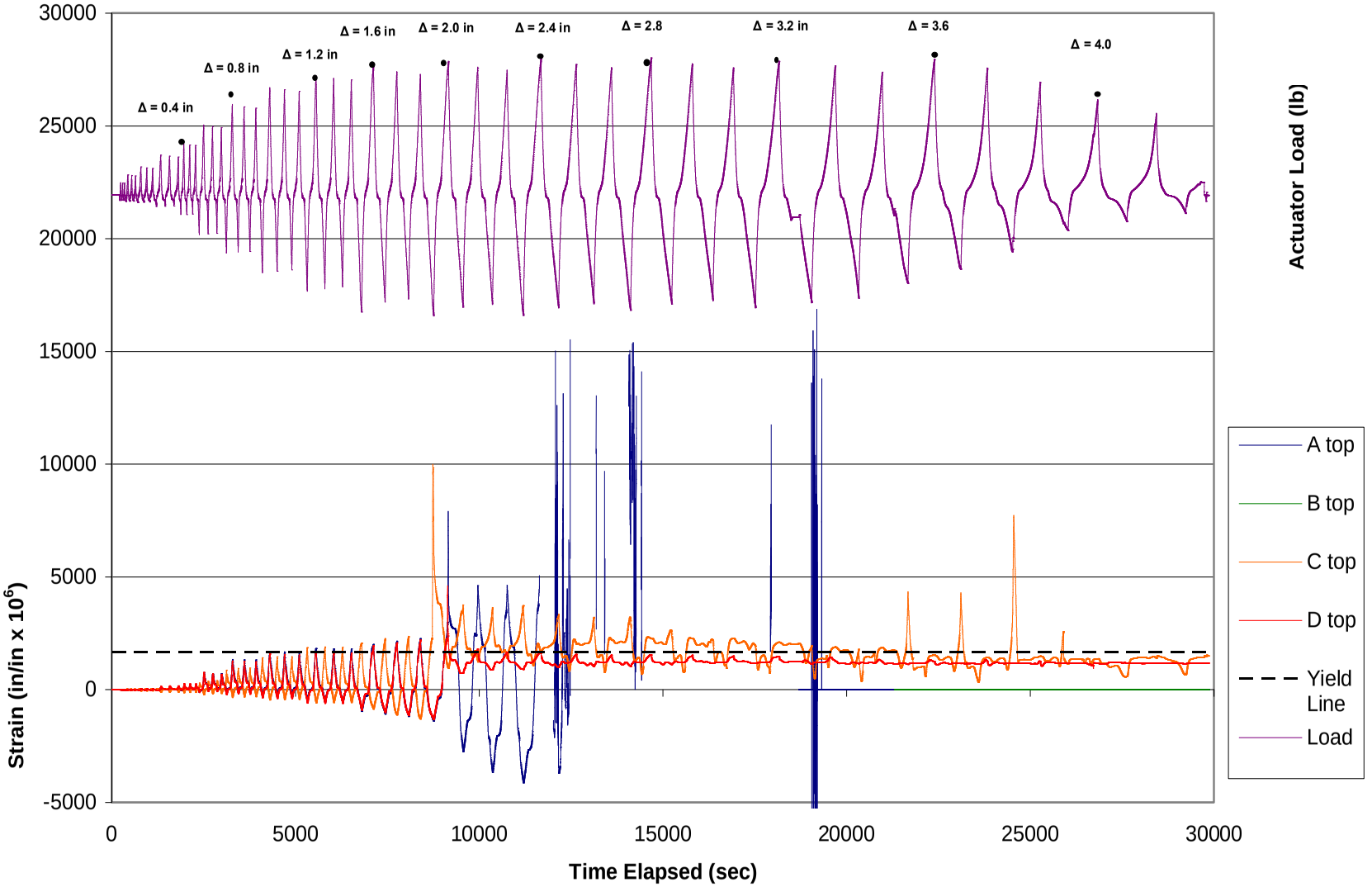

Figure 46 – Column 4 Longitudinal Bar Strain Gage Data at the Top of the Column (1 kip = 4.45 kN, 1 in. = 25.4 mm)

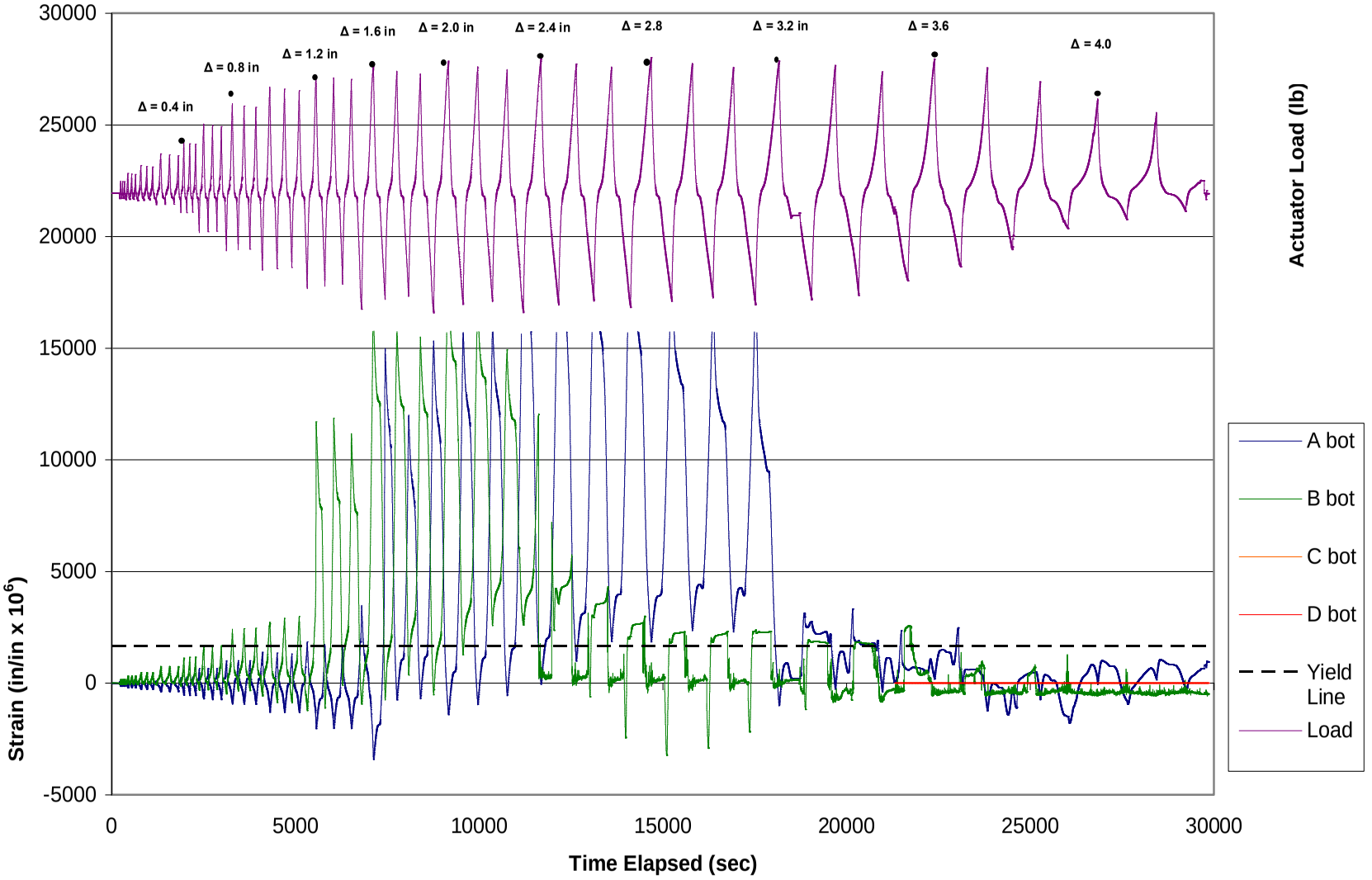

Figure 47 – Column 4 Longitudinal Bar Strain Gage Data at the Bottom of the Column (1 kip = 4.45 kN, 1 in. = 25.4 mm)

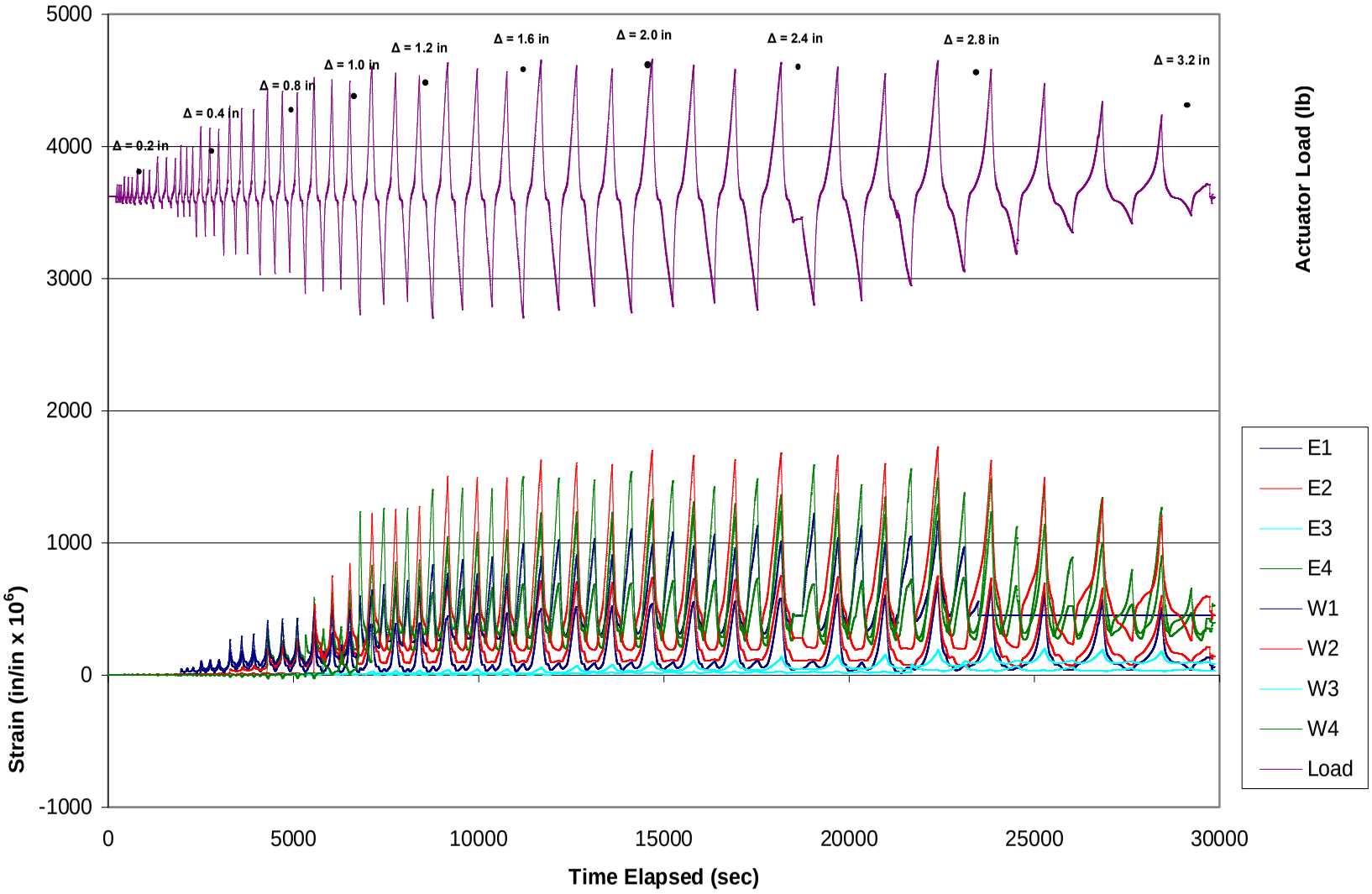

Figure 48– Column 4 Parallel FRP Jacket Strain Gage Data (1 kip = 4.45 kN, 1 in. = 25.4 mm)

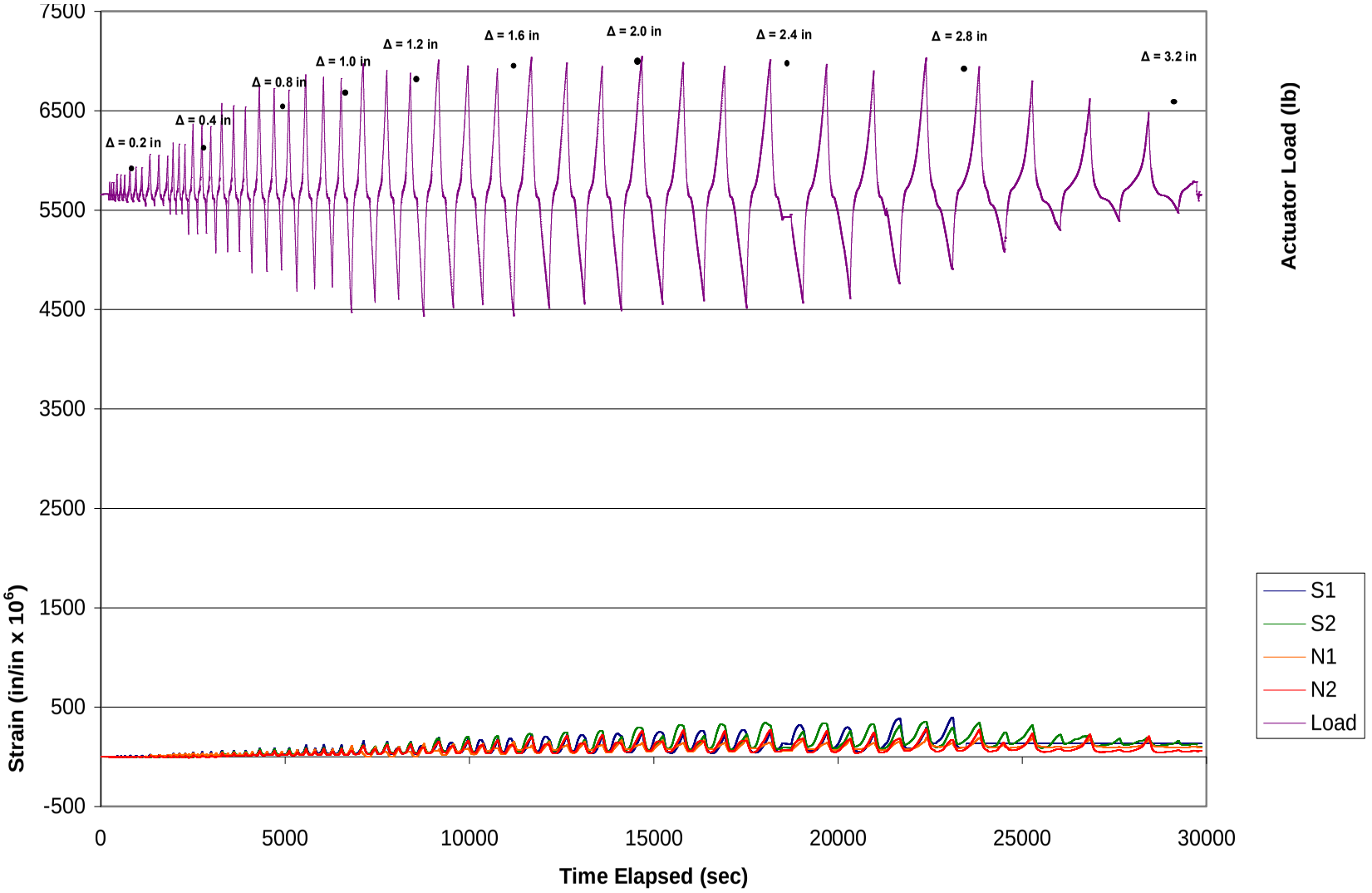

Figure 49– Column 4 Perpendicular Steel Collar Strain Gage Data (1 kip = 4.45 kN, 1 in. = 25.4 mm)

Summary of Retrofitted Solid Column Performance

Tests on as-built Columns 1 and 5 resulted in shear failures at a displacement level of about 2.0 in. (61 mm), accompanied with severe strength and stiffness degradation. Column 2 retrofitted with an FRP jacket but no reentrant corner anchorage or hinge confinement showed a moderate improvement in the energy dissipation capacity of the column but still failed in shear with limited ductility. Column 3 retrofitted with an FRP jacket as well as reentrant corner anchorages consisting of bent plates and epoxied steel anchors showed improvement in the overall seismic response with significant enhancement of seismic energy dissipation and displacement capacity. Failure in Column 3 was caused by bulging of the FRP jacket in the hinge regions, leading to flexural hinge degradation and reentrant corner anchorage failure. Column 4 retrofitted with a FRP jacket with reentrant corner anchorages consisting of FRP anchors along with steel collars in the hinging regions provided the best seismic response. Good seismic energy dissipation along with a ductile response was achieved. Failure in Column 4 occurred due to extensive flexural hinging leading to low-cycle fatigue fracture of several of the longitudinal reinforcing bars.

A summary of various characteristics for the solid column specimens is presented in Table 2. Listed characteristics include the effective secant stiffness and shear force corresponding to the first yield of the longitudinal reinforcement, the maximum observed column shear strength, the maximum displacement ductility and drift ratio attained at the maximum response, and the total amount of energy dissipated throughout the test. Figure 50 shows the envelope lateral load vs. actuator displacement curves for Columns 1-5. Values in Table 2 and Figure 50 for Column 1 were adjusted by removing estimated displacements associated with play between the loading rods and tubes in the loading stub. However, it is likely that this play

influenced the response of Column 1, and as a result the response of Column 5 should be considered as being more representative of the expected performance of the as-built columns.

Table 2 – Solid Column Test Results (1 kip = 4.45 kN, 1 in. = 25.4 mm)

Column	V_y (1)	Δ_y (2)	K_y (3)	V_{exp} (4)	V_{exp}/V_{if} (5)	Δ_{max} (6)	μ_Δ (7)	Drift (8)	E_{total} (9)
1	26.8	0.44	61	98	1.16	2.5	5.6	3.8	290
2	48.5	0.53	91	101	1.19	2.8	5.3	4.3	400
3	50.4	0.62	81	105	1.25	3.2	5.2	4.9	490
4	55.6	0.59	94	113	1.34	4.0	6.8	6.1	650
5	48.7	0.54	90	103	1.21	2.2	4.1	3.3	300

(1): Shear at first yield of longitudinal reinforcement (kips)
(2): Measured actuator displacement at first yield of longitudinal reinforcement (in.)
(3): Effective secant stiffness {(1) / (2)} (kips/in.)
(4): Maximum experimental shear force (kips)
(5): Ratio of maximum experimental shear force to shear force to develop theoretical flexural capacity
(6): Maximum measured actuator displacement (in.)
(7): Displacement ductility at maximum shear force {(6) / (2)}
(8): Drift ratio at maximum shear force (%)
(9): Total energy dissipated during testing (k-in.)

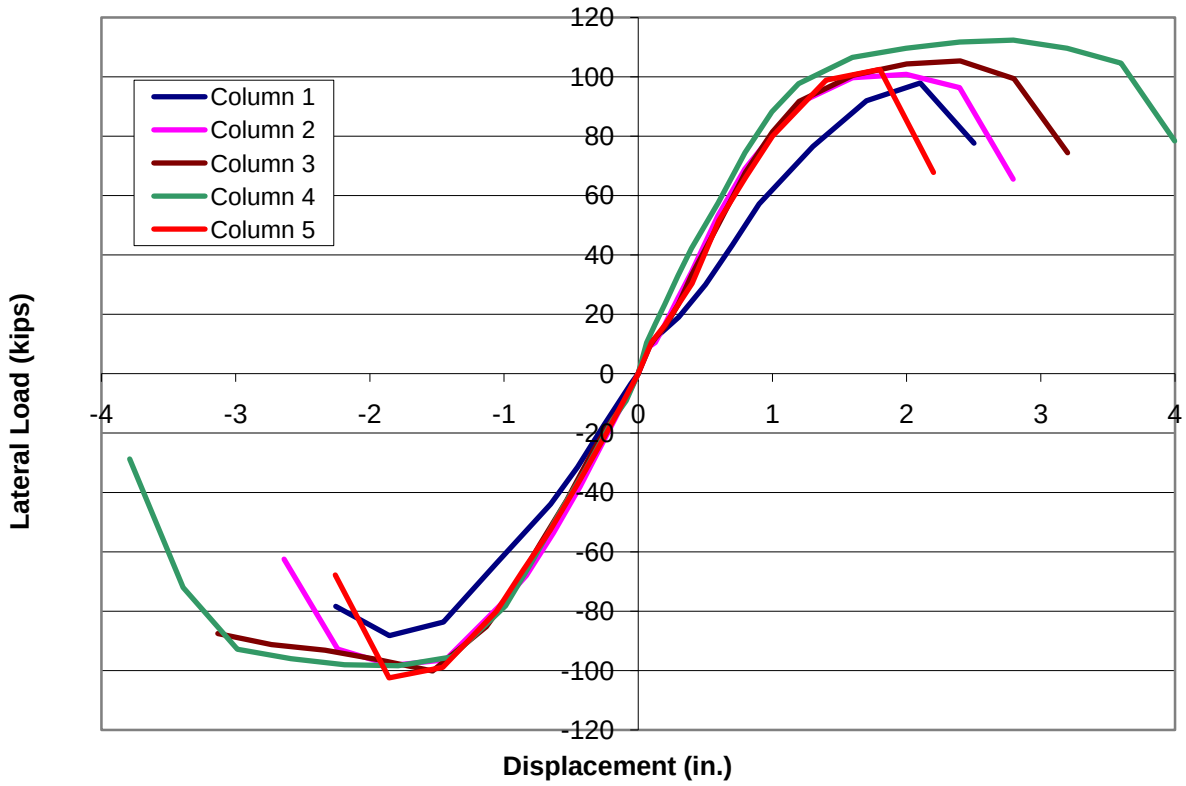

Figure 50 – Envelope Lateral Load vs. Displacement Hysteresis Curves for Solid Columns (1 kip = 4.45 kN, 1 in. = 25.4 mm)

RETROFITTED SPLIT COLUMNS

Columns 6 and 7 modeled the split columns in Bent 11 of the Aurora Avenue Bridge. Retrofitting for both columns consisted of 2-in. (50-mm) diameter cores drilled at 4-in. (100-mm) on center over the full height of the split. The split region and the cored areas were then filled with high-strength grout. The columns were then wrapped with FRP jacketing in exactly the same manner as was used for Column 4, including incorporating FRP inserts in the reentrant corners to anchor the FRP jacket. Finally, steel collars were installed in the bottom hinging regions and filled with high-strength grout. Since the split columns behave as cantilevers, the collars were only installed at the base of the columns.

Column 6

Figure 51 shows the overall hysteretic performance of Column 6 in terms of the lateral force vs. actuator displacement. The peak lateral load achieved was 47 kips (209 kN) and occurred at a lateral displacement of 4.5 in. (110 mm). The flexural response of the column remained stable through three cycles at this displacement level. The peak load dropped rapidly during the second cycle at a displacement level of 6.0 in. (120 mm), and the test was stopped after completing the third cycle at this displacement level.

Flexural hinging developed at the bottom of Column 6 during testing. There was no evidence of any distress in the FRP jacket or in the retrofit collar through cycling to a displacement level of 6 in. (150 mm). The FRP jacket remained fully connected in the reentrant corners and to the flat surfaces of the column. No displacements occurred between the two split sections (both visually, and through measurements at the split location). Final failure of the column was due to fracture of several of the longitudinal column bars from low-cycle fatigue. This is the same failure mechanism that occurred in Column 4. Figure 52 shows the column at the end of testing and illustrates the significant rotation of the plastic hinge regions.

Yielding of the longitudinal bars in Column 6 first occurred at a lateral force level of 36 kips (160 kN). Strains in the transverse tie reinforcement remained small throughout the test (less than 500 με). Figure 53 shows strains in the FRP jacket for gages parallel to the applied load. Peak strains of 700 με were observed at a displacement level of 4.5 in. (110 mm). This peak strain value is substantially less than the peak strains measured in the FRP jackets for the solid columns. Very small strains were measured in the steel retrofit collar during testing (less than 300 με).

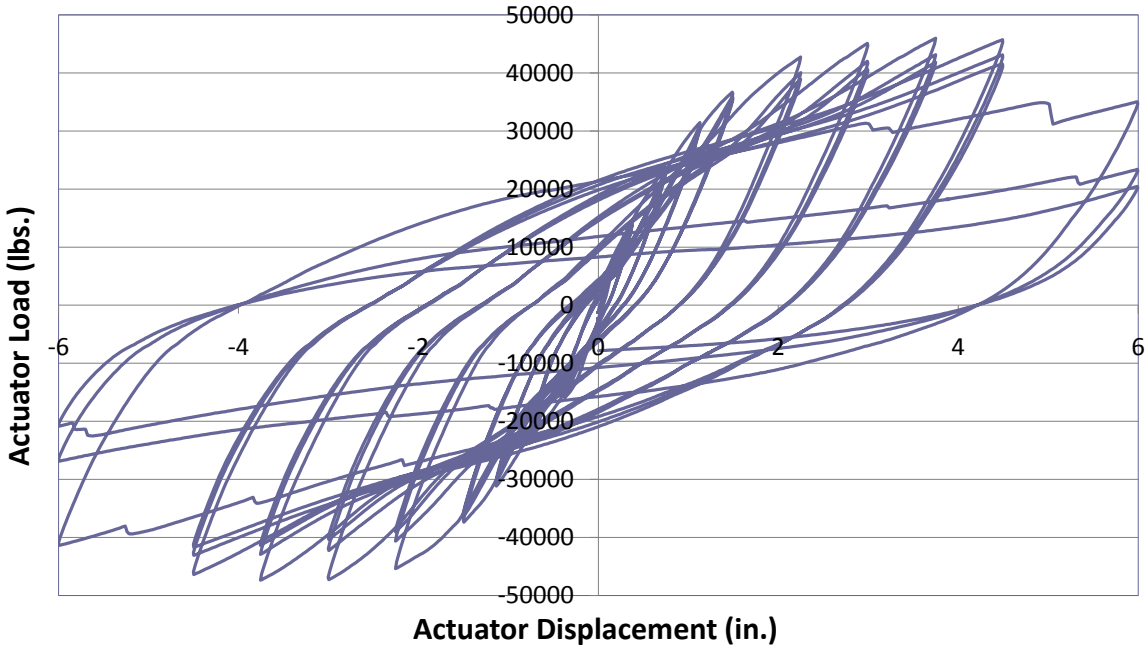

Figure 51 – Column 6 Lateral Load vs. Displacement Hysteresis Curves (1 kip = 4.45 kN, 1 in. = 25.4 mm)

Figure 52 – Column 6 Near the End of Testing

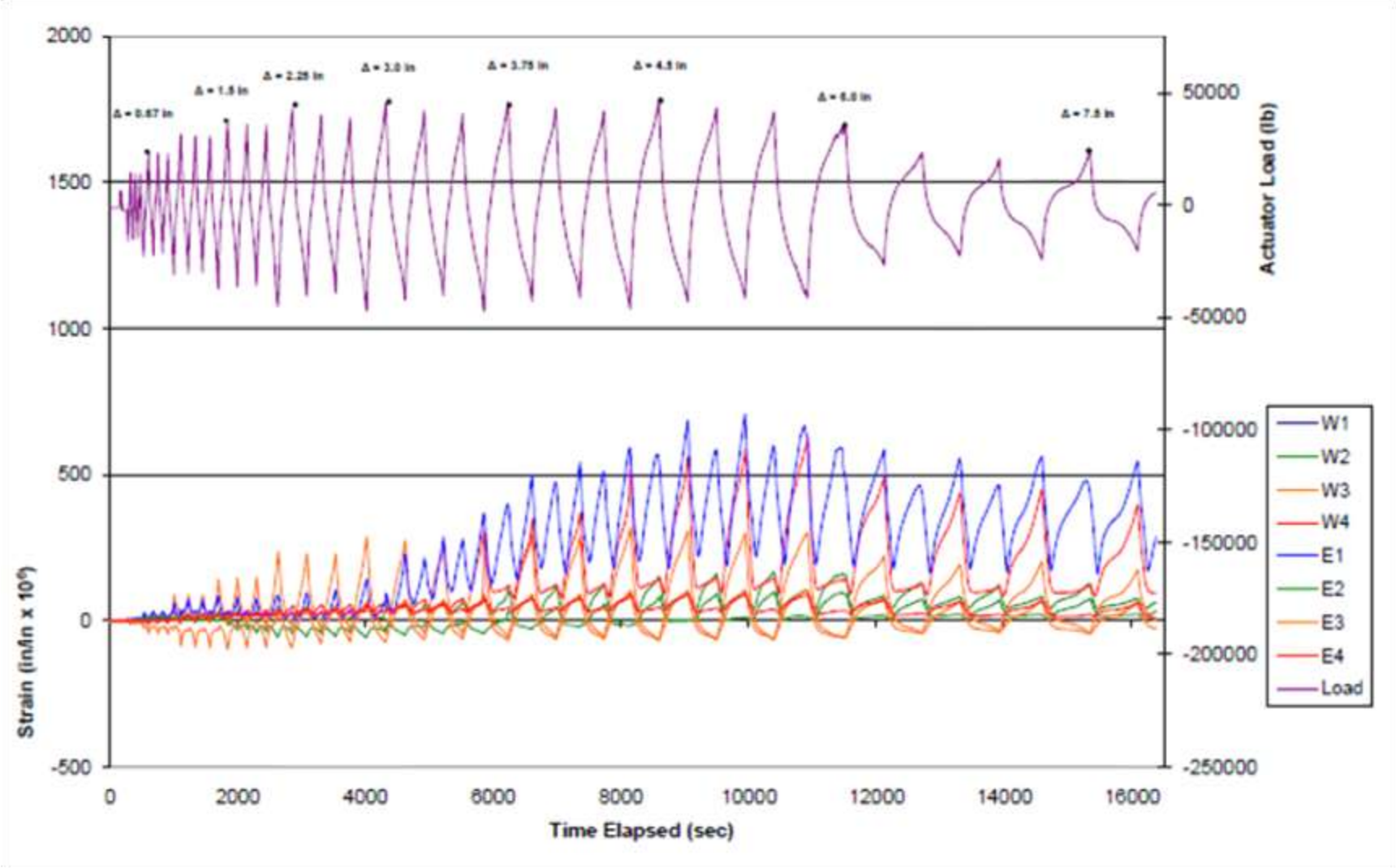

Figure 53– Column 6 Parallel FRP Jacket Strain Gage Data (1 kip = 4.45 kN, 1 in. = 25.4 mm)

Column 7

Figure 54 shows the overall hysteretic performance of Column 7 in terms of the lateral force vs. actuator displacement. The peak lateral load achieved was 49 kips (209 kN) and occurred at a lateral displacement of 6.0 in. (150 mm). The peak load dropped rapidly during the second cycle at a displacement level of 6.0 in. (120 mm), and the test was stopped after completing the third cycle at this displacement level.

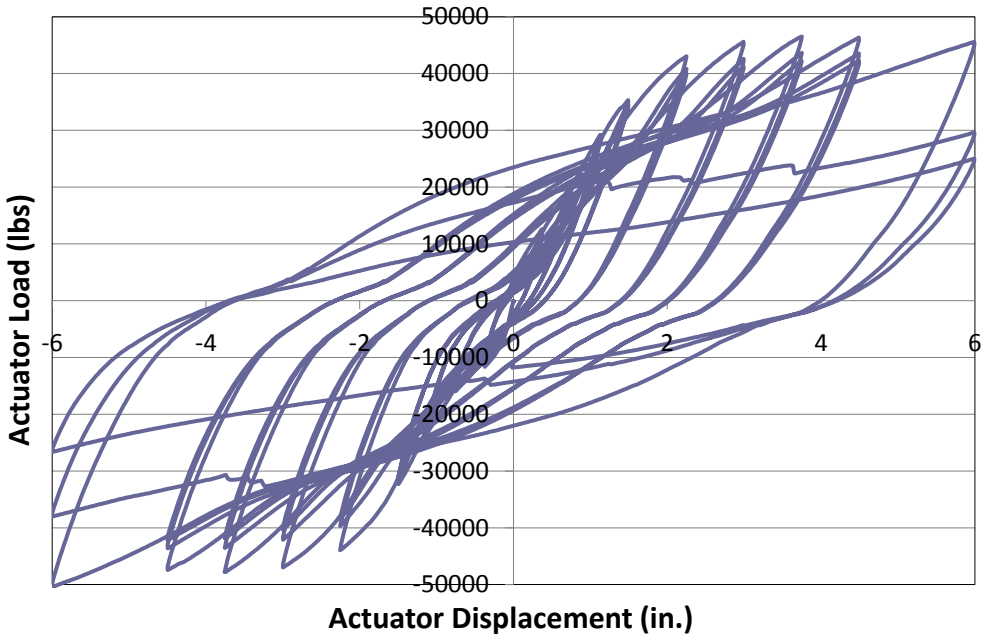

Figure 54 – Column 7 Lateral Load vs. Displacement Hysteresis Curves (1 kip = 4.45 kN, 1 in. = 25.4 mm)

The performance of Column 7 was essentially the same as that obtained for Column 6. Flexural hinging developed at the bottom of Column 7 during testing. There was no evidence of any distress in the FRP jacket or in the retrofit collar through cycling to a displacement level of 6 in. (150 mm). The FRP jacket remained fully connected in the reentrant corners and to the flat surfaces of the column. No movement occurred between the two split sections. Final failure of

the column was due to fracture of several of the longitudinal column bars from low-cycle fatigue.

Yielding of the longitudinal bars in Column 7 first occurred at a lateral force level of 28 kips (124 kN). Strains in the transverse tie reinforcement remained small throughout the test (less than 500 με). Strains in the FRP jacket and in the steel retrofit collar also remained small throughout the test (with values less than 600 με and 300 με, respectively).

Summary of Retrofitted Split Column Performance

The split columns were retrofitted by providing cores over the full height of the split along with FRP jacketing anchored with FRP inserts and steel collars in the hinge regions, similar to those used for Column 4. Good seismic energy dissipation and a ductile response were achieved with both columns. The FRP jackets remained fully connected and no movement occurred between the two split sections throughout testing. Failures were due to extensive flexural hinging leading to low-cycle fatigue fracture of the longitudinal reinforcing bars.

A summary of various characteristics for the split column specimens is presented in Table 3. Listed characteristics include the effective secant stiffness and shear force corresponding to the first yield of the longitudinal reinforcement, the maximum observed column shear strength, the maximum displacement ductility and drift ratio attained at the maximum response, and the total amount of energy dissipated throughout the test. Figure 55 shows the envelope of the lateral load vs. actuator displacement curves for Columns 6 and 7. The characteristics and responses from both columns are very similar.

Table 3 – Split Column Test Results (1 kip = 4.45 kN, 1 in. = 25.4 mm)

Column	V_y (1)	Δ_y (2)	K_y (3)	V_{exp} (4)	V_{exp}/V_{if} (5)	Δ_{max} (6)	μ_Δ (7)	Drift (8)	E_{total} (9)
6	35.9	1.42	25	47	1.19	6.0	4.2	5.6	110
7	27.9	1.32	21	50	1.27	6.0	4.6	5.6	110

(1): Shear at first yield of longitudinal reinforcement (kips)

(2): Measured actuator displacement at first yield of longitudinal reinforcement (in.)

(3): Effective secant stiffness {(1) / (2)} (kips/in.)

(4): Maximum experimental shear force (kips)

(5): Ratio of maximum measured shear force to shear force to develop theoretical flexural capacity

(6): Maximum measured actuator displacement (in.)

(7): Displacement ductility at maximum shear force {(6) / (2)}

(8): Drift ratio at maximum shear force (%)

(9): Total energy dissipated during testing (k-in.)

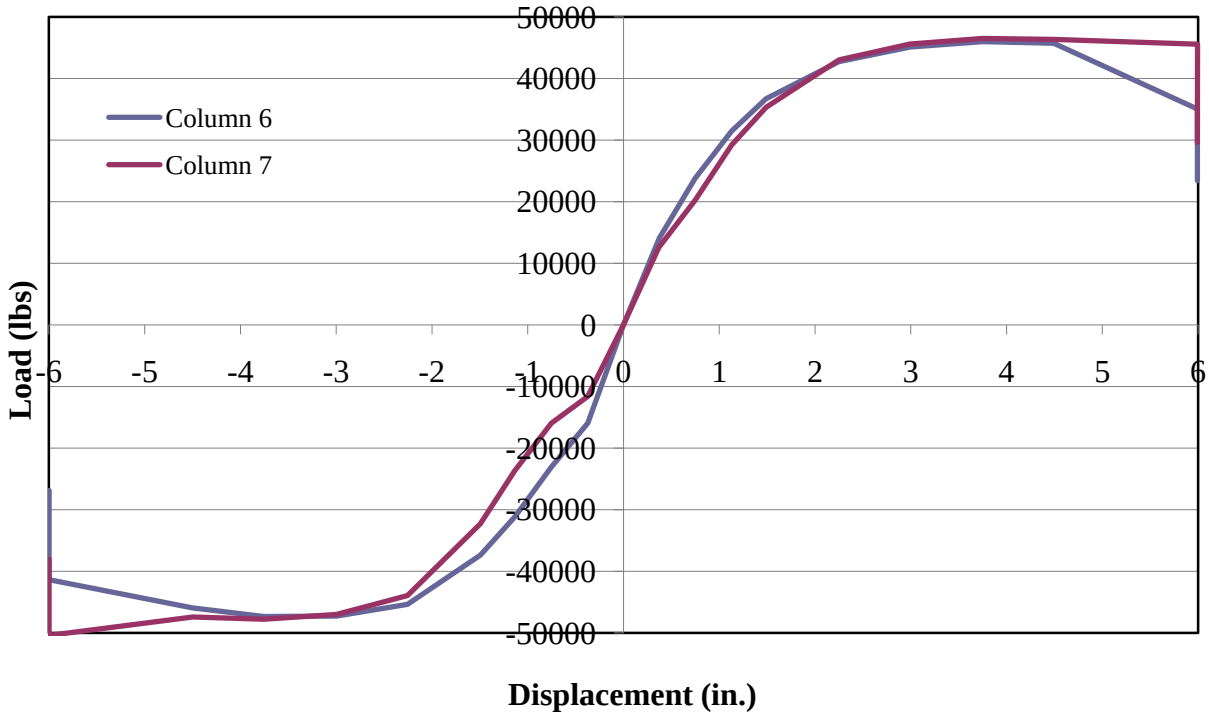

Figure 55 – Envelope Lateral Load vs. Displacement Hysteresis Curves for Split Columns (1 kip = 4.45 kN, 1 in. = 25.4 mm)

CONCLUSIONS AND RECOMMENDATIONS

CONCLUSIONS

The experimental results of this study indicate that the cruciform-shaped columns in the Aurora Avenue Bridge have inadequate shear strength to develop ductile flexural hinging. Tests on column specimens representing as-built conditions resulted in shear failures at modest displacement levels, accompanied by severe strength and stiffness degradation in the columns.

Tests on column specimens representing solid columns in the Aurora Avenue Bridge and which were retrofitted with FRP jacketing resulted in improved performance compared to that obtained for the column specimens representing as-built conditions. The solid column specimen retrofitted with a FRP jacket and no reentrant corner anchorage showed a slight improvement in energy dissipation capacity and ductility compared to the as-built solid specimens. However, pullout of the FRP jacket from the reentrant corners of the column occurred during testing, and the specimen still failed in shear. Inspection of the specimen after testing showed that the pullout of the FRP jacket was caused by concrete spalling under the jacket in the hinging region rather than debonding of the FRP jacket from the concrete. The results of this test indicate that reentrant corner anchorage is required to prevent pullout and develop the required capacity of the FRP jacket.

Both solid column specimens retrofitted with an FRP jacket and reentrant corner anchorages developed flexural hinging and failed in a ductile manner with no evidence of shear distress. The specimen retrofitted with an FRP jacket as well as reentrant corner anchorages consisting of bent steel plates and epoxied steel anchors showed improvement in the overall seismic response with significant enhancement of seismic energy dissipation capacity and displacement levels sustained prior to failure. Failure in this column was caused by bulging of

the FRP jacket in the hinge regions, leading to crushing of the concrete and reentrant corner anchorage failure. To provide confinement in the plastic hinge regions, the final solid column specimen was retrofitted with a grout-filled steel collar at the top and bottom of the column in addition to FRP anchors for reentrant corner anchorage. This specimen achieved significant improvement in energy dissipation capacity and developed the full flexural capacity of the specimen without any bulging in the plastic hinge region. Failure in the specimen was due to extensive flexural hinging leading to low-cycle fatigue fracture of several of the longitudinal reinforcing bars.

Tests on column specimens representing split columns in the Aurora Avenue Bridge and which were retrofitted by providing grout-filled cores over the full height of the split along with FRP jacketing anchored with FRP inserts and steel collars in the hinge regions resulted in a ductile response and good energy dissipation. The FRP jackets remained fully connected and no movement occurred between the two split sections throughout testing. Failures were due to extensive flexural hinging leading to low-cycle fatigue fracture of the longitudinal reinforcing bars.

The results of this study show that FRP jacketing is effective at providing the required shear strength enhancement to prevent a brittle shear failure. The FRP jacket needs to be anchored into the reentrant corners of the column in order to be effective. In addition, due to the cruciform shape of the columns, the FRP jacket does not provide adequate confinement in the hinge regions to develop ductile flexural hinging in the column. A steel collar filled with high-strength grout was effective at providing the required confinement. The final retrofit design incorporating both reentrant corner anchorage and steel collar confinement developed the full flexural capacity of the column and resulted in fracture of the column longitudinal reinforcing

bars. Both the steel bent plates with epoxy anchors and the FRP anchors were effective at anchoring the FRP jacket into the reentrant corners of the column; however, the FRP anchors did not significantly alter the appearance of the bridge columns and were significantly easier to install.

RECOMMENDATIONS

FRP jacketing is effective at improving the seismic performance of cruciform-shaped columns that are deficient in shear. The required effective thickness, t_j, of the FRP jacket can be determined using previously-developed guidelines (Seible et al., 1995) as follows:

$$t_j = \frac{\frac{V_o}{\phi} - (V_c + V_s)}{2 f_{j_d} D \cot\theta} \qquad \text{(Equation 4)}$$

V_o is taken as 1.5 times the shear force required to develop the onset of flexural yielding in the unretrofitted column, and ϕ is taken as 0.85. V_C and V_S are the contributions to shear strength from the concrete and transverse reinforcement of the unretrofitted column, respectively. D is the column dimension in the loading direction, and θ is the inclination of the shear crack of principal compression strut. The design stress level for the jacket, f_{jd}, is specified by the FRP manufacturer. Priestley et al. (1996) recommend that f_{jd} should not exceed $0.004E_j$, where E_j is the elastic jacket modulus in the applied shear direction, in order to limit dilation strains in the concrete. ACI 440 (2006) specifies that f_{jd} should not exceed $0.75\varepsilon_{ju}E_j$, where ε_{ju} is the ultimate strain of the FRP, and imposes an additional safety factor of 0.95 on the contribution of the FRP to the shear strength to account for loss of strength over time.

The results of this study show that both bent steel plates with epoxied steel anchors and FRP anchors were effective at anchoring the FRP jacket to the reentrant corners of the column.

However, the bent plate anchorage significantly alters the appearance of the column due to the heads of the epoxied steel anchors protruding from the face of the column, and the plates impose construction difficulties due to anchors being placed on perpendicular surfaces at very tight clearances. Anchor hole locations have to be held to very tight tolerances to avoid damaging column longitudinal reinforcement and to allow proper fit-up of the steel bent plates in the reentrant corner. In contrast, the FRP anchors do not significantly alter the appearance of the column and are significantly easier to construct due to the flexibility of the location of the anchor holes. Thus, it is recommended that FRP anchors be utilized in the actual retrofit.

Design of the FRP anchors used in this study was based on a required anchor force of 12.8 k/ft (187 kN/m) of column height. Each ½-in. (13-mm) diameter FRP anchor was assumed to provide an effective tensile force of 6.3 kip (28 kN). Anchors were assumed to be effective in tension only, thus a spacing of 4 in. (0.1 m) on center was required on each face of the reentrant corner. This design provided the required anchorage of the FRP jacket to the column, and it is recommended that similar anchor spacing be used in the final retrofit design.

Retrofitting measures consisting of coring and grouting over the length of the split region was found to be effective at achieving full composite action in the split column specimens. Split columns with dimensions or details different than those of the test specimens may require reinforcement across the split interface to achieve composite action.

ACKNOWLEDGEMENTS

This research was conducted through the Washington State Transportation Center (TRAC) and under contract to the Washington State Department of Transportation (WSDOT). Financial support for this project was provided by WSDOT. The contributions and technical assistance provided by Craig Boone, Brian Aldrich and Chyuan-Shen Lee of the WSDOT Bridge Office and by Michael Lamont of TY Lin are appreciated. The authors gratefully acknowledge the assistance provided in conducting the laboratory tests by Tim Vaughan, Jake Sherman, Bob Duncan and Scott Lewis of Washington State University.

REFERENCES

ACI 318-05 (2005). *Building Code Requirements for Structural (ACI 318-05)*. American Concrete Institute, Farmington Hills, Michigan.

ACI 440-02 (2002). *Guide for the design and construction of externally bonded FRP systems for strengthening concrete structures (ACI 440.2R-02)*. American Concrete Institute, Farmington Hills, Michigan.

American Association of State Highway Officials (1931). "Standard Specification for Highway Bridges and Incidental Structures"

California Department of Transportation (1996). "Memo to Designers, 20-4"

Chai, Y. H.; Priestley, M. J. N.; Seible, F. (1991). "Retrofit of Bridge Columns for Enhanced Seismic Performance," *Seismic Assessment and Retrofit of Bridges*, SSRP 91/03, PP. 177-196.

Endeshaw, Mesay A. (2008). "Retrofit of Rectangular Bridge Columns Using CFRP Wrapping," M.S. Thesis, Department of Civil and Environmental Engineering, Washington State University.

Federal Emergency Management Agency (2000). "Prestandard and Commentary for the Seismic Rehabilitation of Buildings"

Haroun, M. A. and Elsanadedy, H. M. (2005). "Fiber-Reinforced Plastic Jackets for Ductility Enhancement of Reinforced Concrete Bridge Columns with Poor Lap Splice Detailing," *ASCE Journal of Bridge Engineering*, Vol. 1, No. 6, 749-757

Iacobucci, R. D.; Sheikh, S. A.; Bayrak, O. (2003). "Retrofit of Square Concrete Columns with Carbon Fiber-Reinforced Polymer for Seismic Resistance," *ACI Structural Journal*, Vol. 100, No. 6, 785-794.

Memon, M. S. and Sheikh, S. A. (2005). "Seismic Resistance of Square Concrete Columns Retrofitted with Glass Fiber-Reinforced Polymer," *ACI Structural Journal*, Col. 102, No. 5, 774-783.

Ozbakkaloglu, T. and Saatcioglu, M. (2009). "Tensile Behavior of FRP Anchors in Concrete," *Journal of Composites for Construction*, March/April, 2009, 82-92.

Priestley, M. J. N. and Seible, F. (1991). "Design of Seismic Retrofit Measures for Concrete Bridges," *Seismic Assessment and Retrofit of Bridges*, SSRP 91/03, University of California, San Diego, pp. 197-234.

Priestley, M. J. N.; Seible, F.; Verma, R. and Xiao, Y. (1993). "Seismic Shear Strength of Reinforced Concrete Columns," SSRP 93/06, University of California, San Diego, 112 pp.

Priestley, M. J. N.; Seible, F. and Calvi, G. M. (1996). *Seismic Design and Retrofit of Bridges*, John Wiley & Sons, Inc., New York.

Seible, F.; Priestley, M. J. N. and Chai, Y. H. (1995). *Earthquake Retrofit of Bridge Columns with Continuous Carbon Fiber Jackets*, Advanced Composites Technology Transfer Consortium, Report No. ACTT-95/08, La Jolla, California.

Seismic Retrofitting Manual for Highway Structures: Part 1 – Bridges (2006). Federal Highway Administration, Report NO. FHWA-HRT-06-032.

SEQAD Consulting Engineers (1993), *Seismic Retrofit of Bridge Columns Using High Strength Fiberglass/Epoxy Jackets*, Solana Beach, California.

Verma, R.; Priestley, M. J. N. and Seible, F. (1993). "Assessment of Seismic Response and Steel Jacket Retrofit of Squat Circular Reinforced Concrete Bridge Columns," SSRP 92/07, University of California, San Diego, 375 pp.

Washington State Department of Transportation (1930). "Bridge 99-560 Approach Span As-Built Plans"

Xiao, Y. and Wu, H. (2003). "Compressive Behavior of Concrete Confined by Various Types of FRP Composite Jackets," *SAGE Journal of Reinforced Plastics and Composites*, Vol. 22, No. 13, 1187-1202.